Department of Civil, Environmental & Construction Engineering

Structures Research

External Post-Tensioning Anchorage

University of Central Florida

4000 Central Florida Blvd

Orlando, Fl 32816

Project Manager:

Charles Boyd and William Potter

Principal Investigator:

Kevin R. Mackie, PhD

Research Assistants:

Elie A. El Zghayar and Zachary B. Haber

Funding Agency:

Florida Department of Transportation

Project No.

BD550 - 11

Final REPORT

May 1, 2011

Disclaimer

The opinions, findings, and conclusions expressed in this publication are those of the authors and not necessarily those of the State of Florida Department of Transportation.

Unit Conversion Table

SYMBOL	WHEN YOU KNOW	MULTIPLY BY	TO FIND	SYMBOL
LENGTH				
in	inches	25.4	millimeters	mm
ft	feet	0.305	meters	m
yd	yards	0.914	meters	m
mi	miles	1.61	kilometers	km

SYMBOL	WHEN YOU KNOW	MULTIPLY BY	TO FIND	SYMBOL
AREA				
in^2	square inches	645.2	square millimeters	mm^2
ft^2	square feet	0.093	square meters	m^2
yd^2	square yard	0.836	square meters	m^2
ac	acres	0.405	hectares	ha
mi^2	square miles	2.59	square kilometers	km^2

SYMBOL	WHEN YOU KNOW	MULTIPLY BY	TO FIND	SYMBOL
VOLUME				
fl oz	fluid ounces	29.57	milliliters	mL
gal	gallons	3.785	liters	L
ft^3	cubic feet	0.028	cubic meters	m^3
yd^3	cubic yards	0.765	cubic meters	m^3
NOTE: volumes greater than 1000 L shall be shown in m^3				

SYMBOL	WHEN YOU KNOW	MULTIPLY BY	TO FIND	SYMBOL
MASS				
oz	ounces	28.35	grams	g
lb	pounds	0.454	kilograms	kg
T	short tons (2000 lb)	0.907	megagrams (or "metric ton")	Mg (or "t")

SYMBOL	WHEN YOU KNOW	MULTIPLY BY	TO FIND	SYMBOL
TEMPERATURE (exact degrees)				
^oF	Fahrenheit	5 (F-32)/9 or (F-32)/1.8	Celsius	^oC

SYMBOL	WHEN YOU KNOW	MULTIPLY BY	TO FIND	SYMBOL
FORCE and PRESSURE or STRESS				
lbf	poundforce	4.45	newtons	N
lbf/in^2	poundforce per square inch	6.89	kilopascals	kPa
kip	kilopoundforce	4.45	kilonewton	kN
ksi	kilopoundforce per square inch	6.89	megapascals	Mpa

Technical Report Documentation

1. Report No.	2. Government Accession No.	3. Recipient's Catalog No.
4. Title and Subtitle External Post-Tensioning Anchorage		5. Report Date 5/1/2011
		6. Performing Organization Code
7. Author(s) Elie A. El-Zghayar, Kevin R. Mackie, and Zachary B. Haber		8. Performing Organization Report No.
9. Performing Organization Name and Address **University of Central Florida** 4000 Central Florida Blvd Orlando, Fl 32816-2450		10. Work Unit No. (TRAIS)
		11. Contract or Grant No. BD550-11
12. Sponsoring Agency Name and Address **Florida Department of Transportation** 605 Suwannee Street, MS 30 Tallahassee, Fl 32399		13. Type of Report and Period Covered Final Report 10/1/2006 - 5/1/2011
		14. Sponsoring Agency Code
15. Supplementary Notes		

16. Abstract

Post-tensioning tendons in segmental bridge construction are often only anchored within the deviator and pier segments. The effectiveness of the post-tensioning (PT) system is therefore dependent on proper functioning of the anchorages. On August 28, 2000, a routine inspection of the Mid-Bay Bridge (Okaloosa County, Florida) revealed corrosion in numerous PT tendons. Moreover, one of the 19-strand tendons was completely slacked, with later inspection revealing a corrosion-induced failure at the pier anchor location. Anchorage failure caused all PT force to transfer to the steel duct located within the pier segment that in turn slipped and caused the tendon to go completely slack. After the application of PT force, the anchorage assembly and steel pipes that house the tendon are filled with grout. These short grouted regions could, in the event of anchorage failure, provide a secondary anchorage mechanism preventing the scenario mentioned above from occurring. This paper presents the results of a full-scale experimental investigation on anchorage tendon pullout. The study focuses on the length required to develop the in-service PT force within the pier segment grouted steel tube assembly. Seven, twelve, and nineteen 0.6 inch diameter strand tendons with various development lengths were considered. Recommendations for pier section pipe detailing and design will be discussed.

17. Key Word External Post-Tensioning, Anchorage, Transfer Length, Development Length, De-bonding	18. Distribution Statement No Restrictions

19. Security Classif. (of this report) Unclassified	20. Security Classif. (of this page) Unclassified	21. No. of Pages 149	22. Price N/A

Acknowledgements

The authors would like to express gratitude to the Florida Department of Transportation for funding this project (Project BD550-11), the staff at the FDOT Structures Research Center in Tallahassee, Florida, Dr. Lei Zhao for his contributions to this work, and Robert Slade for his assistance with the project.

Executive Summary

Background

On August 28, 2000, a routine inspection of the Mid-Bay Bridge, a 19,265 ft precast segmental bridge located over the Choctawhatchee Bay in Okaloosa County, Florida, revealed that the polyethylene duct of one of the bridge's 19-strand tendons was cracked. It was also observed within the cracked housing that several tendon strands had fractured. The discovery of the de-stressed tendon led to an immediate walk-though inspection of the bridge's remaining spans to confirm if other tendons were displaying similar signs of de-stress. The resulting walk-through led to the discovery of a tendon found to completely slacked between the pier expansion joint diaphragm and the mid-span deviator. Slacking was caused by a substantial level of slip that occurred between the embedded steel pipe tendon duct (Figure 1), located within the expansion joint pier segment, and the surrounding concrete. An inspection of the slacked tendon anchorage device revealed that a substantial level of corrosion had led to the brittle fracture of numerous strands within the anchorage (Figure 2). Failure of the anchorage caused all post-tensioning (PT) force to transfer to the steel duct located within the pier segment. The force transfer resulted in the significant slippage of the steel pipe and resulted in the complete tendon slacking (FDOT 2001).

Figure 1. Mid-Bay Slipped Pipe

Figure 2. Mid-Bay Anchorage

An experimental program was initiated in this project to determine, in the event of anchorage failure, whether secondary anchorage of PT tendons can be developed within span pier segments and to develop recommendations for the transfer length for future design. To date, little information is available in the literature and design codes on the length required to fully develop a PT tendon with different numbers of individual strands in a cementitious material. The experimental program was developed to isolate the transfer of PT force within the grout-duct assembly through the use of shear transfer devices on the outside of the duct. In addition, in accordance with the FDOT specifications at the time the project started, steel-based ducts and assembly components were specified.

Findings

As is common with provisions containing inherent conservatism or factors of safety, the code provisions for the transfer length yielded larger predicted transfer lengths than those measured experimentally as part of this project. Table 1 presents a summary of the observed transfer and development lengths for the 7-, 12-, and 19-strand specimens. The tendons were stressed between 70% to 74% of the guaranteed ultimate tensile strength (GUTS) per American Association of State Highway and Transportation Officials (AASHTO) Table 5.9.3-1, grouted within the post-tensioning duct, and then de-stressed. The transfer length was estimated at this point for those specimens that did not experience a drop in load. Subsequently, the tendons were subjected to a pullout load of 90% of GUTS to estimate the development length. The results

show that the 7-strand tendon requires 38 inches of length for the 90% of the guaranteed ultimate tensile strength (GUTS) force to be developed into the system without failure or slip, while the 12-strand tendon requires roughly 50”. These values are approximate due to the spacing of the instrumentation on the pipe enclosure. The predicted code values obtained from ACI 318-05 and AASHTO LRFD exceeded the measured development lengths by 55% for both the 7- and 12-strand tendons. (ACI is American Concrete Institute and AASHTO LRFD is American Association of State Highway and Transportation Officials Load and Resistance Factor Design).

The development lengths obtained from the experimental tests in this study are limited to the specimen configuration utilizing shear transfer devices on the exterior of the steel duct. For the 7-, 12-, and 19-strand specimens tested utilizing standard VStructural, LLC (VSL) assembly products, a ductile failure mechanism was observed that consisted of large expansive and axial compressive strains at the stressing (free) face due to the larger diameter of grout present in the trumpet and bearing plate region. The failure mechanism was characterized by gradual slip of the grout relative to the pipe and development of the PT force primarily through the Hoyer Effect enhanced by the confining stress provided by the grout and steel pipe in the region near the bearing plate.

The results of the 19-strand test indicate that the pipe was not strong enough for VSL anchorage specifications. The high strains induced on the pipe (both axial and circumferential) due to the grout plug formation allowed the local failure of the pipe and the resultant expansive failure of the concrete block. When the VSL assemblage was altered so that it contained only straight pipe, the grout plug did not form at the free face and failure was characterized by slip of the grout at lower loads. In all the 19-strand specimens, the secondary anchorage mechanism was not able to reach or maintain the intended 90% of GUTS.

Table 1. Results Summary for 9 Specimens

Specimen	Transfer Length (in)	Development Length (in)	Grout Plug Anchored Tendon?	Pullout Load sustained by Specimen (kips)
1st 7-strand specimen (4 ft)	38	38	No	Full 90% GUTS
2nd 7-strand specimen (2 ft)	19*	Not applicable (N/A)	Yes	336
3rd 7-strand specimen (1.5 ft)	18*	N/A	Yes	340
1st 12-strand specimen (5 ft)	50	50	No	Full 90% GUTS
2nd 12-strand specimen (2.5 ft)	28*	N/A	Yes	607
3rd 12-strand specimen (2 ft)	21*	N/A	Yes	605
1st 19-strand specimen (6 ft)	60*	N/A	Yes	Specimen Failed
2nd 19-strand specimen (6ft with shear flanges at center of pipe)	55*	58	Yes	770
2nd 19-strand specimen (6ft with shear flanges spread out on pipe)	50*	55	No	870

* Not a true transfer length for 70-74% of GUTS. Transfer shown is estimate based on strain readings of the sustained load after loss.

Recommendations

At project inception, FDOT specifications designated the use of shear transfer devices external to the steel post-tensioning ducts investigated in this study. Since that time, FDOT specifications have been amended and no longer qualify the shear transfer devices due to potential masking of tendon condition. The findings and recommendations from the experimental results in this study are therefore applicable to the existing structures that were built with the specifications that include steel pipes and shear transfer devices. In addition, they provide guidance on the potential failure mechanisms that may develop and therefore be visible in maintenance and inspection. The experimental results cannot therefore be used directly to evaluate existing guidelines; however, the use of PVC pipes and no shear transfer devices are discussed in the analytical modeling section (Chapter 6) based on predictive modeling.

Based on the experimental results, the recommended minimum development length for a 7- strand tendon is 38” and that for the 12-strand is 50” to prevent failure at 90% of GUTS. Given the width of existing expansion joint pier segments, it is anticipated that such a secondary anchorage mechanism could be mobilized after anchor head failure. When VSL systems with shear transfer devices (similar to the experimental set-up in this study) are used, the failure of the 7- and 12-strand secondary anchorage zone is gradual and ductile and may allow time for

inspection and repair. The shear transfer devices may play an important role in load transfer and development. Shear transfer devices may also increase stiffness of the pipe giving the grout plug a stronger support to provide the secondary anchorage. Therefore further inspection of such anchorages may be required to determine whether loss of anchorage has occurred.

To use the same development for the 19-strand tendon as those recommended in sections 5.8 and 5.9 of this report, a stronger pipe that can resist more expansive forces is required in order to allow ductile failure and time for inspection and repair. However, the 6 ft specimen length used in this study exhibited either progressive slip or significant expansive failure of the surrounding concrete and may therefore be more detectable. Per the FDOT Structures Design Guidelines (SDG) Table 4.5.6-1, the diaphragms are allowed to be 4 ft long. Based on this study, with such a dimension reduction, the recommendations for a stronger pipe may still apply to slow down and/or prevent fast and brittle failure of the 19 strand. However, based on the experimental specimens, it is not known whether 4 ft would be sufficient to allow full transfer or development.

Table of Contents

List of Figures

List of Tables

Chapter 1: Introduction

1.1 Problem Statement

Post-tensioning (PT) tendons are external in many structural systems except at the anchor piers and deviator pads. The steel tubes that house the tendons are filled with a non-shrink and non-bleed grout after the PT force is applied on the tendons. The entire duct that houses the tendon is grouted; however, the short grouted section at the deviator and pier segment may develop a bond between the tendon and the concrete block, which may provide a secondary anchorage zone when the anchorage head is lost. The purpose of this research is to determine this capacity and recommend the minimum transfer length. In addition, an objective is to properly specify the detailing required to effectively utilize this secondary anchorage in the case of anchor head failure.

The current design procedures do not take advantage of this secondary anchorage mechanism, nor explicitly account for the development length. In the Mid-Bay bridge (located over the Choctawhatchee Bay in Okaloosa County, Florida), this secondary anchorage did not sufficiently develop. Improving the quality of grout and pipe detailing had been studied by other researchers, including research sponsored by the FDOT. The research is this study focuses on recommending a reliable transfer length to provide anchorage for the post-tensioned tendons based on the grout-to-steel pipe interface and the grout-to-tendon interface, specifically assuming slip of the steel pipe with respect to concrete can be mechanically arrested.

1.2 Research Objectives

Objectives of the experimental program were (1) to determine how to promote secondary anchorage of PT tendons in span pier segments in order to maintain some effectiveness of the post-tensioning system in the event of primary anchorage failure and (2) to develop design recommendations for the transfer length. If the PT force can be developed within the pier segment, this would allow bridge owners time to determine the proper course of action, possibly including closure, maintenance, further inspection, or allowing service to continue. The experiments in this study were based on 7-, 12- and 19-strand tendons made of 0.6” diameter loss-relaxation strand. For each tendon size, multiple development lengths were considered. The

study presented in this report considered nine specimens; a 7-strand tendon with a 4ft, 2ft and 1.5ft development length, a 12-strand tendon with a 5ft, 2.5ft, and 2ft development length, and a 19-strand with a 6ft development length with three different pipe configurations for shear resistance.

1.3 Report Outline

This report presents a literature review of previous experimental work and code provisions that control the design and the calculations of the transfer length. Chapter two presents several variables that can affect the transfer length are identified along with previous studies on tendon-cementitious material interfaces. The experimental set-up and design of the test fixture and specimens are detailed in chapters 3 and 4. Testing protocols and procedures are introduced during discussion of the test set-up. Results and data analysis for all three strand configurations are presented in chapter 5. Chapter 6 presents a finite element model (FEM) that predicts the elastic behavior of the experiment and investigates the implementation of different pipe materials that conform to the new FDOT specifications. Following the FEM, standard component-level tests aimed at quantifying the pullout behavior of specimens containing 7-strand tendons are detailed in Chapter 7, along with results and recommendations for the implementation of the test. Chapter 8 presents conclusions from the existing specimen testing matrix and recommendations for design and future work that could be drawn from this project.

Chapter 2: Literature Review

2.1 Introduction

Unlike prestressed concrete members without anchorage, the stress in the tendon of post-tensioned members achieves the prestress at the anchorage block. Therefore, there are no codes that specify requirements of transmission length or development length in post-tensioned members because the case of anchor head failure is never taken into consideration. In this chapter a brief review on bond mechanism, transfer length, development length, and factors affecting them is presented.

2.2 Definitions

2.2.1 Transfer Length or Transmission Length

In prestressed members, the prestress force in the tendons is transferred into the concrete by bond. The length that is required to develop this bond is called the transfer length or transmission length. It can also be defined as the length required to fully develop the effective prestress f_{se}.

2.2.2 Development Length

Development length is the length that is required to develop the force, f_{ps}, which is the stress in the strands caused by the application of the ultimate design loads. Figure 3 shows the ideal stress distribution for an underdeveloped strand (PCI, 1978) and the difference between the transfer length and development length.

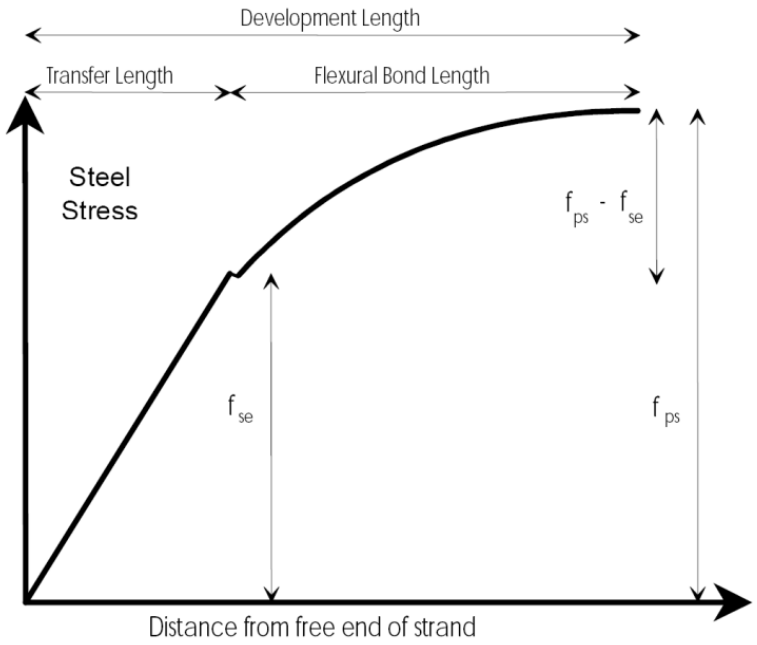

Figure 3. Stress Distribution in a Strand (PCI, 1978)

2.2.3 Flexural Bond Length

The flexural bond length is defined as the length of the bond required to develop the stress in the strand from f_{se} to f_{ps}. In other words, it is the difference between the development length and transfer length.

2.2.4 Embedment Length

This is defined as the length of the bond from beginning of the bond, where de-bonding starts and the bond stresses are negligible, to the critical section.

2.2.5 Hoyer Effect

After stressing the tendon, the diameter decreases from the original value according to Poisson's ratio. When de-stressed, the tendon regains its original diameter at the ends outside the concrete or grout, and it tapers from its original value to a reduced value at the transmission length, which creates a wedge effect. This helps in the transfer of prestress from the tendon to the

concrete. As the tendons are de-stressed, radial compressive forces are generated on the surrounding concrete. This is idealized in Figure 4. This is known as the Hoyer Effect (Hoyer & Friedrich, 1939).

In post-tensioned members where larger numbers of tendons are run through ducts, the compressive force magnitudes can get very large increasing the magnitude of friction significantly. The Hoyer Effect plays the most critical role in the secondary anchorage for the tendons in case of anchor head failure.

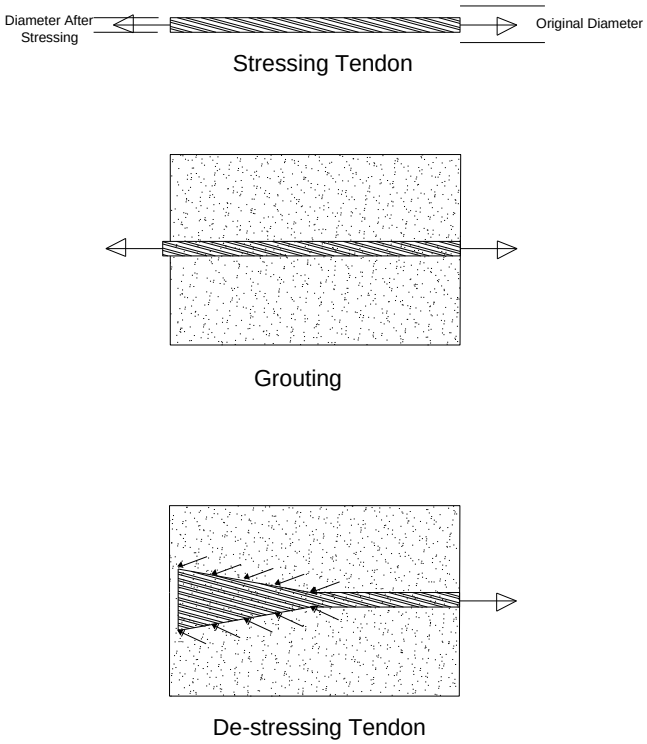

Figure 4. Hoyer Effect

2.3 Stress Transfer Mechanism in Post-Tensioned Members

In post-tensioned members, where the transmission is primarily through external anchorages, high compressive stresses are generated just behind the anchorages, and after small distances, tension stresses are developed in a direction normal to the direction of the compression stresses. The tensile forces within the anchor zone are called splitting forces. Spalling forces (also tensile) similarly develop in the zones away from anchorage zones along the transmission

length of the tendon. The stress field, especially in the end zones, therefore, gets complicated and the need for special design of transverse reinforcement is required. Since the objective of this research is not the transmission of prestress though external anchorages but rather through transmission and development length after anchor head failure, this mechanism will not be detailed any further.

When considering the secondary anchorage provided by the grout and concrete in case of anchor head failure in post-tensioned systems, the transmission length and development length mechanisms of the tendons are similar to prestressed members. Differences between the two mechanisms arise from the factors affecting the transmission length, such as the confinement of the tendons.

2.4 Stress Transfer in Prestressed Members

2.4.1 Bond Mechanisms

For a prestressed member with no anchorage devices, the bond between the concrete and the tendons transmits the prestress. This bond is achieved by three mechanisms:

1. Adhesion between the tendons and concrete: The effect of adhesion is considered very small and is often neglected. Note that when slip occurs between the concrete and the tendons, adhesion does not exist anymore in the bond mechanism.
2. Mechanical bond or bearing at the steel/concrete interface: Because of the helical shape of the strands, a mechanical interlock mechanism exists due to the normal forces between the strand and the concrete/grout.
3. Friction which increases with the increase of transverse compression: The Hoyer Effect, therefore, plays the most important role in affecting this bond mechanism.

2.4.2 Transfer and Bond Stresses

The prestress is transferred over a certain length called the transmission length or transfer length (L_t). After de-stressing, the stress in the tendon is zero at the ends. It increases over the transfer length to reach the effective prestress magnitude (f_{se}) under service loads and remains

practically constant beyond it. Figure 5 shows the variation of the prestress in the tendon. It can be seen that the bond length is marginally smaller than the transmission length (Rajagopalan, 2002). In the transfer zone where the stresses in steel are increasing from zero to the effective prestress, f_{se}, strong enough bond stresses between the concrete and the steel must exist to develop this effective prestress.

The bond stresses, as seen in Figure 5, are assumed to be parabolic, with the maximum value near the free end (Rajagopalan, 2002). It is assumed that the bond stress is directly proportional to the slope of the stress in the anchorage zone (Marshall, 1966).

The strain compatibility between the grout/concrete and strands is not achieved until after the transfer zone. Friction and wedge forces, governed by the Hoyer Effect, anchor the strand near the beam ends. Proceeding down the transfer zone away from the ends into the concrete, the Hoyer Effect is reduced. The mechanical bond in this area starts to play a more important role because the Hoyer Effect anchoring the tendon behind this area prevents the tendons from twisting. Further away the mechanical bond becomes fully accountable for the entire transfer bond.

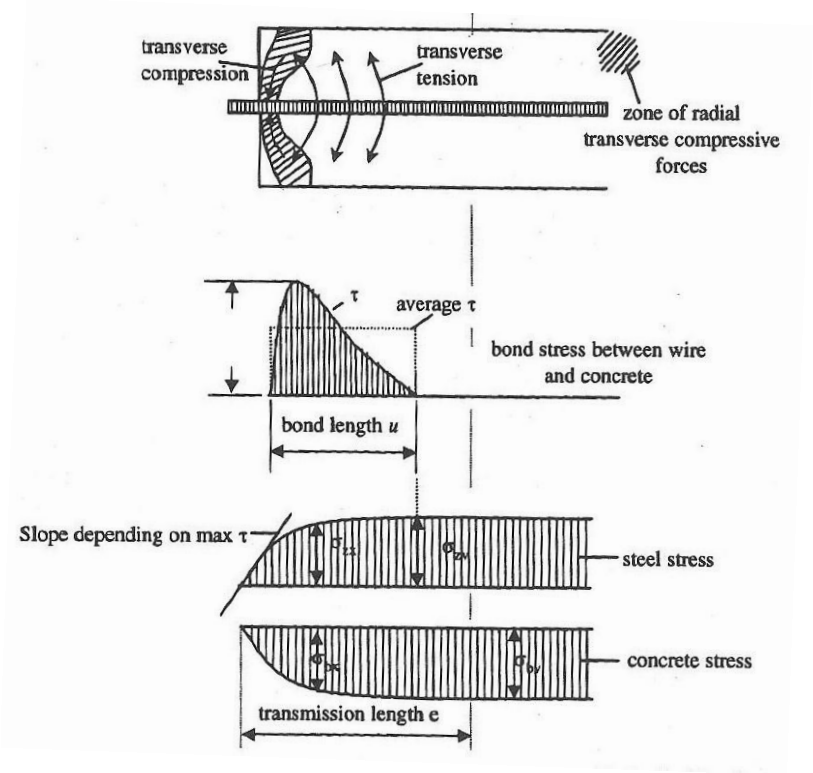

Figure 5. Bond Stress Distribution in a Prestressed Beam without Anchorage (Rajagopalan, 2002)

2.4.3 Bond Failure

It was suggested by Janney (1954) that in prestressed beams if a wave of high flexural bond stresses reaches the transfer zone, bond failure will occur. Flexural bond stresses are the stresses required to develop the increased tensile forces in the strands due to the applied load. After cracking, the concrete has no tensile resistance therefore increasing the strand stresses. To resist this wave of increased tensile stresses, high bond strength is required. If the bond stresses were not able to resist the increased tensile stresses, slip will occur to relieve these stresses. It was also suggested by Janney (1954) that this increase in tension in the strand results in reduction of Hoyer Effect. Therefore, twisting of the tendon might occur affecting the mechanical bond. A sudden failure could therefore occur.

Russel and Burns (1993) suggested that anchorage failure also occurs when web-shear cracks, which develop mainly in the transfer zone at the ends of the beams, propagate to the level of the strand. The ultimate failure mechanism in this case is the same as flexural cracking in the transfer zone discussed in the previous paragraph.

Therefore, bond failure can occur due to the increase in the tensile forces in the strand at the anchorage.

2.5 Factors Affecting Transfer Length

Some of the factors that affect the bond length and transfer length are the shape, surface characteristics, and ductility of steel in addition to the strength of concrete and the magnitude of prestress. A combination of certain characteristics such as strength of concrete, surface friction and ductility of steel, and applied prestressing force leads to the Hoyer Effect. Other factors include cover and spacing of strands, confinement, and method of release.

2.5.1 Strand Diameter

Research has shown that strand diameter is the key parameter in transfer length as the strand transfers the prestressing force to the concrete over its surface area. Therefore, larger diameters will allow more force to be transferred per unit length of the strand. ACI and AASHTO LRFD code specifications use the following equations to estimate the transfer length:

1/3 $f_{se}d_b$, *50*d_b, and 60d_b, where d_b is the nominal diameter of the strand (ACI is the American Concrete Institute, and AASHTO is the American Association of State Highway and Transportation Officials). As seen from these equations the stress transfer is directly proportional to the strand diameter. However, according to Russel et. al. (1996), beyond a certain diameter, this linear relationship no longer applies based on several experimental results.

2.5.2 Strand Surface Condition

The effect of strand surface condition on the transfer length is also very important and has been thoroughly researched. Research programs investigating the effects of strand surface conditions were performed since the early 1950s (Janney, 1954). According to the research, lubricated and clean wires required longer transfer lengths over the rusted wires which had the best performance in transfering the prestress force. This could be obvious because friction plays the most important role as compared to the other two bond mechanisms. Increasing the coefficient of friction would alternatively increase the friction and therefore improve the bond stresses leading to a shorter transfer length. In 1990 further research was performed on epoxy covered strands (Cousins et. al., 1990). The research proved that epoxy coated strands required shorter transfer length to develop the prestress than the uncoated strand.

2.5.3 Method of Release

Prestressing and Post-tensioning applications have two main methods for releasing the tendon or de-stressing. The first is the sudden release method which involves flame cutting the tensioned strand. Cutting the strands causes the tensioned strands to abruptly and suddenly release large magnitudes of force into the member. The second method is the gradual release. In this method, detensioning of the strand is done using hydraulic jacks for slower and gradual release for the forces into the system. Sudden abrupt release of the tendons can cause eccentric loading and it was proved that gradual release will actually result in shorter transfer lengths than the sudden release method (Russel and Burns, 1997).

2.6 Other Related Research

2.6.1 Diephuis, Xia, VSL and FDOT on Pipe Slippage

The tendency of shear-slip failure occurring between concrete and the rigid steel piping typically used in segmental bridge pier diaphragms and deviator sections has been explored experimentally. Diephuis (2004) reported the findings of an experimental study on the factors affecting bond of multi-strand PT tendons used in segmental bridge construction. Four different bond lengths and tendon curvatures were considered along with different duct materials, i.e., rigid steel pipe, high-density polyethylene (HDPE) corrugated duct, and galvanized steel corrugated duct. Specimens with short duct length incorporating rigid steel pipe ducts failed in shear slip occurring between the duct and the surrounding concrete. It was recommended that anchorage be provided to prevent shear slippage of smooth steel ducts from concrete.

The FDOT and VSL Structural investigated the use of three different types of shear transfer devices to prevent pipe slippage (Xia 2004). The first of such devices, proposed by VSL, was a single 6.4 mm weld bead around the circumference of the embedded steel PT duct. The second, proposed by the FDOT, employed five 0.5 inch thick circular steel discs or "shear flanges" welded to the steel duct. The third device was similar to the first but employed up to 5 welded beads. All devices were tested by performing a simulated anchorage failure and pullout tests with VSL ECI6-19 bearing plates, 0.6 inch diameter grade 270 ksi strand, and 19-strand tendons. Tests indicated that shear slippage was significantly reduced or completely prevented using devices 1 (shear flanges) and 3 (multiple welded beads).

2.6.2 Construction Technology Laboratories Bonded and Un-bonded Post-Tensioned Systems

In 1984, a major study by Construction Technology Laboratories (Sowlat et. al., 1984) on post-tensioning systems included a similar system to the one under investigation in this study. The CTL studies compared the behavior of external post-tensioning systems that are partially bonded to completely bonded systems. In addition, the results were compared with theoretical analyses, and it was discovered that the measured flexural strengths exceeded the calculated strengths by 15% to 24%. The experimental tests included three types. The first type was

bonded-tendon girders that were post-tensioned with internal tendons. The second type was the un-bonded girder that had un-bonded tendons and was post-tensioned with external tendons. The third type was the modified un-bonded tendon girder, which was similar to the second girder type, except that a secondary concrete cast was placed on the bottom of the flange after post-tensioning. The tendon ducts were grouted after post-tensioning for all three types. At the end of the loading cycles, the wedges of the two top strands were burned off, and strains measured on these strands indicated loss of prestress in the pier segments and draped portions of the three types. Releasing the anchor wedges in the un-bonded girders affected the behavior of these girders. However, the measured strengths were higher than the calculated values based on total bond loss of the two top strands. Partial loss of prestress in two top strands led to compression failure in the top flange at the joint (Sowlat et. al., 1984).

2.6.3 Theoretical Approach for Transfer Lengths

An analytical study of the transfer length was conducted to predict the transfer lengths of prestressed concrete members (Oh et al. 2006). They considered the radial expansion of prestressing steel due to prestress load transfer that causes cracking of the surrounding concrete in the radial direction depending upon the magnitude of stress. The study took into account the effects of partial and full cracking due to expansive pressure in constructing the governing equations. The reduction of the elastic modulus and tensile strength of damaged concrete due to cracking was taken care of by employing a tensile stress-crack width relation. Using equilibrium and compatibility equations, the strain development curves from the ends of pretensioned concrete members were generated. Various variables, including concrete strength, strand diameter, cover and thickness and strand spacing were considered by conducting comprehensive tests (Oh et. al., 2006). The comparison of the theoretical results with the present test data showed good agreement.

2.7 Transfer and Development Length Equations

AASHTO LRFD and ACI 318 development length equations are very simple and nearly identical. The following are the AASHTO code provisions:

9.28.1 Three- or seven-wire pretensioning strand shall be bonded beyond the critical section for a development length, in inches, not less than

$$(f_{ps} - 2/3\ f_{se})D$$

Where D is the strand diameter in inches and f_{ps} and f_{se} are expressed in kips per square inches.

9.28.2 Investigation may be limited to cross sections nearest each end of the member that are required to develop their full ultimate capacity.

1/3 f_{se} D accounts for the transfer length portion of the development length.

AASHTO section 9.20.4 and ACI 318 section 11.4.4 assume a transfer length of 50 strand diameters to calculate the resistance to web-shear cracking of the concrete. This is a simplified equation of the transfer length portion of the development length.

Table 2 lists some suggested equations for the development and transfer lengths in prestressed members.

Table 2. Different Suggested Equations for Transfer and Development Length

Transfer Length Equation	**Development Length Equation**	**Author (Year Published)**
$L_t = \frac{f_{se}}{3} d_b$ $L_t = 50\ d_b$	$L_d = L_t + (f_{ps} - f_{se}) d_b$	AASHTO / ACI 318 (1963)
$L_t = 80\ d_b$	$f_{ps} \le \frac{L_e}{80\ d_b}\left(\frac{135}{d_b} + 31\right) \qquad L_e \le 80 d_b$ $f_{ps} \le \frac{135}{d_b^{1/6}} + 0.39\ L_e \qquad L_e > 80 d_b$	Martin & Scott (1976)
$L_t = \frac{f_{se}}{2} d_b$	$M_{cr} > L_t\ V_u \qquad Fully\ Bonded$ $\frac{L_b + L_t}{Span} \le \frac{1}{2}\left[1 - \sqrt{1 - \frac{M_{cr}}{M_u}}\right] \qquad Debonded$	Russel & Burns (1993)
$L_t = \frac{f_{si} d_b}{3}\sqrt{\frac{3}{f_{ci}'}}$	$L_d = L_t + (f_{ps} - f_{se})\ d_b \sqrt{\frac{4.5}{f_c'}}$	Mitchell, Cook, Khan, & Tham (1993)
$L_t = \frac{f_{se}}{3} D$	$L_d = L_t + \frac{3}{2}(f_{ps} - f_{se}) d_b$	(Buckner, 1994)

Chapter 3: Specimen Design and Details

Specimens were designed to simulate the expansion joint pier segment in segmental externally post-tensioned bridge structures. General specimen details can be found in Table 3. All specimens, except the second and third 19-strand specimens, incorporated anchorage components produced by VSL; ECI 6-7, 6-12, and 6-19 dead-end anchorage bearing plates were use for 7-strand, 12-strand, and 1st 19-strand specimens respectively. Schedule 40 galvanized steel pipes were used within the specimen blocks as would be found in the field. Figure 6 provides a general schematic of the main components incorporated in the first 7 and 12 strand specimens and all 3 19-strand specimen blocks. The 7 and 12 strand specimens were designed with different development lengths and different shear flange locations. To accommodate the shorter development length design in the 2nd and 3rd 7- and 12-strand specimens, a hollow section in the concrete block was introduced to allow the grout termination in the pipe at each corresponding development length. A general Schematic for this design is show in Figure 7.

Table 3. Specimen Block Details

Specimen	Height (ft)	Width (ft)	Length (ft)	Pipe Diameter (in)	DSI Post-tensioning Force per Bar (kip)	No. of Shear Flanges
7-Strand	2	6.5	4	2.5	20	3
12-Strand	2	7	5	3	30	4
19-Strand	2	7	6	3.5	40	5

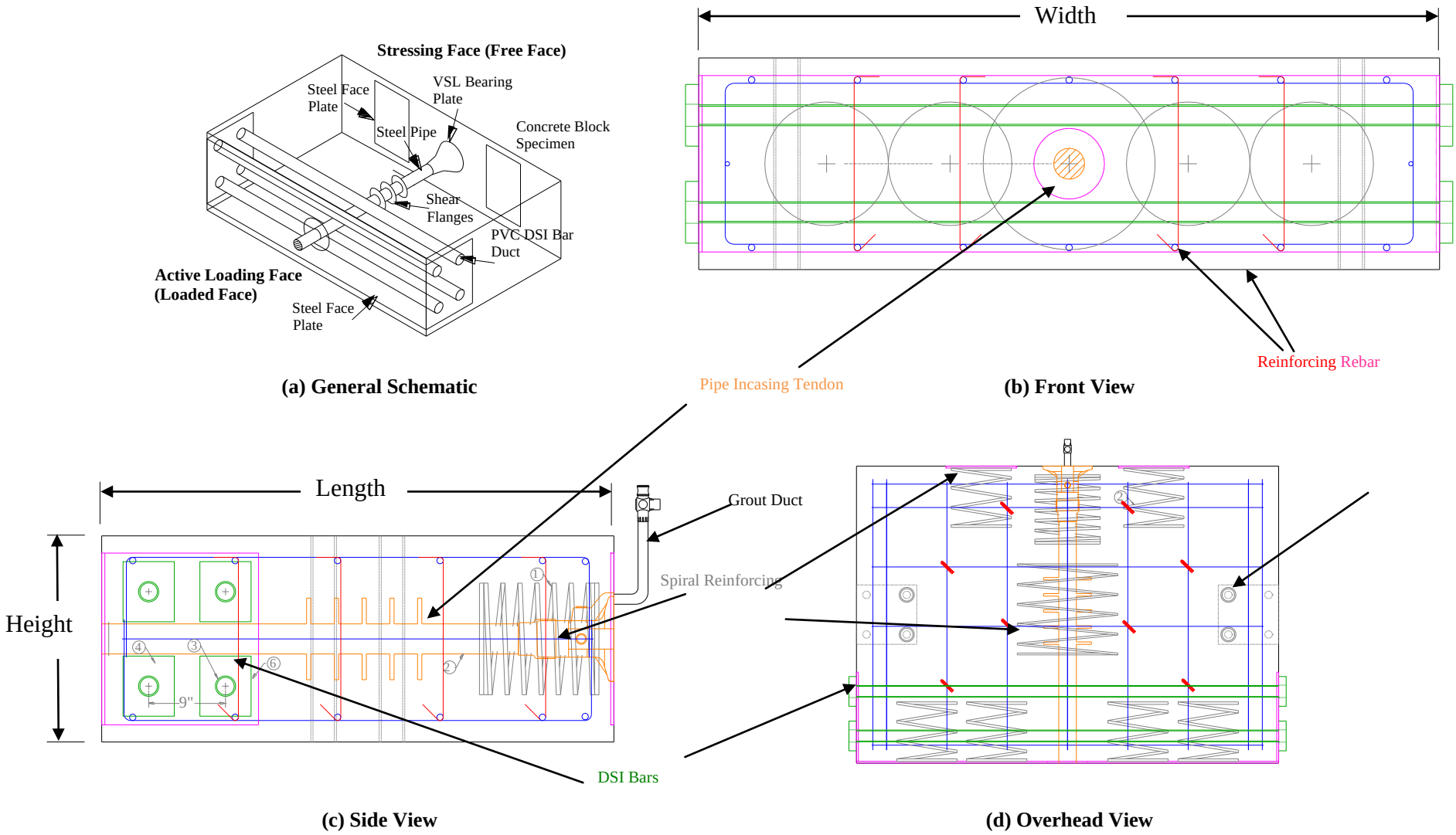

Figure 6. General Specimen Details – Without Hollow Section

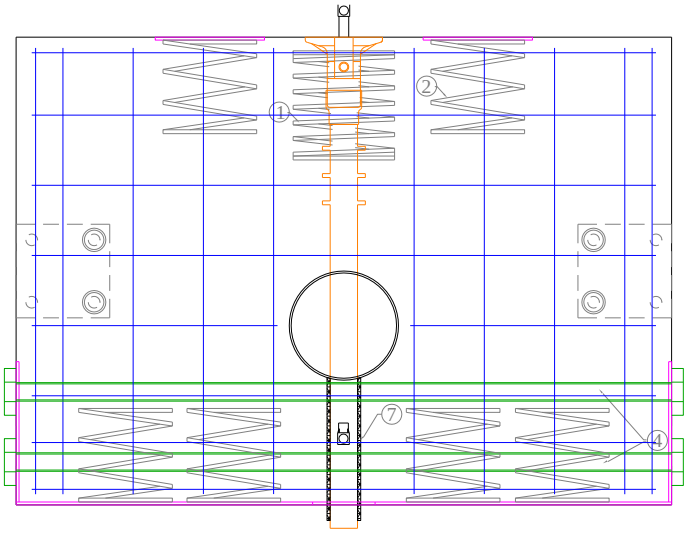

(a) Overhead View

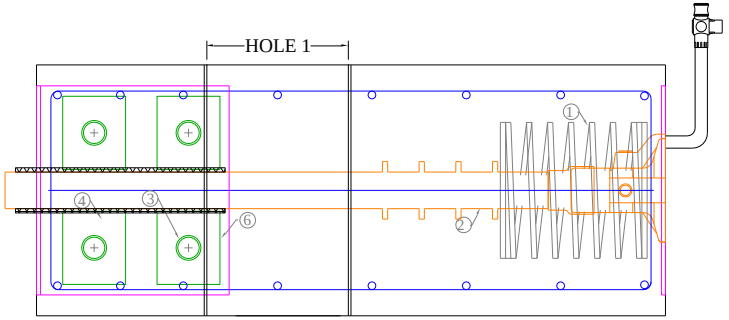

(c) Side View

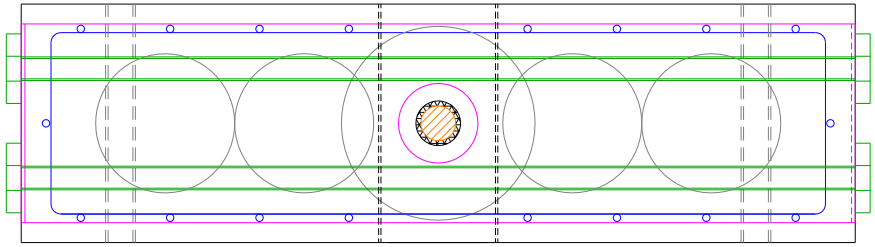

(c) Side View

Figure 7. General Specimen Details - With Concrete Hollow Section to Accommodate Shorter Development Length

To prevent shear slippage between the steel pipe and surrounding concrete, shear flanges similar to those described by Xia (2004) were used. Flanges protruded approximately 1" from the steel pipe. Flange locations for the first set of specimens can be seen in Figure 8 and those for the 2nd and 3rd sets for the 7, 12, and 19-strand specimens are shown in Figure 9. Specimens were reinforced longitudinally and transversely with conventional grade 60ksi mild steel rebars. Reinforcement details can be found in Figure 6. In order to prevent cracking during active loading procedures, specimens were also reinforced with 4 DSI 1.25" diameter thread bars (A DSI bar is a Dywidag-Systems International product). Prior to any loading, the DSI bars were prestressed and locked off. The DSI bars were inserted through PVC ducts, that were cast into the specimens, and were anchored to the side faces of the specimen block using steel bearing plates and lock-off nuts.

Foil-backed resistive strain gage biaxial rosettes were installed at various lengths along the steel pipe and at two different locations around the pipe's circumference. Details of gage locations can be found in Figure 8 and Figure 9. At each strain gage location on the pipe two strain gages were installed, one at 0˚ and the other at 120˚.

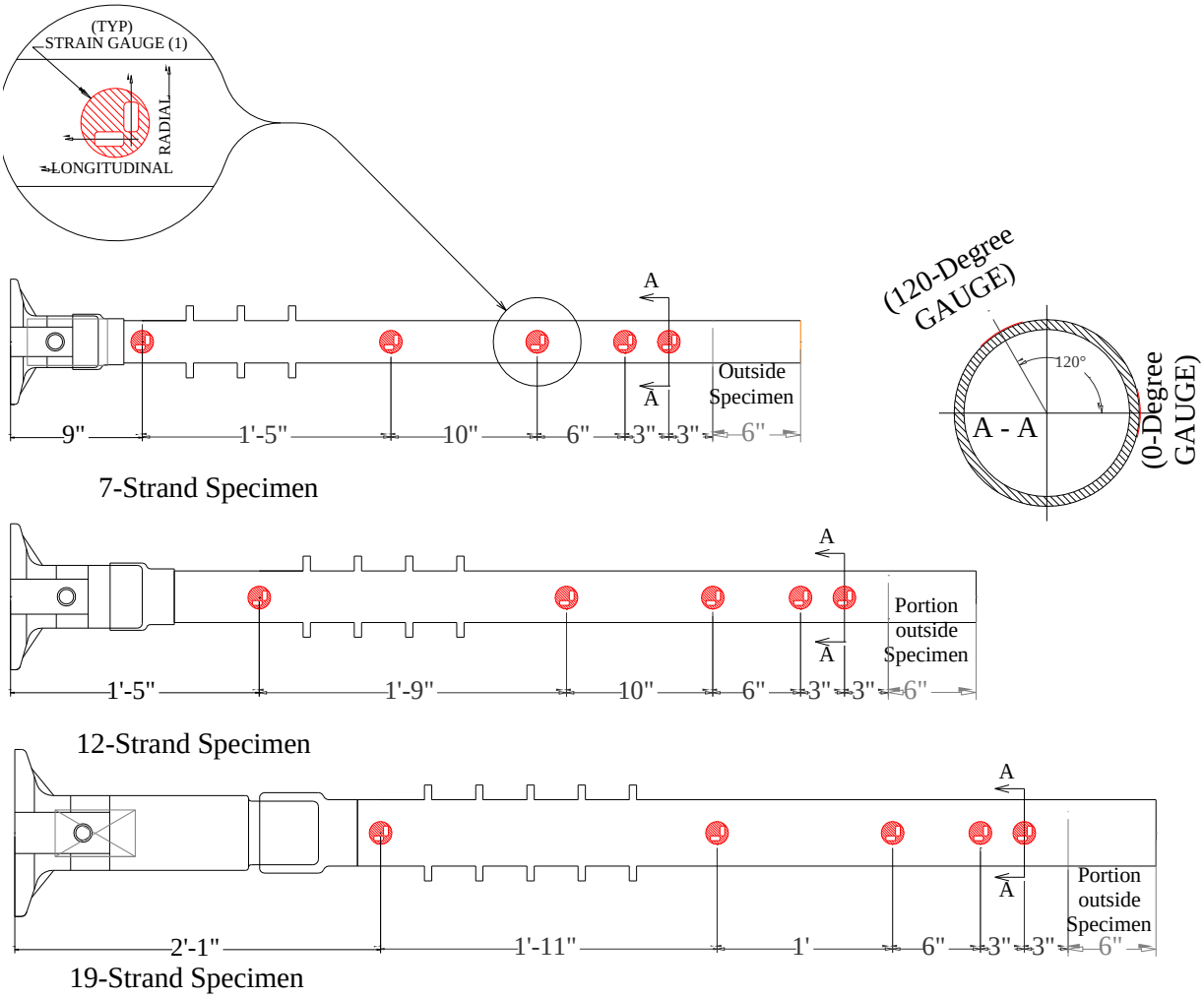

Figure 8. First Set of Specimens - Pipe Details

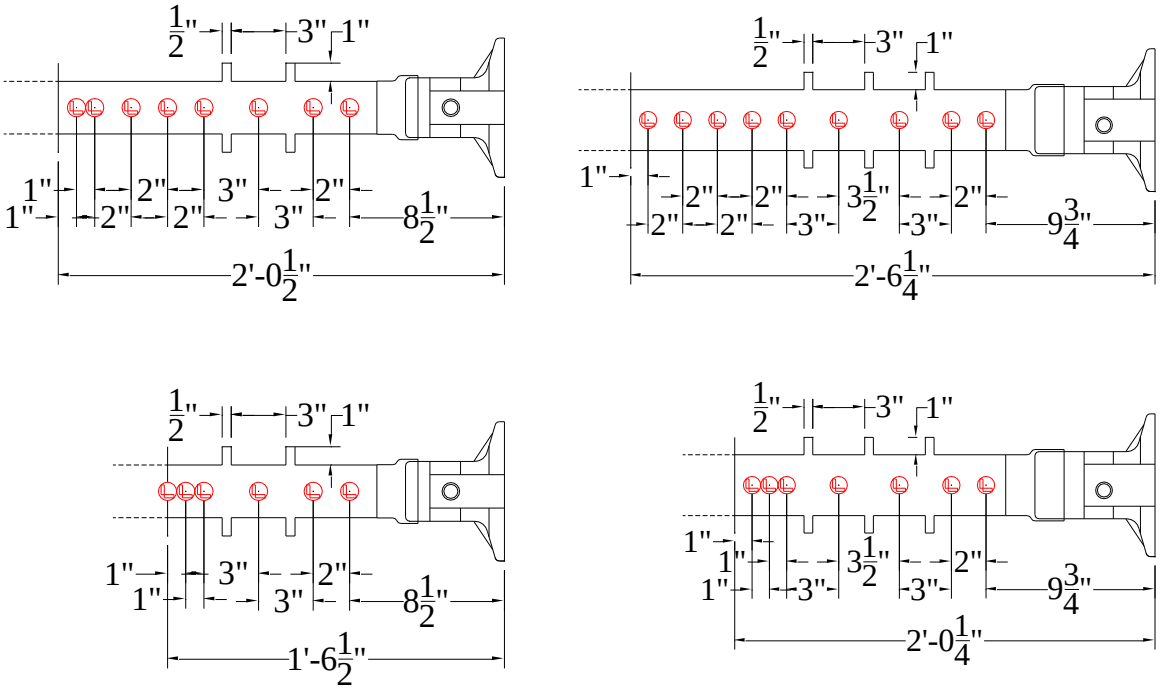

(a) 7-Strand **(b) 12-Strand**

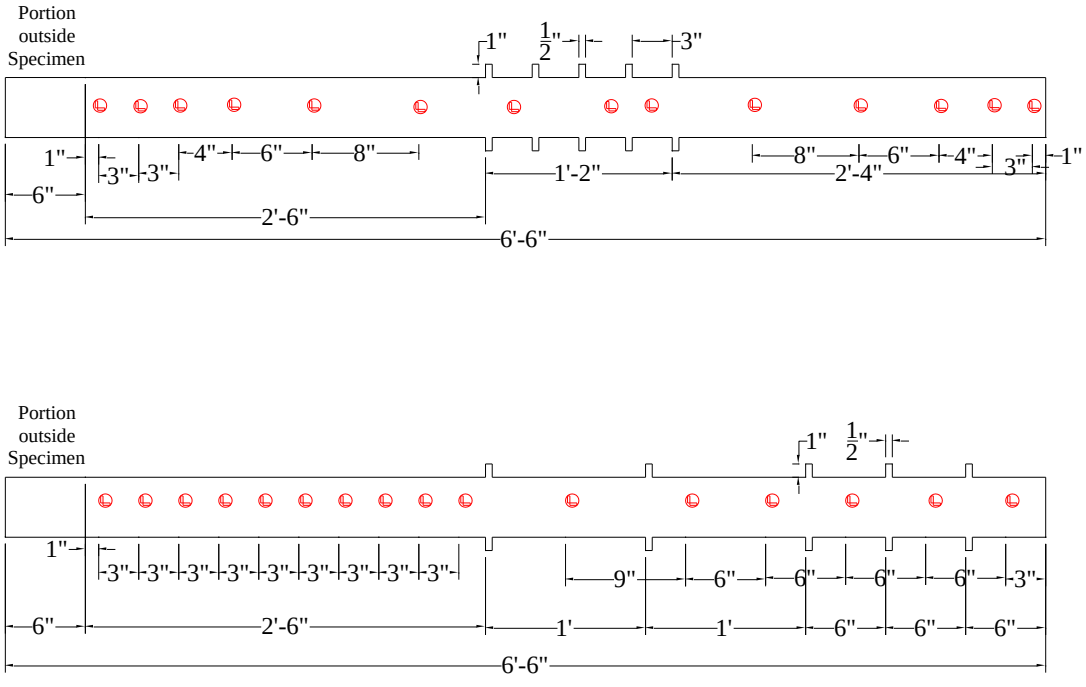

(c) 19-Strand

Figure 9. Second and Third Set of Specimens - Pipe Details

The specimen blocks were cast using 5 ksi Portland cement concrete at the FDOT Structures Research Center in Tallahassee, FL. Figure 10 shows formwork, reinforcement cages, PVC pipes, and the hollow section in the middle of the concrete block that allowed a shorter bond length in-place prior to casting the concrete.

(a) Specimen Formwork Before Casting

(b) Shear Flange Detailing

(c) DSI Bar and Tie-Down Piping

(d) Hollow section for shorter bond length - 2nd and 3rd 7 and 12 strand specimen

Figure 10. First Set of Specimen Blocks Prior to Casting

Chapter 4: Experimental Design & Set-up

4.1 Testing Reaction Fixtures

Two specially designed reaction fixtures were used to restrain specimens during strand stressing, de-stressing, and active loading. The first reaction fixture was a 55ft sliding reaction frame composed of 2 W36x150 sections welded continuously along the flanges. This frame can be seen in Figure 11-b and -c. A long frame length was used to minimize prestress losses due to wedge seating and strand relaxation. This frame also provided an enclosed space to house the tendons during testing. The sliding reaction frame was mounted between 3 sets of rollers to allow for longitudinal translation during stressing but prevent out of plane translation. The second reaction frame, entitled the dead-end reaction frame, was used to anchor the tendons on the opposite side of the specimen (Figure 11-a). This frame would be allowed to slide during active loading to apply increased load to the tendon grouted within the specimen block.

(a) Dead-end Reaction Frame **(b) Sliding Fixture – Anchor End** **(c) Sliding Fixture – Jacking End**

Figure 11. Reaction Fixtures

4.2 Experimental Set-up

The configuration of the specimen and reaction fixtures used during all portions of the large-scale experimental investigation can be found in Figure 12. Both reaction fixtures were secured from translating out of axis by tie-down beams (Figure 13-a and -c). Both hydraulic jack locations i.e. stressing and active loading, can been identified. The jacks can be seen in Figure 13-b in the stressing position. The specimen block was mounted on three grout pads cast on the strong floor and was tied down to the strong floor using four 100kip capacity threaded rods.

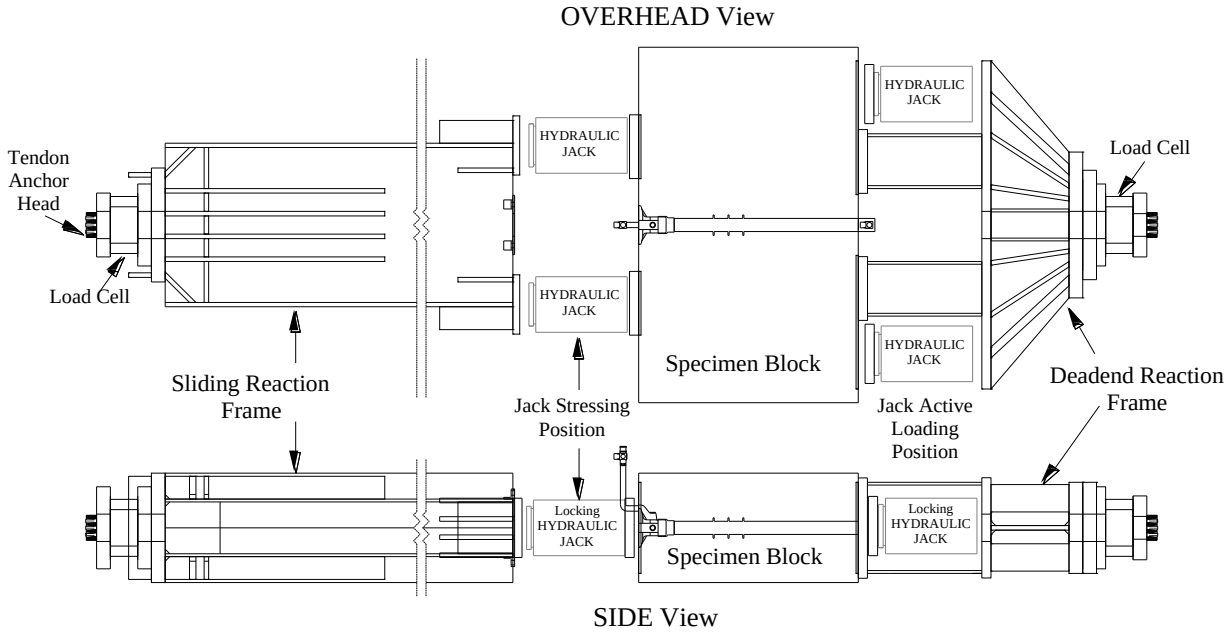

Figure 12. Experimental set-up

(a) Sliding reaction frame

(b) Stressing Jacks

(c) Dead-end reaction fixture

Figure 13. Test set-up photos

4.3 Instrumentation

Instrumentation was installed on the test fixtures and the specimen block. Test fixtures were monitored to ensure proper functionality and safety during testing. Specimens were instrumented for test measurement (such as pipe slip), safety, and control during the testing procedures. The following section describes the various types of instrumentation utilized for test fixtures and specimen blocks.

4.3.1 Test Fixtures

There were three main sets of instrumentation employed on the test fixture; Load cells at anchor point, sliding fixture instrumentation, and dead-end fixture instrumentation. Both the sliding and dead-end fixtures were instrumented for strain and displacement measures critical locations.

Two Geokon 3000 Series 1,500 kip hollow-core load cells were used to measure the applied load at the anchor points of the multi-strand tendons. As recommended by the manufacturer, 3” thick bearing plates were used on either side of the cells to minimized error due to eccentric loading. The load cells and respective locations can be seen in Figure 14.

Figure 15 depicts a schematic of the instrumentation used to monitor the sliding reaction fixture during testing. Longitudinal displacement measurements were also taken at both the sliding and dead-end fixtures.

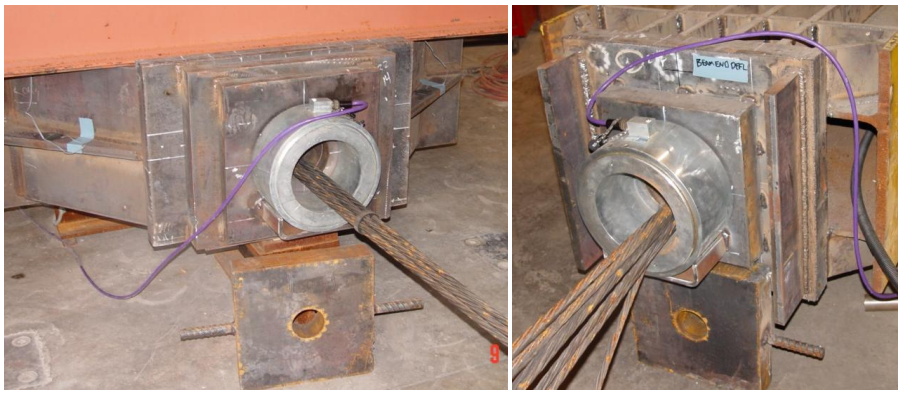

(a) Dead-end Fixture Location **(b) Sliding Fixture Location**

Figure 14. Load Cell Locations

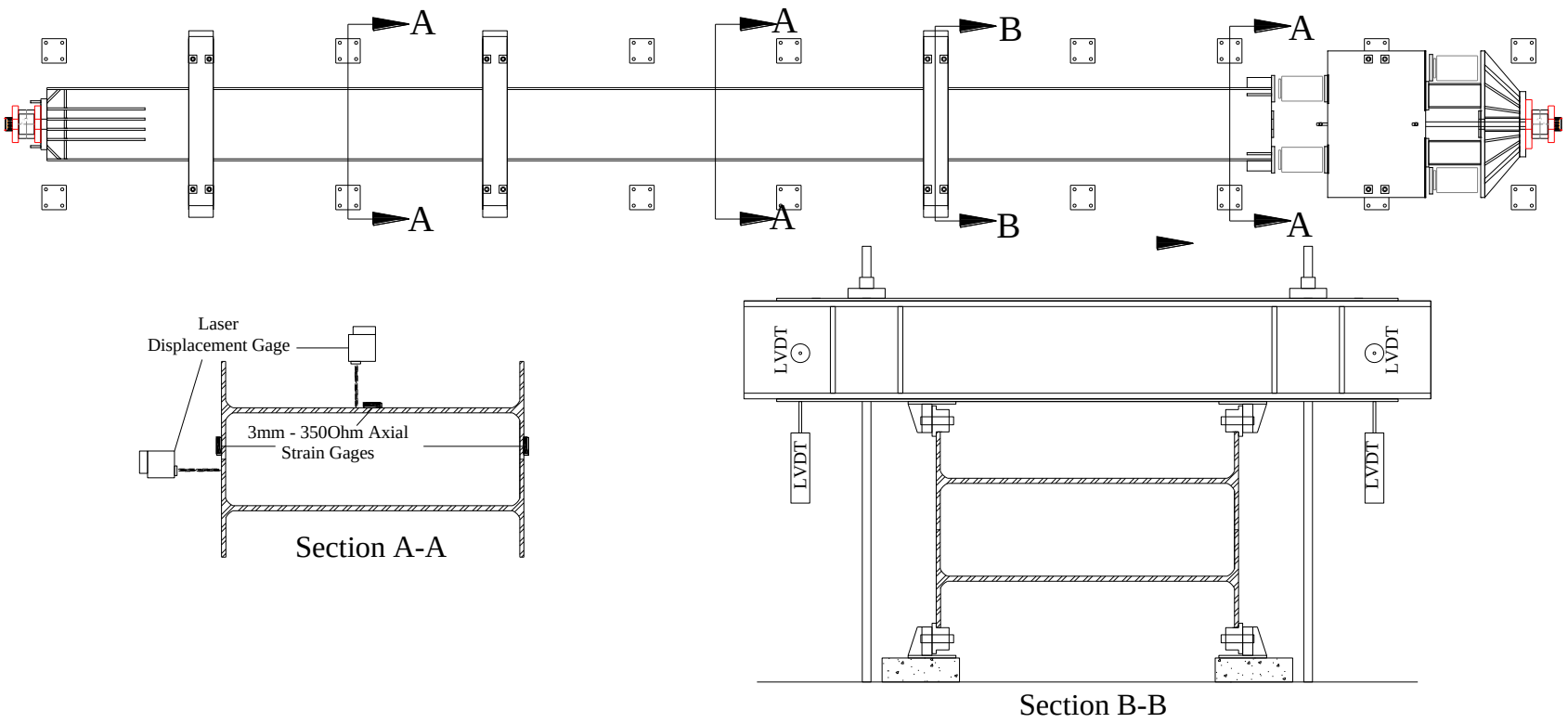

Figure 15. Sliding Fixture Tie-downs and Instrumentation

4.3.2 Specimen Block

The instrumentation utilized on the exterior portion of the specimen block can be found in Figure 16. Two string POT linear displacement transducers were mounted on the stressing face of the specimen block in order to measure hydraulic jack piston extension during the stressing procedure (Figure 16-b). Two LVDT displacement transducers were also placed on the stressing face. These sensors were offset approximately 3ft from the centerline of the specimen to measure rotation during loading procedures (Figure 16-a). Lastly, an LVDT was mounted against an L-bracket attached to the portion of pipe that protruded from the active loading face of the specimen block (Figure 16-c). This sensor was only utilized during de-stressing and active loading procedures to measure the slip between the steel pipe and surrounding concrete.

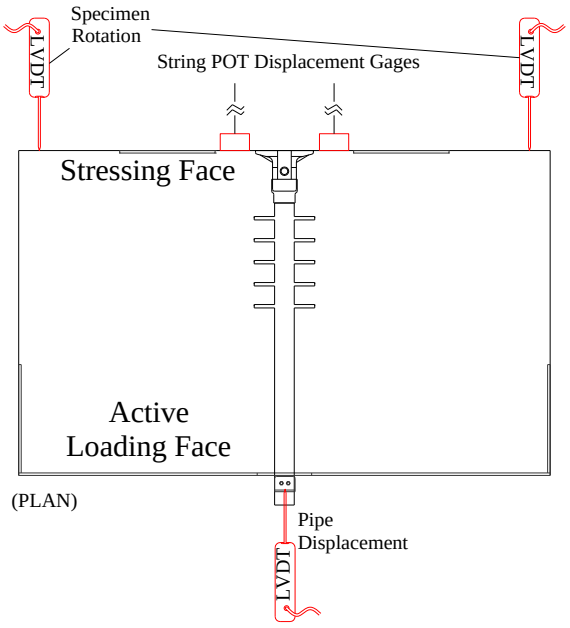

(a) External Specimen Instrumentation Plan

(b) String Gages

(c) Pipe LVDT

Figure 16. Specimen Instrumentation Details

4.4 Loading Procedures

Two 600kip Enerpac CLL series hydraulic jacks (Figure 17) with lock nut cylinders, located between the sliding frame and specimen, were used for all major loading procedures. A manual flow value coupler (Figure 18) was used to operate the two jacks simultaneously during stressing. Since the Enerpac CLL series jacks only had single action hydraulic flow, the value coupler was also used during the de-stressing procedure to control the rate of return.

Figure 17. Enerpac Jacks

Figure 18. Enerpac Flow Coupler

4.4.1 Tendon Stressing Procedure

Prior to applying the full PT force to the tendons, each individual strand was tensioned with a mono-strand jack with a force of 1.5kip to relieve excess slack within the sliding frame. The stressing procedure took place over a period of approximately 15min for both the 7- and 12-strand specimens. Tendons were tensioned between 70% and 75% of the guaranteed ultimate tensile strength (GUTS). Once the dead-end reaction frame load cell reached approximately 70% GUTS, stressing was considered to be complete and the lock off nuts on the hydraulic jacks were screwed into the locking position.

After completing the stressing procedure, locations where the tendon exited the specimen block were blocked with rigid-cure expanding foam to prevent leakage during the grouting procedure. Specimens were then allowed to remain undisturbed for a 24-hour period to allow for stand relaxation and a full cure of the foam. After 24 hours, the grouting procedure commenced. The grout selected for both specimens was SikaGrout 300PT which is a sand-free, high-flow, non-bleed, cementitious grout typically used in post-tensioned segmental construction. Grout was proportioned and mixed according to manufacturer specifications. Grouting of specimen pipes was completed using a manual grout pump. Once completed, the grout within the specimen block was allowed to cure for 6 days prior to the de-stressing procedure. During the 6-day curing period continuous load, displacement, and strain measurements were taken once a minute.

4.5 De-stressing Procedure

After the 6-day grout curing period, the lock rings on the hydraulic jacks were released. Since the loading jacks only operated with one-way flow action, a specialized flow value device was used to control piston retraction. Piston retraction or “de-stressing” took place over a period of approximately 10 minutes for each specimen. The data acquisition sampling frequency was set at 10 Hz. Full de-stress was taken to be the instance when the load cell at the far end of the sliding reaction frame read approximately zero load. Once full de-stress was reached, specimens were allowed to sit undisturbed for 24 hours prior to active loading.

4.6 Active Loading Procedure

If tendon pullout or a significant amount of slippage was not observed during or after de-stressing, additional load was applied until tendon pullout or a load of approximately 90% of GUTS was reached. Load was applied using the same hydraulic jacks used for application of the initial PT force. However, for active loading the jacks were re-positioned between the specimen block and the dead-end reaction frame. The active loading procedure took place over a period of 10 minutes for both specimens. If 90% of GUTS was reached the load was held for 15 minutes. During the active loading procedure data was acquired at a rate of 1kHz.

Chapter 5: Test Observations, Results, and Discussion

The following section presents the observations and measurement results taken during experimental testing. Tests for each specimen type are described separately. For each specimen, a complete account of the observations prior to all loading procedures, observations taken during loading, numerical results from tests, and post-test inspection are presented.

For an ideal experiment that produces results as predictable by theoretical approaches, the following trends are true for the strains in the pipe. During stressing, small compressive strains will develop in the axial gages, while the circumferential gages remain constant except for small confining strain induced in the region of the DSI bars. During de-stressing, compressive axial strains will develop at the free face and would decrease to reach zero at the end of the transfer length. Also tensile circumferential strains will develop in the transfer length region with the highest strains closest to the free face decreasing to zero at the end of the transfer region. Ideally, no strains, axial or circumferential, should develop after the transfer length close to the active loading end. During active loading, tensile strains are expected to develop within the region of the transfer length on the active loading face and decrease to zero at the end of it. Compression strains in the circumferential direction are also expected in the same region due to the reduction in strand diameter.

5.1 First 7-strand Tendon Specimen (4 ft Bond Length)

5.1.1 Test Details

During preparation for stressing of the 7-strand specimen, it was noticed that the dead-end reaction fixture did not sit plumb against the specimen block. Prior to proceeding with tendon stressing, it was decided to pour hydrostone gypsum cement between the specimen block and reaction fixture to ensure a flush bearing surface. This can be seen in Figure 19.

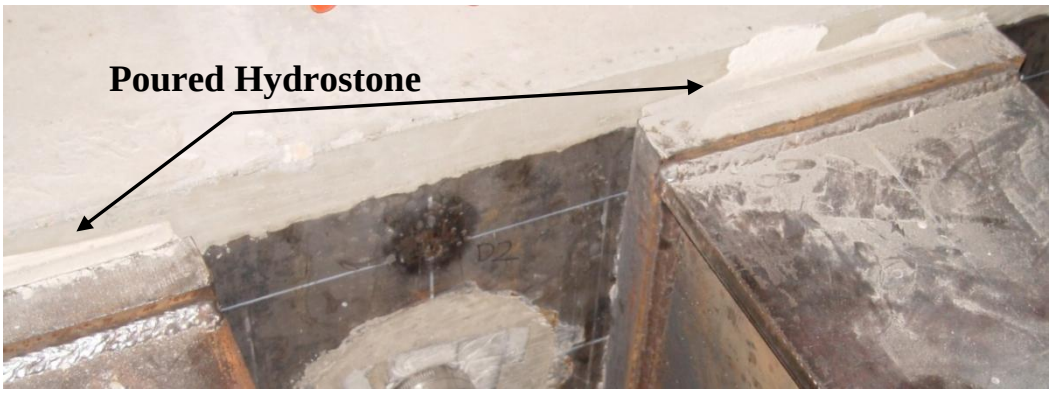

Figure 19. Hydrostone Joint

The 7-strand specimen was stressed on 11/12/2009. During the stressing procedure, it was observed that the sliding fixture tie-down located closest to the specimen block was deflecting significantly (approximately 1") in the sliding direction. Although, as stressing continued, the tie-down abruptly relocated to its original location. Furthermore, it was observed that as the stressing load increased, a discrepancy between load cells began to develop. At the point of jack lock-off, the load discrepancy was approximately 50kip.

Specimen grouting proceeded the following day (11/13/2009). The specimen block and test fixture were monitored overnight. There were no significant problems observed during the grouting procedure. Moreover, little to no grout leakage/wicking was observed. De-stressing and active loading procedures commenced on 11/19/2009 and 11/20/2009, respectively. There were no problems observed with the DAQ system or loading procedures. Results from cylinder tests conducted on 11/23/2009 can be found in Table 4.

Table 4. 7-strand Concrete Cylinder Strengths

Sample	Strength
1	8775
2	8865
3	8817
Average	8819

5.1.2 Numerical Test Results

Results of load and strain are presented here in reference to time. Plots show the initial stressing of the tendon, transfer of load to the pipe (de-stressing), and active loading of the tendon. The results are presented sequentially in the plots; however, the portions where load was maintained and the tendon monitored for losses were excluded; therefore the horizontal axis is not representative of time required for the entire test. Once zero load was achieved in the jacks after de-stressing, the load in the dead-end reaction frame load cell was monitored overnight until active loading. Negligible losses were measured, on the order of 1 kip.

The tendon load, as monitored throughout the various portions of the testing procedure is shown in Figure 20. The regions of increasing load (stressing), decreasing load due to transfer to the secondary mechanism (de-stressing), and final load increase to 90% of GUTS (active loading) are clearly delineated in the figure. In Figure 20, the readings from the load cell located at the free face (destressing end) were used in the stressing and destressing phases, and the readings from the load cell located at the active loading end was used during the active loading phase. The change in load with time can be correlated with the strain changes observed in the two subsequent plots. Figure 21 and Figure 22 show the strain history in gages R1/R6 and R5/R10 (the 2 sets of gages located at each end of the pipe) in the axial and circumferential directions on the pipe, respectively. Over the course of the test, several discontinuities in recorded strain values were observed due to environmental and accident interference. Data was post-processed to remove these discontinuities.

The greatest change in strain during de-stressing occurs on the free face in the region of R1 and R6. It can be observed in these plots that there are differences between the top (R1/R5) and side gages (R6/R10). Preliminary interpretation of the data attributed these differences to the warping and flexure of the pipe that began during stressing and increased as the specimen was de-stressed. This conclusion was drawn based on observing the relative displacements of the specimen block sides at the free face with respect to the sliding reaction frame (Figure 23).

From the stressing region of Figure 21, the axial strain on the side ($R6_0$) of the tube is increasing in tension while the axial strain on the top of the tube ($R1_0$) is increasing in compression with a larger magnitude. This provides another indication that the tube seems to be warping/flexing. During de-stressing, the strains follow the expected trend, where the grout compresses axially and the circumferential strains reflect the expansion of the grout inside the tube. During this phase, the axial strain increases by 617με in compression at the free face where the load transfer is occurring, while the circumferential strain increases in tension by 267με. The strain changes on the other end of the specimen (R5/R10) are minimal in comparison.

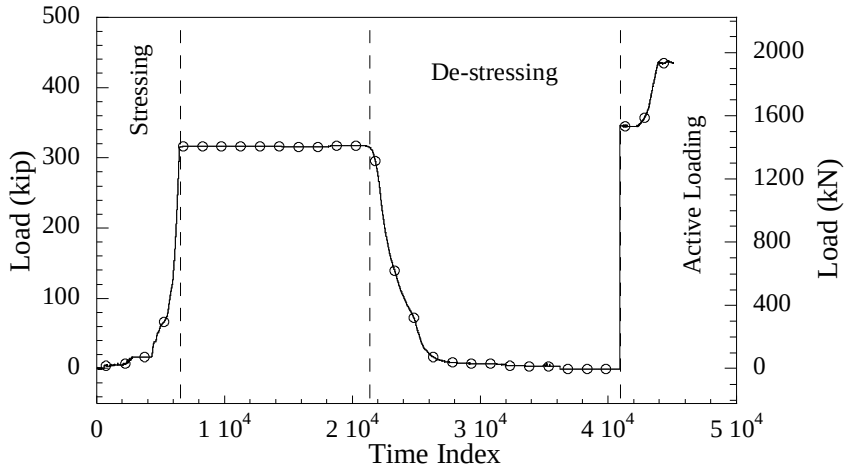

Figure 20. 7-strand tendon load history

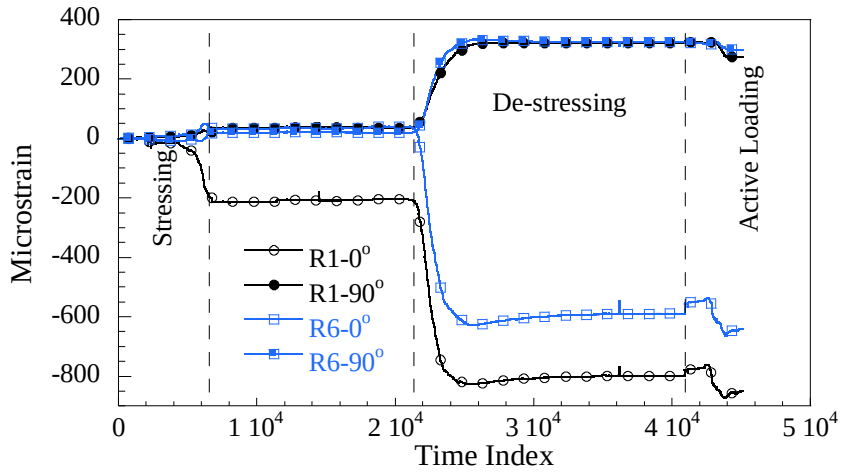

Figure 21. 7-strand strain history: gages R1 and R6

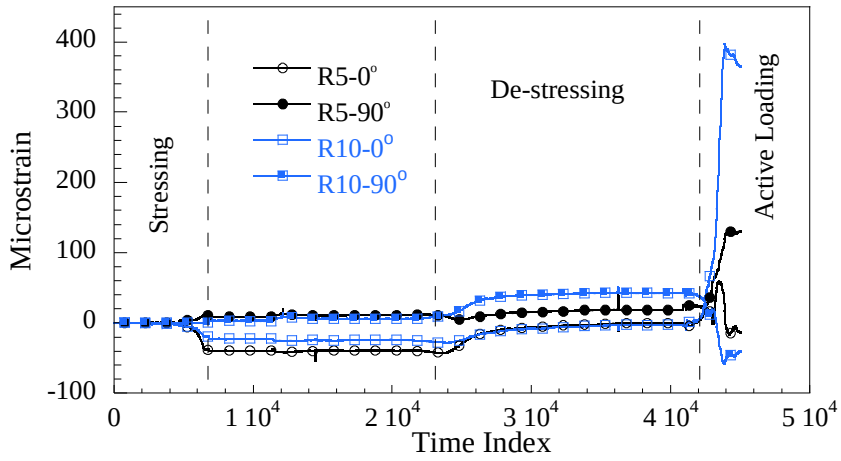

Figure 22. 7-strand strain history: gages R5 and R10

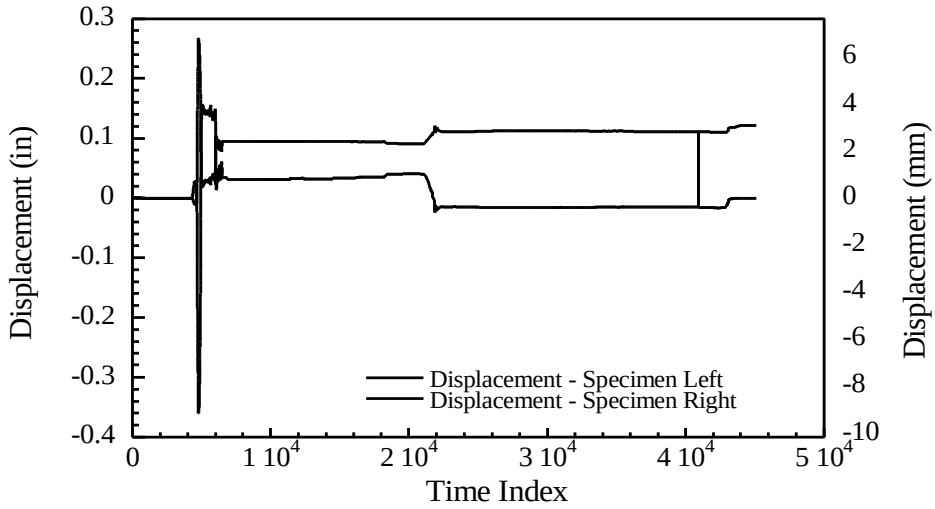

Figure 23. Corner Displacements of the Specimen

The strain profile at several locations along the length of the pipe was generated at different load increments during the de-stressing and active stressing. The axial strain profiles for the top ($R1_0$-$R5_0$) and side ($R6_0$-$R10_0$) gages during de-stressing are shown in Figure 24 and Figure 25 respectively. Similarly, the circumferential strain profile for the top ($R1_{90}$-$R5_{90}$) and side ($R6_{90}$-$R10_{90}$) gages is shown in Figure 26 and Figure 27 respectively. The trends in the axial strain are consistent between the two axial gages, and the transfer length can conservatively be estimated as 38". Due to the spacing of the gages, it is not known how much shorter the true

transfer length may be. The circumferential strain profiles illustrate the Hoyer Effect clearly as the peak tensile strains occur at the location of peak axial strain.

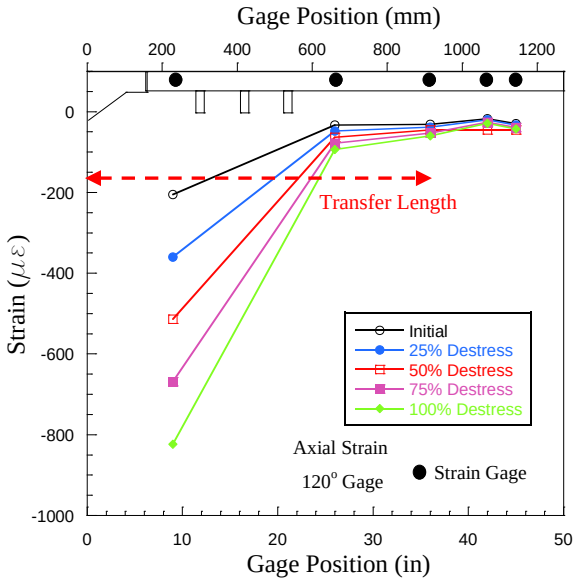

Figure 24. Axial top strain profile during 7-strand de-stressing

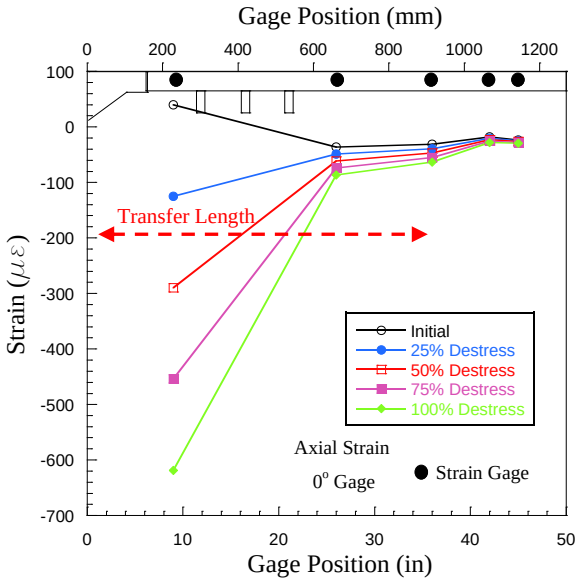

Figure 25. Axial side strain profile during 7-strand de-stressing

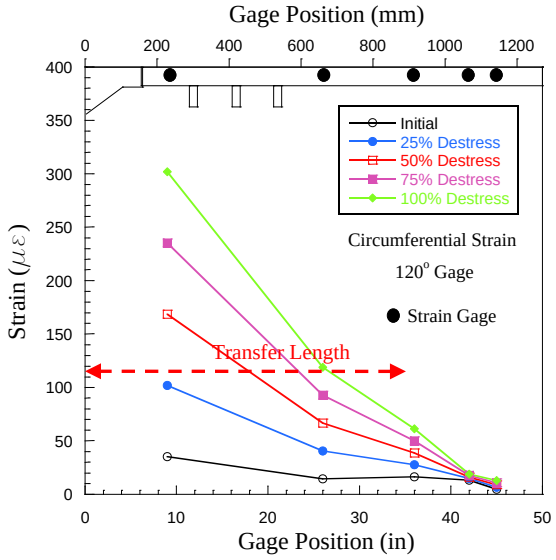

Figure 26. Circumferential top strain profile during 7-strand de-stressing

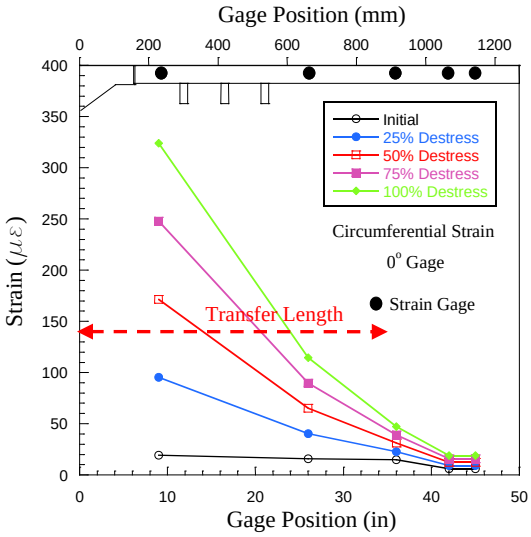

Figure 27. Circumferential side strain profile during 7-strand de-stressing

Strain profiles were also generated for the active loading phase and are shown for the axial top and side gages in Figure 28 and Figure 29. The circumferential strain is shown in Figure 30 and Figure 31. During active loading it is observed from the axial strain profile that the tendon pulling is causing the pipe to be in two different states, compression on the free face and tension on the active loading face. This means that the locked forces in the tendon due to the Hoyer Effect during de-stressing anchored the tendon at the free face while it was being pulled from the active loading face creating compression strains on the free face and tensile strains on the active loading face.

The axial strain behavior during active stressing was different from the theoretically expected values. The strains increase with distance from R5 to R2, which is the fourth gage from the active loading end. This could mean that slippage is occurring between the pipe and grout or grout and tendon. The peak tensile strain occurs at gage $R2_0$. The circumferential strains follow the opposite trend, i.e., gage $R1_{90}$ is in tension (due to the Hoyer Effect).

It is also observed that as the load increases, the axial and circumferential top strain in the gage closest to the active loading face ($R5_0$) does not increase significantly relative to the other strain gages (Figure 28 and Figure 28). This trend suggests that de-bonding between the grout and the pipe is occurring in the region of the first gage from the free face (R5/R10). The strain profiles for the side gages in Figure 29 and Figure 31 still suggest that de-bonding is occurring as the strains are changing least closer to the active loading end and the change starts to increase further down the pipe to reach a maximum at R2/R7 where the strains start to decrease in magnitude due to the secondary anchorage mechanism. From the active loading strain profile, it can be seen that the strand is being fully developed at a point between gage R1 and R2, therefore, the development length can be estimated at approximately 38 in.

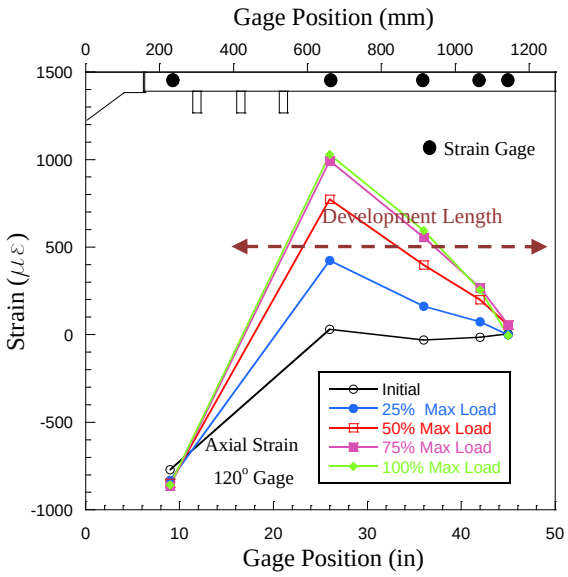

Figure 28. Axial top strain profile during 7-strand active loading

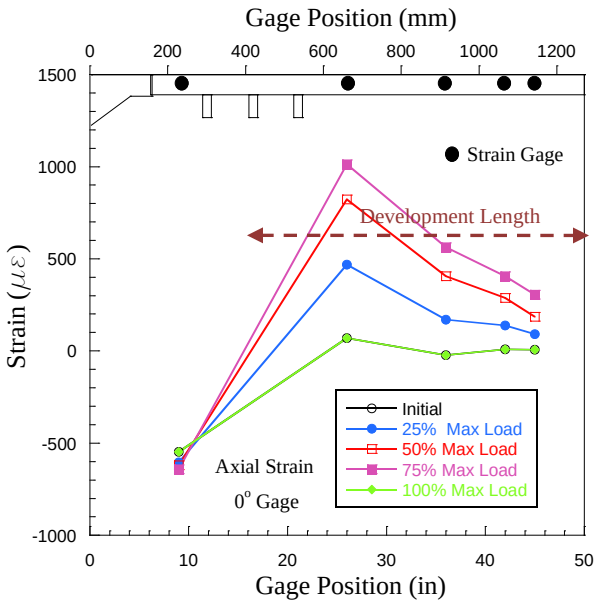

Figure 29. Axial side strain profile during 7-strand active loading

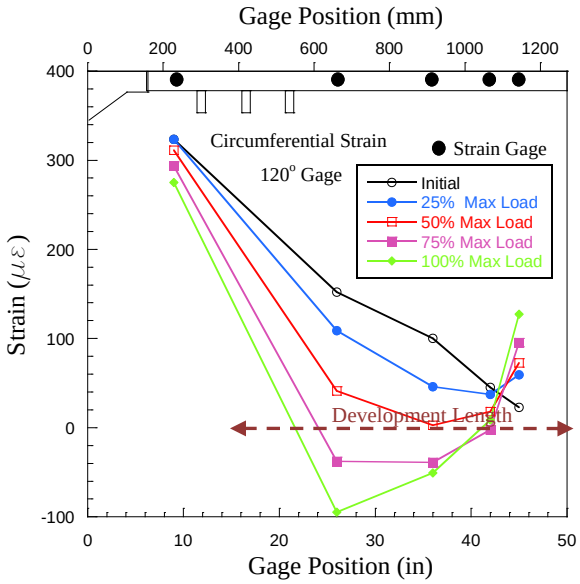

Figure 30. Circumferential top strain profile for 7-strand during active loading

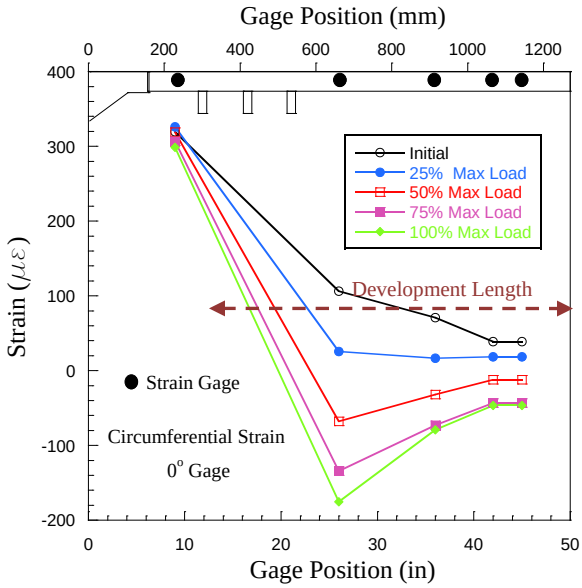

Figure 31. Circumferential side strain profile during 7-strand active loading

5.1.3 Post-test Observations

Upon completing active loading, instrumentation, hydraulic jacks, and reaction fixtures were removed such that the specimen could be inspected. There was no visual indication of slippage between the embedded steel pipe and concrete or between the steel pipe and PT grout. Although, once the grout blocker (Figure 32) was removed from the free end of the specimen, a significant amount of radial cracking was observed within the anchor bearing plate (Figure 33), which is a sign of the significant role the Hoyer Effect had played in the anchorage of the tendon. No cracking was seen to have occurred in the specimen block due to the active loading procedure.

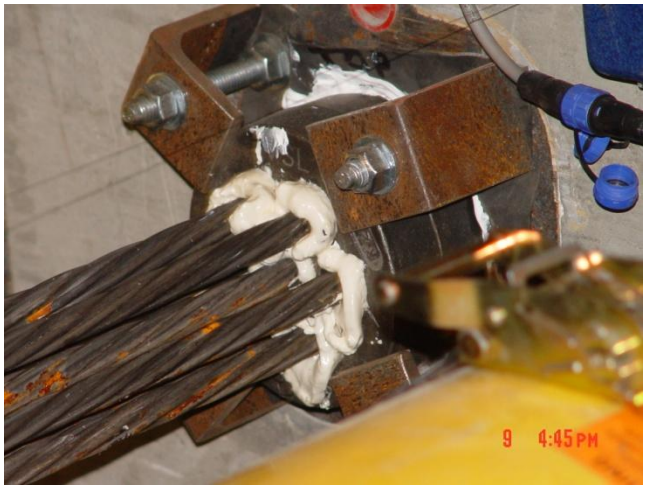

Figure 32. Grout Blocker at Free End

Figure 33. Crack Pattern Within Bearing Plate

5.2 Second 7-strand Tendon Specimen (2 ft Bond Length)

5.2.1 Test Details

The second 7-strand specimen was stressed on 8/10/2010. Unlike the first 7-strand specimen, there were no significant deflections of the specimen recorded during the stressing phase. The two load cells were reflecting loads with no discrepancies during stressing. During de-stressing, the load cell at the active loading end showed 53 kips of load loss.

Specimen grouting proceeded the following day (8/11/2010). The specimen block and test fixture were monitored overnight. There were no observed changes in specimen or fixture measurements. There were no problems observed during the grouting procedure and no grout leakage or bleeding was observed. De-stressing and active loading procedures were carried on 8/17/2010 and 8/18/2010 respectively. There were no problems observed with the DAQ system or loading procedures. The concrete cylinders and grout cubes were tested on 8/18/2010. The results are shown in Table 5.

Table 5. 7-strand - 2nd Specimen - PT Grout Cube and Concrete Cylinders Strengths

Cubes		**Cylinders**	
Test Date	8/18/2010	*Test Date*	8/18/2010
Sample	Strength (psi)	Sample	Strength (psi)
1	--	1	6607
2	7520	2	6485
3	6559	3	5560
Average	7040	Average	6217

5.2.2 Numerical Test Results

The plots presented in this section similarly show the three major stages of the experiments uniquely identified on them. The horizontal axis does not reflect the real time of which the experiment was performed. These time history plots are meant to show the continuity of the loads and strains through the different stages: Stressing of the tendon, load transfer from the tendon into the system de-stressing, and active loading.

The tendon load throughout various portions of the testing procedure is shown in Figure 34. Two different load cells are used to produce this plot. During stressing and de-stressing, the data from load cell at the free end (de-stressing end) was used. During active loading, the data from the load cell at the active loading end was used. The increasing load is shown in the stressing phase, then the decrease in the tendon load due to the load transfer into the pipe in the de-stressing phase. During active loading, the load is increased to 370 kips. The specimen was unable to hold the 90% of GUTS. The load dropped and the specimen was able to hold 336 kips. The change in load with time can be correlated with the strain changes observed in the two subsequent plots. Figure 35 shows the strain history in gages R1/R9 (the 2 sets of gages located at the free face) in the axial and circumferential directions on the pipe. There were abrupt discontinuities in gages like those seen in the first 7-strand specimen. Therefore, the data was normalized to get rid of these discontinuities.

Figure 36 shows the load at the active loading end during de-stressing. This plot shows a load loss of 53 kips during de-stressing. Therefore, the stressing load was not fully transferred into the specimen during de-stressing and slip could have happened. After the 53 kip load loss, the specimen was able to hold the remaining load.

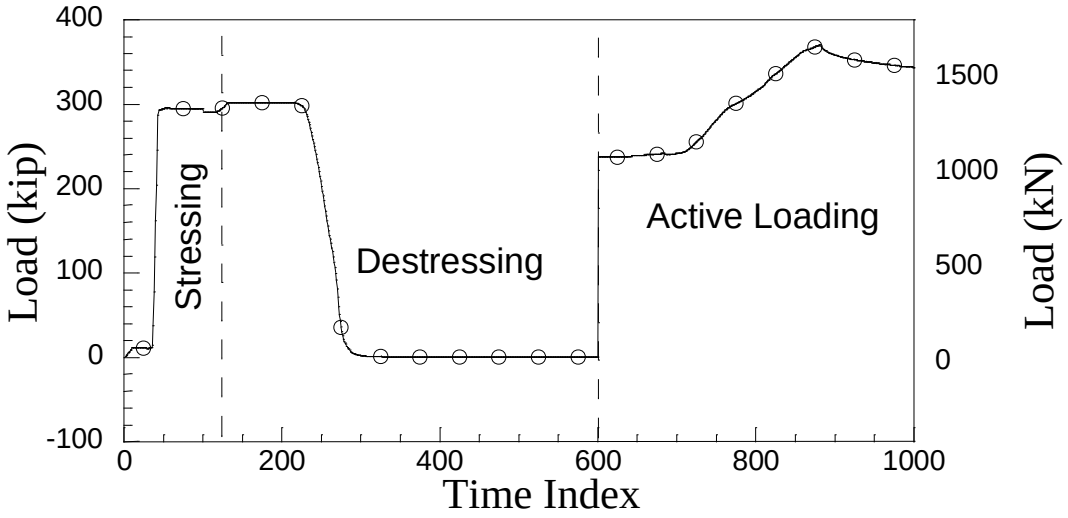

Figure 34. 7-strand - Second Specimen - Tendon Load Time History

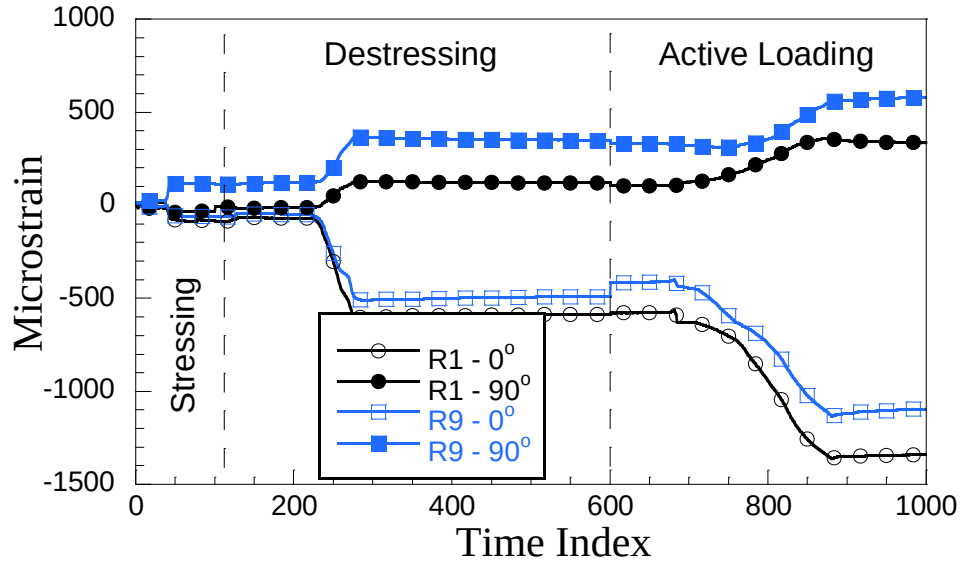

Figure 35. 7-strand - Second Specimen - R1 and R9 Time History

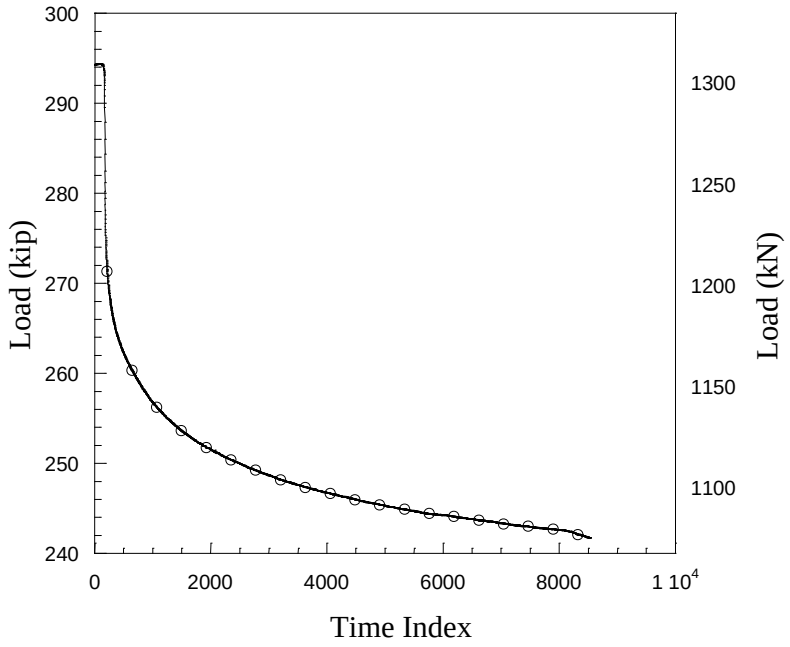

Figure 36. 7-Strand – Second Specimen - Load at Active Loading End During De-stressing

The strain profile at several locations along the length of the pipe was generated at different load increments during the de-stressing and active stressing. The axial strain profile for the top ($R1_0$-$R8_0$) gages during de-stressing is shown in Figure 37 and axial strain profile for the side ($R9_0$ – $R12_0$) gages is shown in Figure 39. Similarly, the circumferential strain profile for the top ($R1_{90}$-$R8_{90}$) gages and the side ($R9_0$ – $R12_0$) gages are shown in Figure 38 and Figure 40 respectively. The last 4 side gages from the active loading end (R13-R16) malfunctioned, and data from them was not recorded. The trends in the axial strain are consistent between the two axial gages (top and side). Since this specimen experienced a load loss of 53 kips of during de-stressing, the stressing force was not fully transferred; however, the specimen was able to sustain the load after the load loss. From the strain profiles the transfer length of this load (after the 53 kips of lost load) can be estimated at 19". The irregularities observed on the active loading end of the pipe that are attributed to the errors in the strain gage readings and not any physical phenomena. The circumferential strain profiles illustrate the Hoyer Effect clearly as the peak tensile strains occur at the location of peak axial strain.

Strain profiles were also generated for the active loading phase and are shown for the axial top and side strain gages in Figure 41 and Figure 43 respectively, and the circumferential

strain for the top and side gages in Figure 42 and Figure 44 respectively. During active loading it is observed from the axial strain distribution that the tendon pulling is causing the pipe to be in two different states, compression on the free face and tension on the active loading face. As the tendon is pulled, the axial strains were increasing in compression while the circumferential strains were increasing in tension. This explains the formation of a grout plug at the free face. This grout plug anchored the tendon therefore placing the pipe in axial compression at the free face.

Estimating the development length from the active loading phase (Figure 41 through Figure 44) is not as obvious as the estimation of the transfer length from the de-stressing data due to grout plug formation. Moreover it is noted that the system was unable to carry the full 90% GUTS load. The strand did not fully develop for this specimen. After the load drop, 336 kips were sustained by the "grout plug" formation, which is the main secondary anchorage mechanism for this specimen.

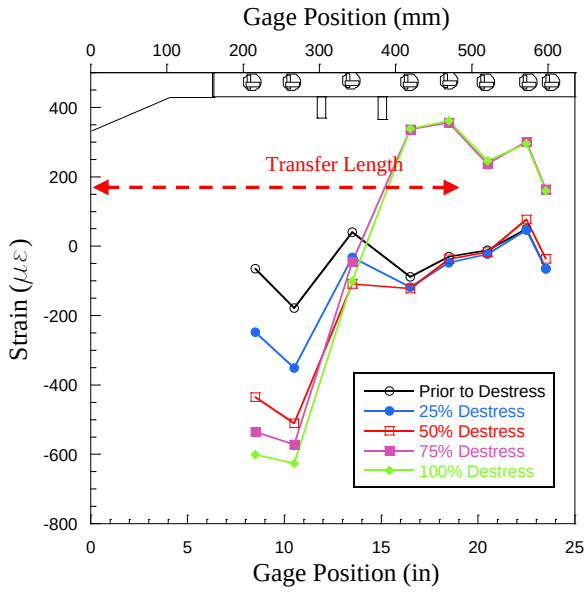

Figure 37. 7-strand - Second Specimen - Top Axial Strain Profile During De-stressing

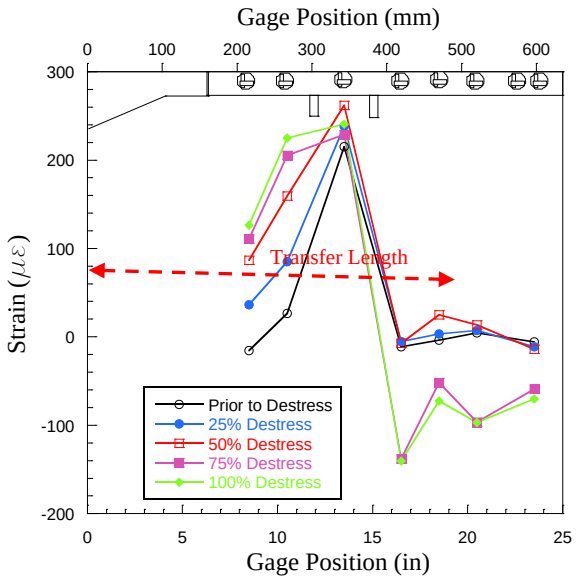

Figure 38. 7-strand - Second specimen - Top Circumferential During De-stressing

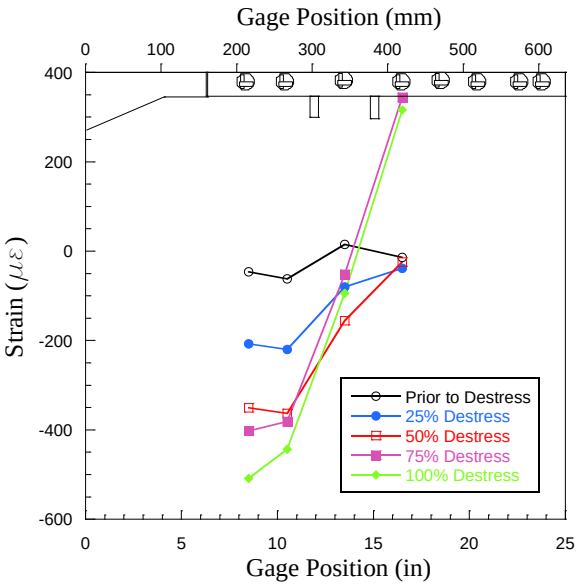

Figure 39. 7-strand - Second Specimen - Side Axial Strain Profile During De-stressing

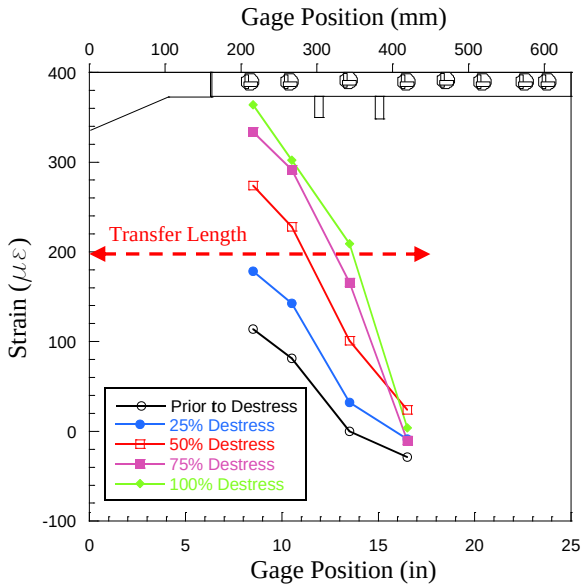

Figure 40. 7-strand - Second specimen - Side Circumferential During De-stressing

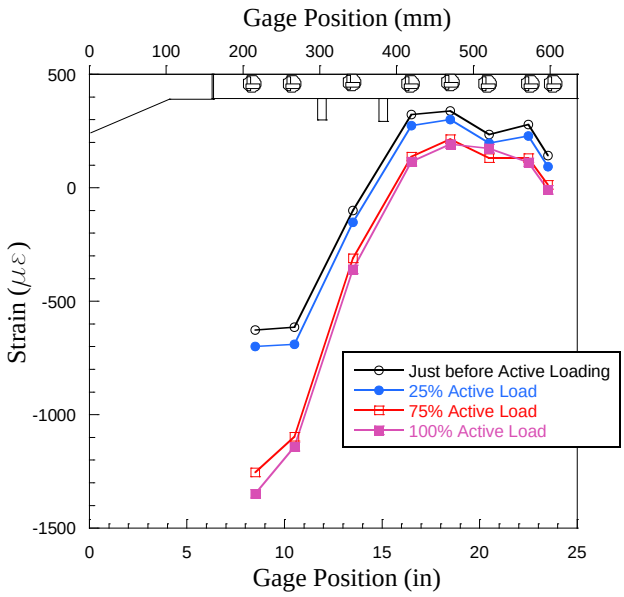

Figure 41. 7-strand - Second Specimen - Top Axial Strain Profile During Active Loading

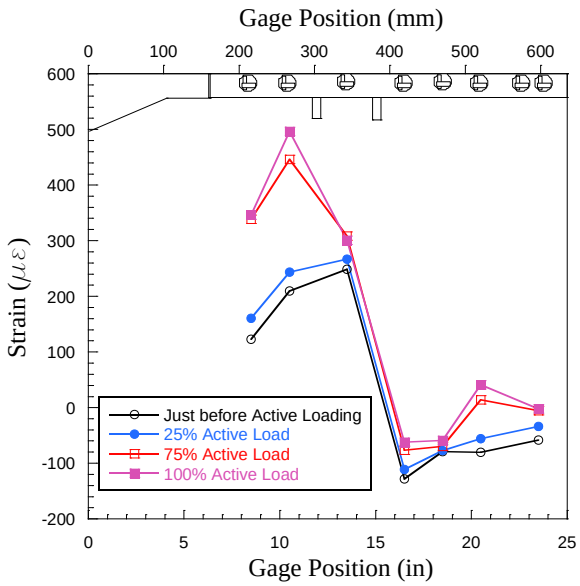

Figure 42. 7-strand - Second Specimen - Top Circumferential Strain Profile During Active Loading

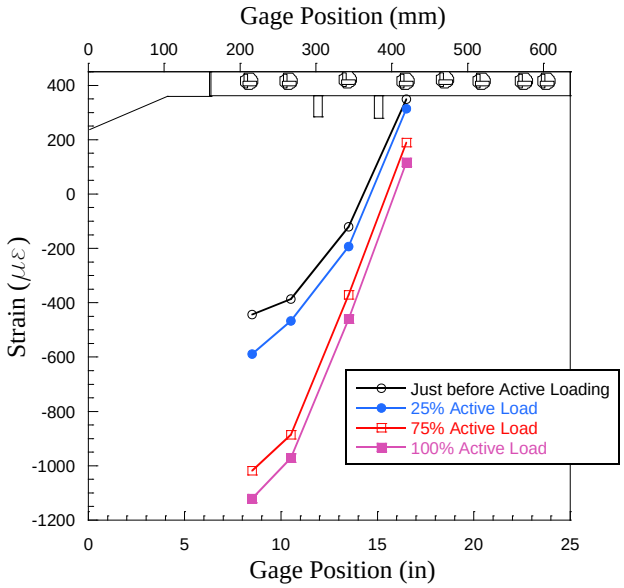

Figure 43. 7-strand - Second Specimen - Side Axial Strain Profile During Active Loading

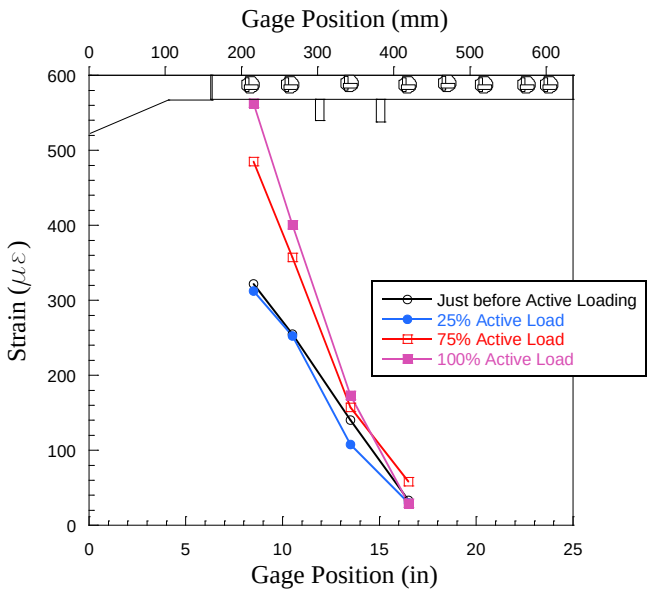

Figure 44. 7-strand - Second Specimen - Side Circumferential Strain Profile During Active Loading

5.2.3 Post-test Observations

After active loading, the hydraulic jacks, and reaction fixtures were removed and DSI bars were de-stressed and the specimen was inspected. There was visual indication of slippage between the steel pipe and PT grout from the active loading end (Figure 45). Once the grout blocker was removed from the free end of the specimen, slippage between the tendon and the grout was observed as well as a significant amount of radial cracking within the anchor bearing plate (Figure 46). No cracking was seen to have occurred in the specimen block due to the active loading procedure.

Figure 45. 7-strand - Second Specimen - Grout Slip Photo

Figure 46. 7-strand - Second Specimen - Tendon Slip at Free face

5.3 Third 7-strand Tendon Specimen (1.5 ft Bond Length)

5.3.1 Test Details

The third 7-strand specimen was stressed on 8/31/2010. There were no significant deflections of the specimen recorded during the stressing phase. The two load cells were reflecting loads with no discrepancies during stressing. During de-stressing, the load cell at the active loading end showed 68 kips of load loss.

Specimen grouting proceeded the following day (8/32/2010). The specimen block and test fixture were monitored overnight. There were no observed changes in specimen or fixture measurements. There were no problems observed during the grouting procedure. No grout leakage or bleeding was observed. De-stressing and active loading procedures were carried on 9/7/2010 and 9/8/2010 respectively. There were no problems observed with the DAQ system or loading procedures. The concrete cylinders were tested on 9/1/2010. The results are shown in Table 6.

Table 6. 7-strand – Third Specimen - PT Grout cubes and Concrete Cylinder Strengths

Cubes		**Cylinders**	
Test Date	9/1/2010	*Test Date*	9/1/2010
Sample	Strength (psi)	Sample	Strength (psi)
1	9657	1	7601
2	9711	2	7760
3	10006	3	7855
Average	9791	Average	7739

5.3.2 Numerical Test Results

The time history plots presented in this section show the three major stages of the experiments uniquely identified on them. The horizontal axis does not reflect the real time of which the experiment was performed. These time history plots are meant to show the continuity of the loads and strains through the three major phases of the experiment: Stressing of the tendon, load transfer from the tendon into the system de-stressing, and active loading.

The tendon load throughout the various portions of the testing procedure is shown in Figure 47. Two different load cells are used to produce this plot. During stressing and de-stressing, the data from load cell at the free end was used. During active loading, the data from

the load cell at the active loading end was used. The increasing load is shown in the stressing phase, then the decrease in the tendon load due to the load transfer into the pipe in the de-stressing phase. During active loading, the load is increased to 370 kips before the strand slipped. The 90% of GUTS was not carried by the secondary anchorage mechanism. After the slip of the tendon, the specimen was able to sustain 340 kips. The specimen was reloaded to a maximum of 400 kips and the same load of 340 kips was sustained. The reloading is not shown in Figure 47. The change in load with time can be correlated with the strain changes observed in the two subsequent plots. Figure 48 shows the strain history in gages R1/R7 (the 2 sets of gages located at the free face) in the axial and circumferential directions on the pipe. Some strain data were normalized due to abrupt discontinuities in strain gage readings like those seen in the first 7-strand specimen. Their contribution to the strain profile analysis which follows is, therefore, ignored.

Figure 49 shows the load at the active loading end during de-stressing. This plot shows a load loss of 68 kips during de-stressing. Therefore, the stressing load was not fully transferred into the specimen during de-stressing and slip could have happened. After the 68 kip load loss, the specimen was able to hold the remaining load.

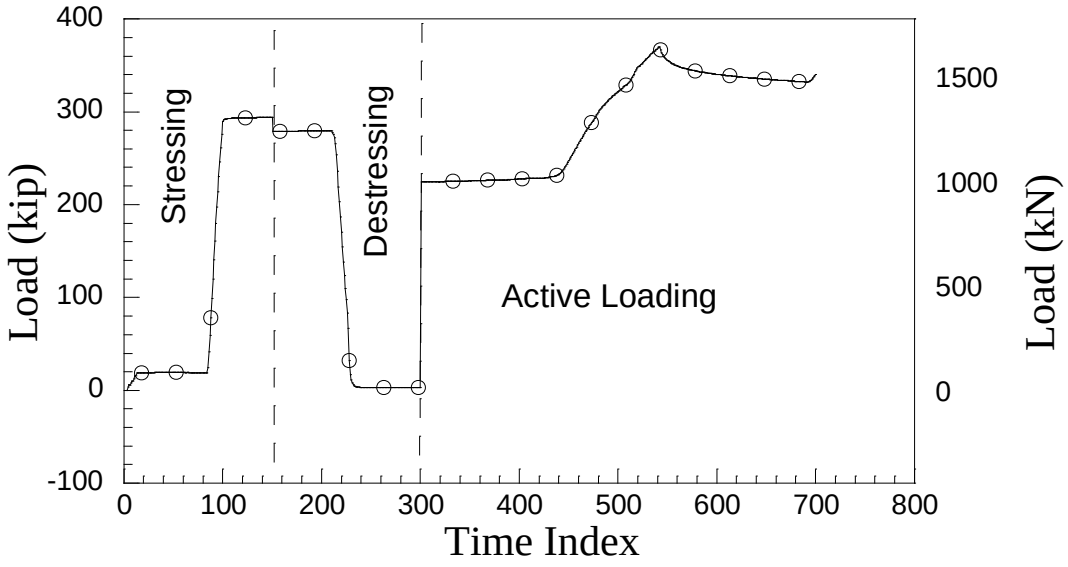

Figure 47. 7-strand - Third Specimen - Load History

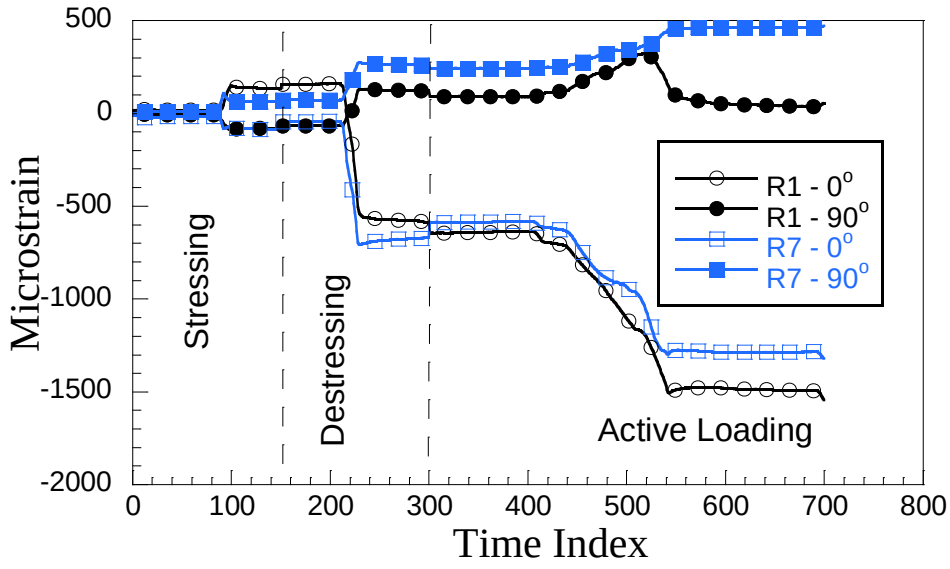

Figure 48. 7-strand - Third Specimen - R1 and R7 Strain History

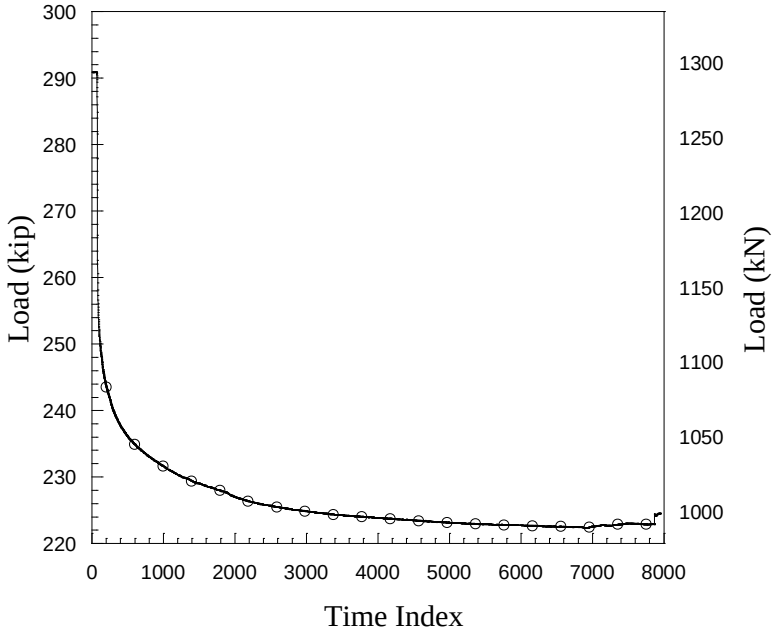

Figure 49. 7-strand – Third Specimen - Load at Active Loading End During De-stressing

Similar to the previous specimens, the strain profile at several locations along the length of the pipe was generated at different load increments during the de-stressing and active stressing. The axial strain profile for the top ($R1_0$-$R6_0$) gages during de-stressing is shown in Figure 50 and axial strain profile for the side ($R7_0$ – $R12_0$) gages is shown in Figure 52.

Similarly, the circumferential strain profile for the top ($R1_{90}$-$R6_{90}$) gages and the side ($R7_0$ – $R12_0$) gages are shown in Figure 51 and Figure 53 respectively. Since this specimen experienced a load loss of 68 kips of during de-stressing, the stressing force was not fully transferred; however, the specimen was able to sustain the load after the load loss. From the strain profiles the transfer length of this load (after the 68 kips of lost load) can be estimated at 18". The circumferential strain profiles illustrate the Hoyer Effect clearly as the peak tensile strains occur at the location of peak axial strain.

Strain profiles were also generated for the active loading phase and are shown for the axial top and side strain gages in Figure 54 Figure 56 respectively, and the circumferential strain for the top and side gages in Figure 55 and Figure 57 respectively. The same behavior observed in the second 7-strand specimen (2 ft development) was observed in this one. It is observed from the axial strain distribution that the tendon pulling is causing the pipe to be in two different states, compression on the free face and tension on the active loading face. As the tendon is pulled, the axial strains were increasing in compression while the circumferential strains were increasing in tension. This explains the formation of a grout plug at the free face. This grout plug anchored the tendon therefore placing the pipe in axial compression at the free face.

Due to aforementioned behavior, estimating the development length from the active loading phase (Figure 54 through Figure 57) is not as obvious as the estimation of the transfer length from the de-stressing data due to grout plug formation. The PT force did not fully develop during active loading. The anchorage of the tendon was provided by the formation of this grout plug. The after the load drop, the specimen was able to sustain 340 kips.

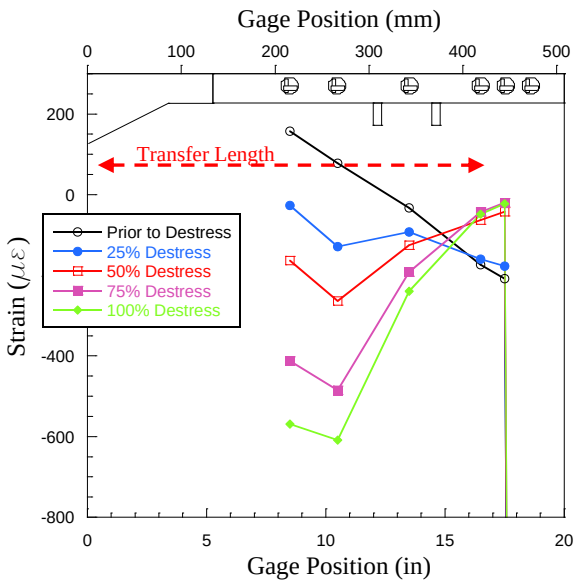

Figure 50. 7-strand - Third Specimen - Top Axial Strain Profile During De-stressing

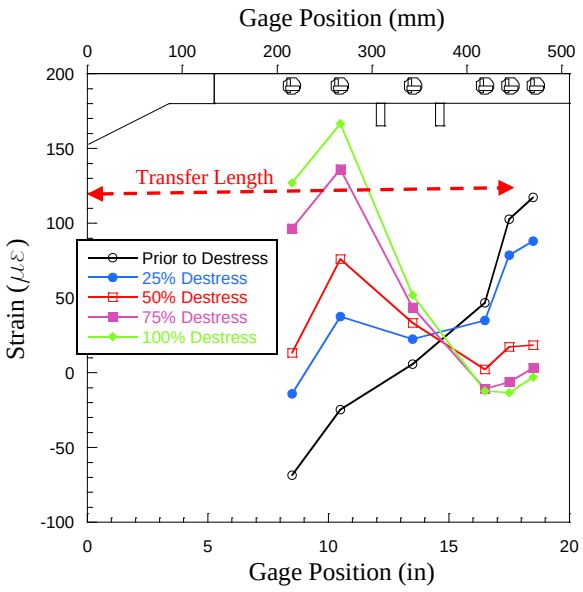

Figure 51. 7-strand - Third Specimen - Top Circumferential During De-stressing

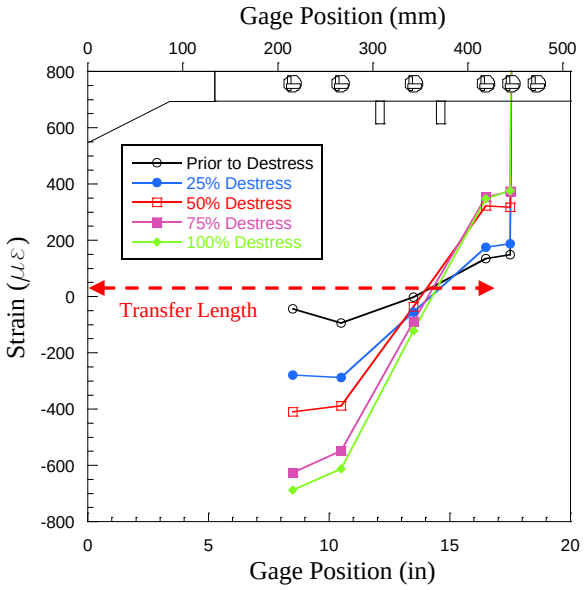

Figure 52. 7-strand - Third Specimen - Side Axial Strain Profile During De-stressing

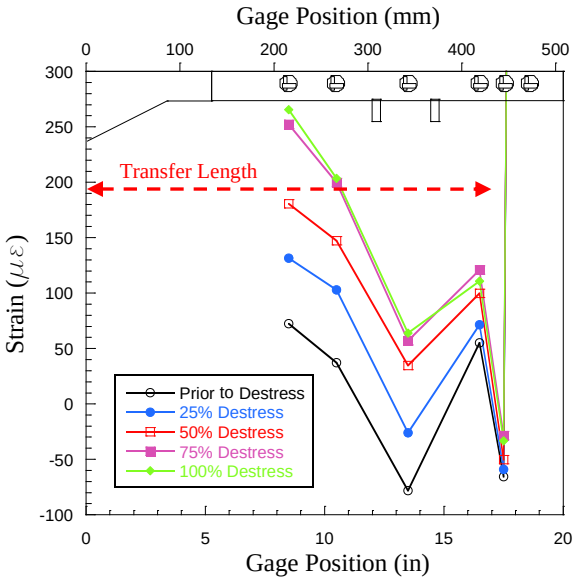

Figure 53. 7-strand - Third Specimen - Side Circumferential During De-stressing

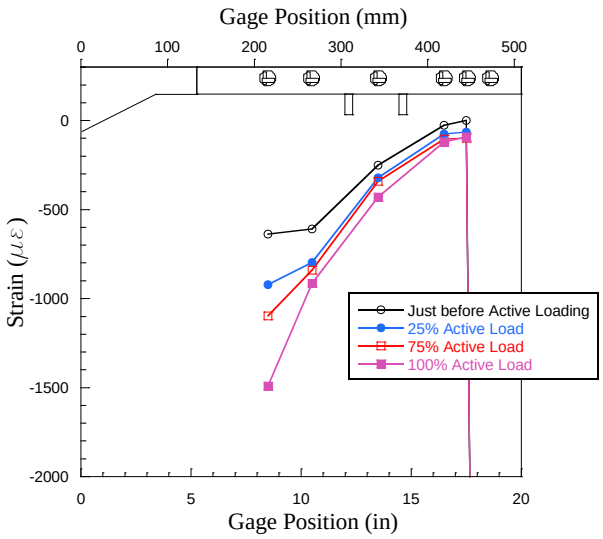

Figure 54. 7-strand - Third Specimen - Top Axial Strain Profile During Active Loading

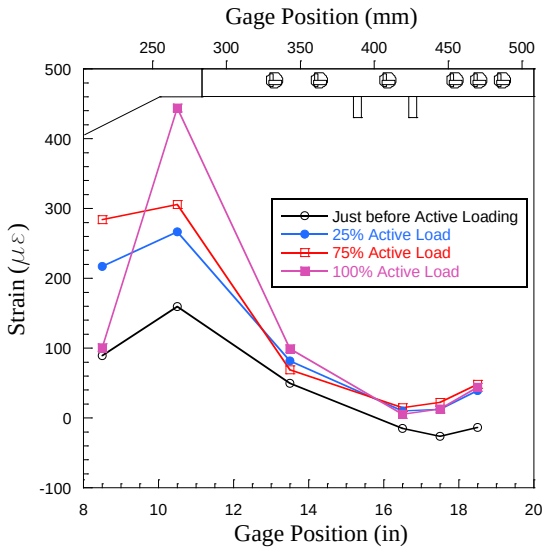

Figure 55. 7-strand - Third Specimen – Top Circumferential Strain Profile During Active Loading

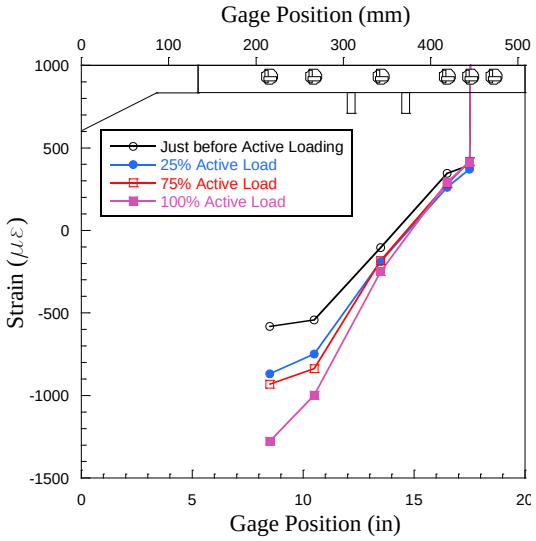

Figure 56. 7-strand - Third Specimen – Side Axial Strain Profile During Active Loading

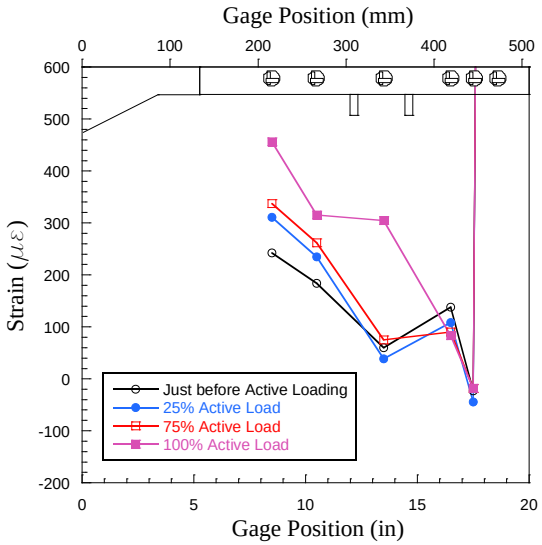

Figure 57. 7-strand - Third Specimen – Side Circumferential Strain Profile During Active Loading

5.3.3 Post-test Observations

After active loading, the hydraulic jacks, and reaction fixtures were removed and DSI bars were de-stressed allowing the visual inspection of the specimen. There was visual indication of slippage between the tendons and PT grout as well as slip between the grout and the pipe from the active loading end (Figure 58). Once the grout blocker was removed from the free end of the specimen, slippage between the tendon and the grout was observed (Figure 59). No cracking was seen to have occurred in the specimen block due to the active loading procedure.

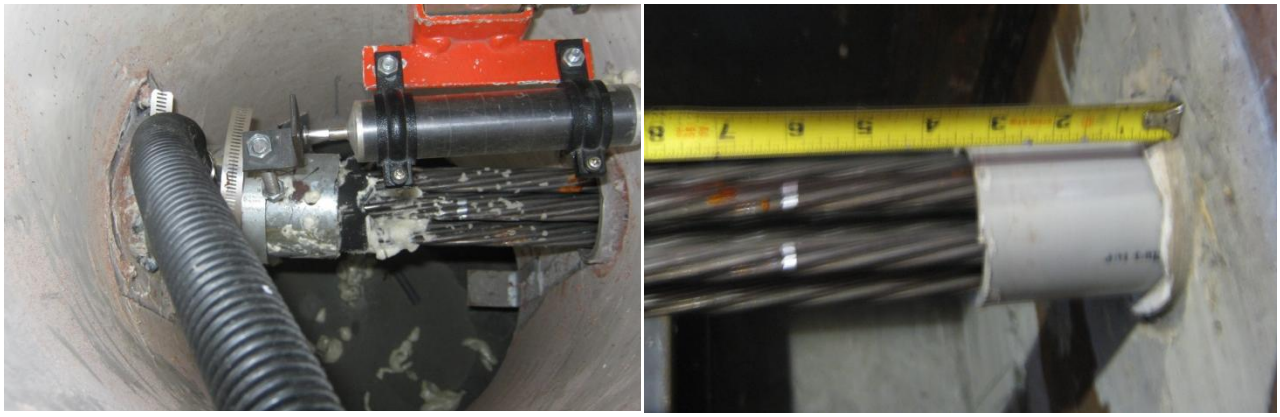

Figure 58. 7-Strand - Third Specimen – Post-Active Loading – Active Loading End Photo

Figure 59. 7-strand – Third Specimen - Tendon Slip at Free face

5.4 First 12-strand Tendon Specimen (5 ft Bong Length)

5.4.1 Test Details

The 12-strand specimen was stressed on 12/11/2009. During the stressing procedure, there were no issues observed with the testing fixture. Although, like the 7-strand specimen, it was observed that as the stressing load increased, a discrepancy between load cells began to develop. At the point of jack lock-off, the load discrepancy was approximately 75kip.

Specimen grouting proceeded the following day (12/12/2009). The specimen block and test fixture were monitored overnight and no substantial change was observed. There were some minor issues regarding the foam blockage applied the previous day. The foam appeared to be in poor quality. Although, it was noted that little to no grout leakage/wicking was observed. De-stressing and active loading procedures commenced on 12/17/2009 and 12/18/2009 respectively. There were no problems observed with the DAQ system or loading procedures.

5.4.2 Numerical Test Results

Similar to the 7-strand specimen, results of load and strain are presented here in reference to time: Figure 60 shows the tendon load, Figure 61 shows the strain history (axial and circumferential) in gages R1/R6, and Figure 62 shows the strain history in gages R5/R10. Gage $R10_0$ (axial gage on the top side of the tube) malfunctioned and the data is excluded from Figure 62. From Figure 61 and Figure 62, the strains measured differ minimally between the top and side gages; therefore, the apparent warping/flexure of the tube exhibited by the 7-strand specimen was not observed. Pipe axial strains increase in compression and circumferential strains increase in tension during de-stressing of the tendon indicating force transfer due to the Hoyer Effect.

During de-stressing the strains in R1 and R6 at the free face reflect the most significant changes as the PT force starts to be released at that face. During active loading strain gages R5 and R10 experience the largest strain changes. In Figure 62 both the side and top gages reflect an increase in tensile strain. This indicates one or both of the following mechanisms could be occurring: de-bonding at the active loading face or excessive confining forces due to the DSI bars affecting the changes in the strain at the active loading face.

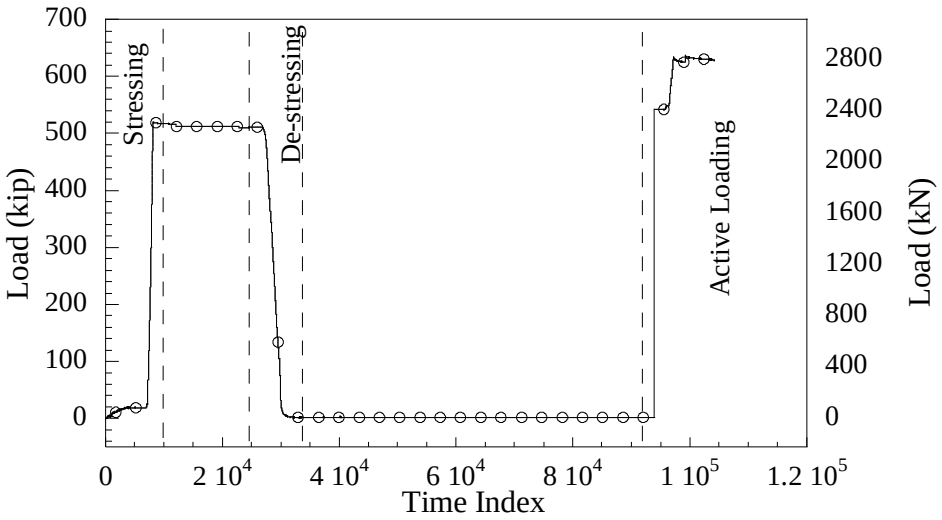

Figure 60. 12-strand tendon load history

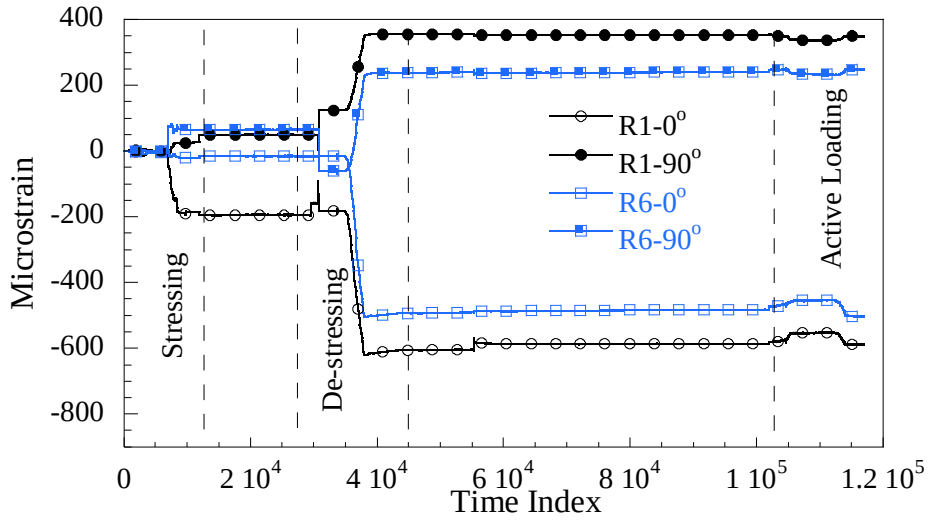

Figure 61. 12-strand strain history: gages R1 and R6

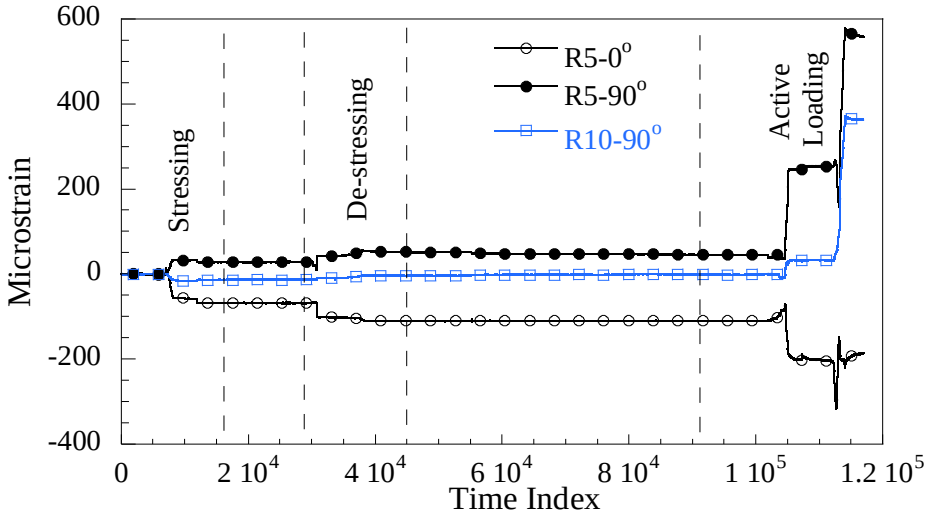

Figure 62. 12-strand strain history: gages R5 and R10

Strain profiles at several locations along the length of the pipe were generated for different loads during the de-stressing and active loading phases. During de-stressing it is observed that the PT force is transferred into the system at approximately 50" from the free face (between R1/R6 and R3/R8). This is apparent in Figure 64 and Figure 65 where the axial strains increase in compression as the load increases and decrease along the pipe length from the free face to the active loading face. The circumferential strains also reflect what is expected from the Hoyer Effect where the magnitude of tensile strains, due to the expansion of the tendon as it is released, decrease in magnitude to a value close to zero at roughly 50" from the active loading end.

Axial strain profiles for the side gages ($R6_0$-$R10_0$) during active loading are shown in Figure 68 and Figure 69. Similarly, the circumferential strain profile for the side gages is shown in Figure 70 and Figure 71. The trend in axial strain profile was not observed to be as consistent between the two gage locations as observed in the 7-strand specimen, specifically within the three gages (R3/8, R4/9, and R5/10) closest to the active loading face of the specimen. During active loading, it is observed from the axial strain distribution that the tendon pulling is causing the pipe to be in two different states, compression on the free face and tension on the active loading face. Figure 68, Figure 70 and Figure 71 explain the same phenomenon that took place in the first 7-strand specimen. The locked forces in the tendon due to the Hoyer Effect during de-stressing anchored the tendon at the free face while it was being pulled from the active loading

face. This resulted in compression strains on the free face and tensile strains on the active loading face. It also means that there is grout-pipe or grout-tendon slippage in a similar manner as observed in the 7-strand specimen. From the circumferential profile strains in Figure 70 and Figure 71, upon full de-stress, the PT force is developed between the anchorage bearing plate and gage R2/R7. The transfer and development lengths can be estimated as 50". Yet, due to the spacing of gages, there is not an ability, through experimental results, to make a more precise estimate as to the transfer length.

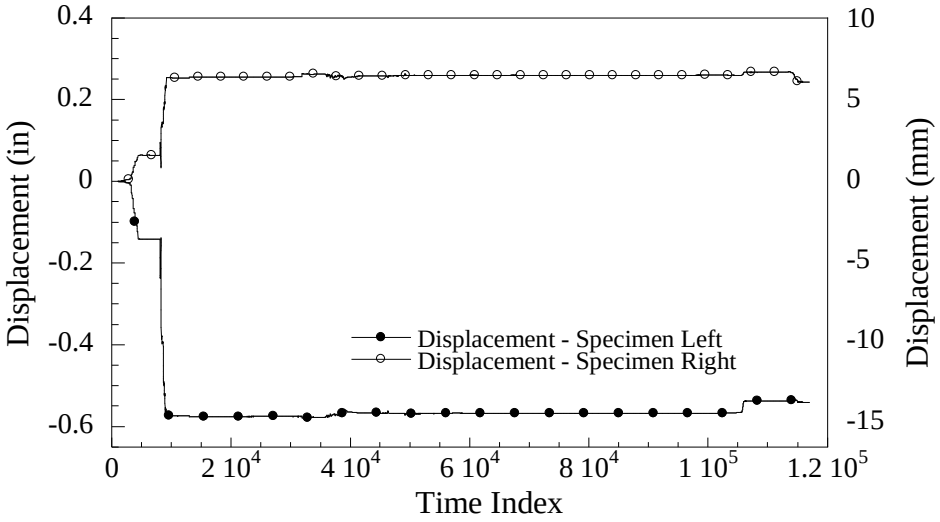

Figure 63. Specimen Displacement

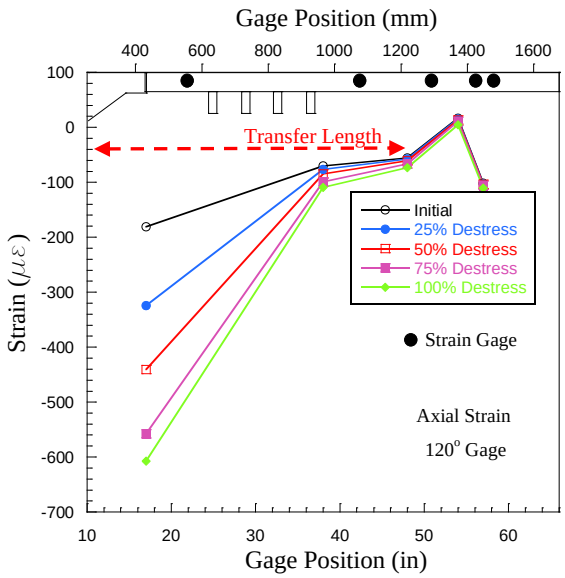

Figure 64. Axial top strain profile during 12-strand de-stressing

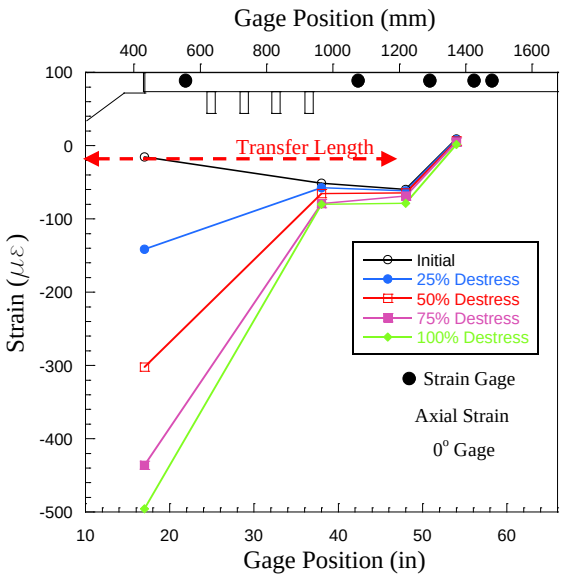

Figure 65. Axial side strain profile during 12-strand de-stressing

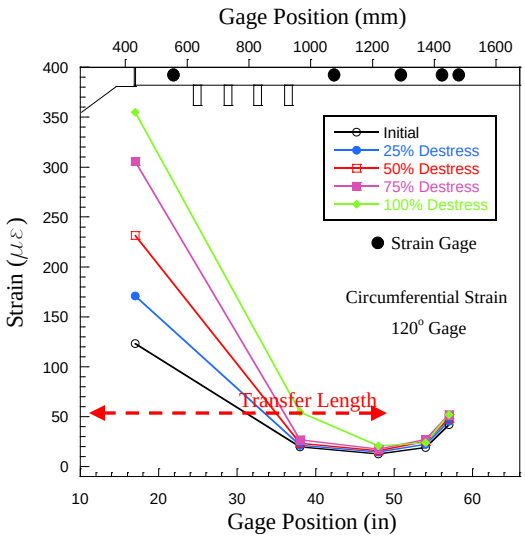

Figure 66. Circumferential top strain profile during 12-strand de-stressing

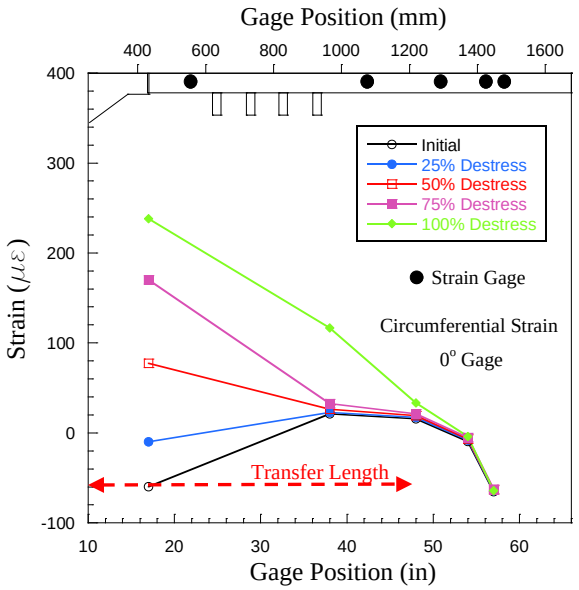

Figure 67. Circumferential side strain profile during 12-strand de-stressing

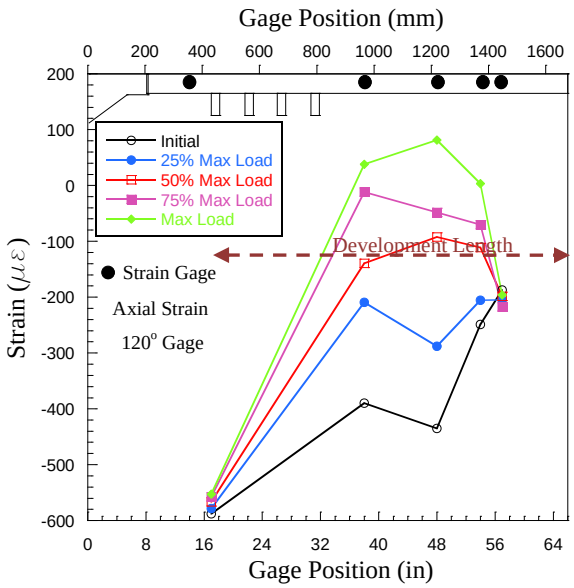

Figure 68. Axial top strain profile during 12-strand during active loading

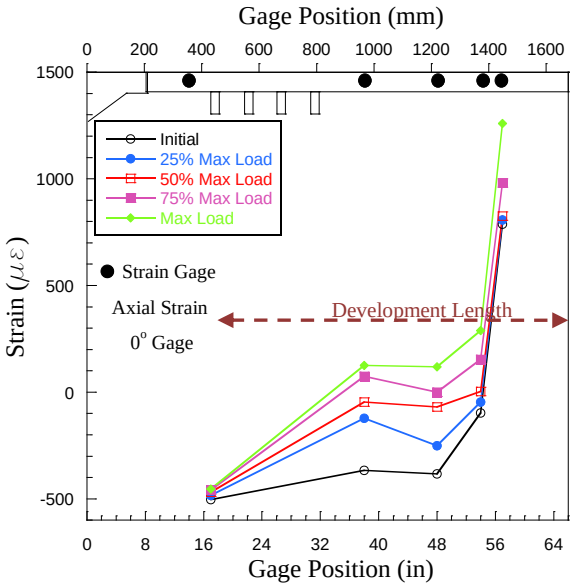

Figure 69. Axial side strain profile during 12-strand active loading

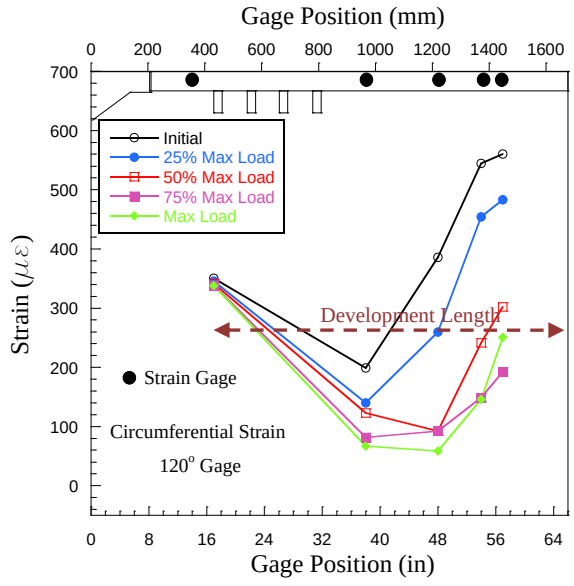

Figure 70. Circumferential top strain profile during 12-strand active loading

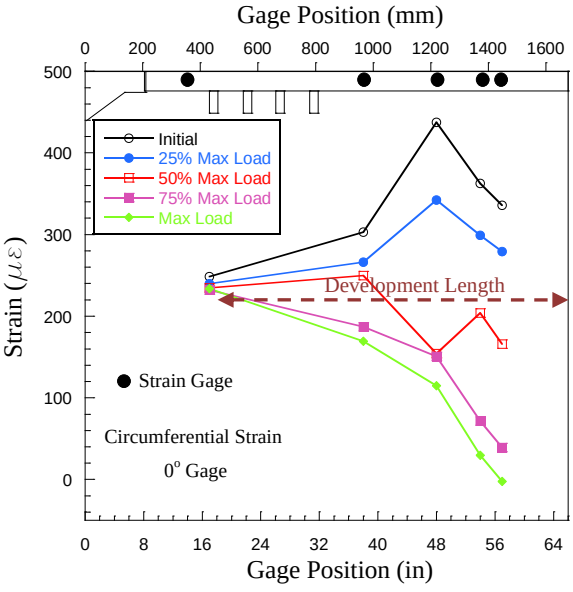

Figure 71. Circumferential side strain profile during 12-strand active loading

5.4.3 Post-test Observations

Minor cracking of the grout around the strand on the free face was seen during post-test inspection (Figure 72). Cracks were observed to propagate in the radial direction from the embedded strands. There was no cracking found to have developed on the specimen block.

Figure 72. Photos of 12-Strand after Active Loading

5.5 Second 12-strand Tendon Specimen (2.5 ft Bond Length)

5.5.1 Test Details

The second 12-strand specimen was stressed on 9/21/2010. There were no significant deflections of the specimen recorded during the stressing phase. The two load cells were reflecting loads with no discrepancies during stressing. During de-stressing, the load cell at the active loading end showed 84 kips of load loss.

Specimen grouting proceeded the following day (9/22/2010). The specimen block and test fixture were monitored overnight. There were no observed changes in specimen or fixture measurements. There were no problems observed during the grouting procedure and no grout leakage or bleeding was observed. De-stressing and active loading procedures were carried on 9/28/2010 and 9/29/2010 respectively. There were no problems observed with the DAQ system or loading procedures.

5.5.2 Numerical Test Results

The time history plots are shown in Figure 73, Figure 74 and Figure 75. The horizontal axis does not reflect the real time of which the experiment was performed. These plots are meant to show the continuity of the loads and strains through the different stages: Stressing of the tendon, load transfer from the tendon into the system de-stressing, and active loading.

The tendon load throughout the various portions of the testing procedure is shown in Figure 73. During stressing and de-stressing, the data from load cell at the free end was used. During active loading, the data from the load cell at the active loading end was used. The load increases in the stressing phase, then during de-stressing the load is transferred to the system (grout, pipe and concrete block). During active loading, the load is increased to 633 kips. The specimen was unable to hold the load. After the load drop, a load of 607 kips was sustained by this specimen even after reloading the specimen to 90% GUTS. As seen in Figure 73 the load decreases exponentially to a constant value allowing the tendon to slip. Then the load was increased to 90% of GUTs and the same behavior occurred where the specimen was unable to hold the load. The latter part is not shown in the time history plot. The change in load with time can be correlated with the strain changes observed in the two subsequent plots. Figure 74 shows

the strain history in gages R1/R10 (the 2 sets of gages located at the free face) in the axial and circumferential directions on the pipe and Figure 75 shows a similar plot for the gages on the active loading end (R9/R11). There were abrupt several discontinuities in many readings of the strain gages like those seen in the previous specimens. These discontinuities were repaired.

Figure 76 shows the load at the active loading end during de-stressing. This plot shows a load loss of 84 kips during de-stressing. Therefore, the stressing load was not fully transferred into the specimen during de-stressing and slip could have happened. After the 84 kip load loss, the specimen was able to hold the remaining load.

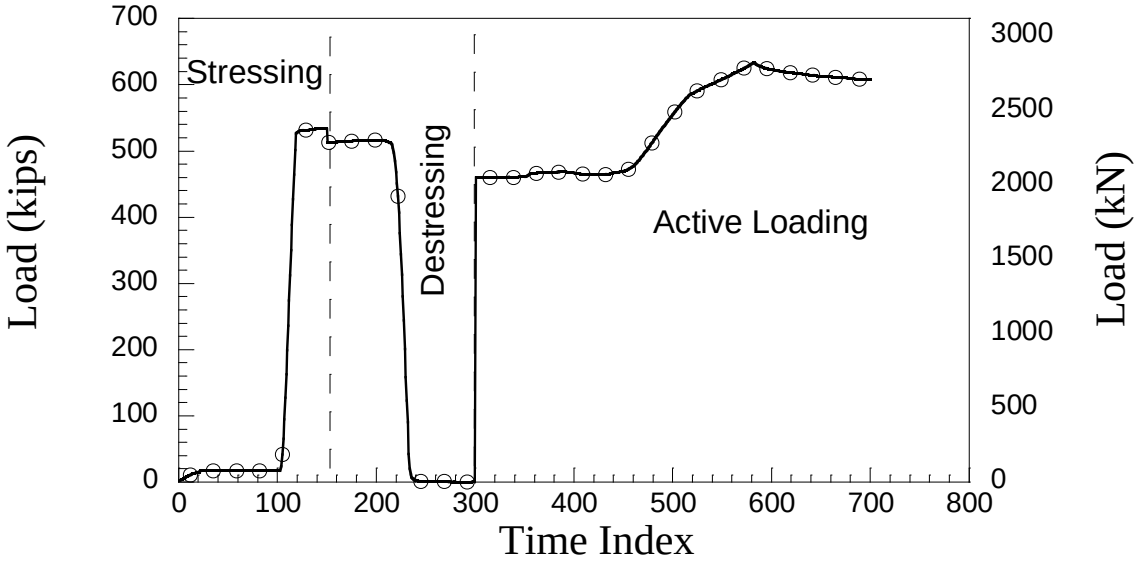

Figure 73. 12-strand - Second Specimen - Tendon Load Time History

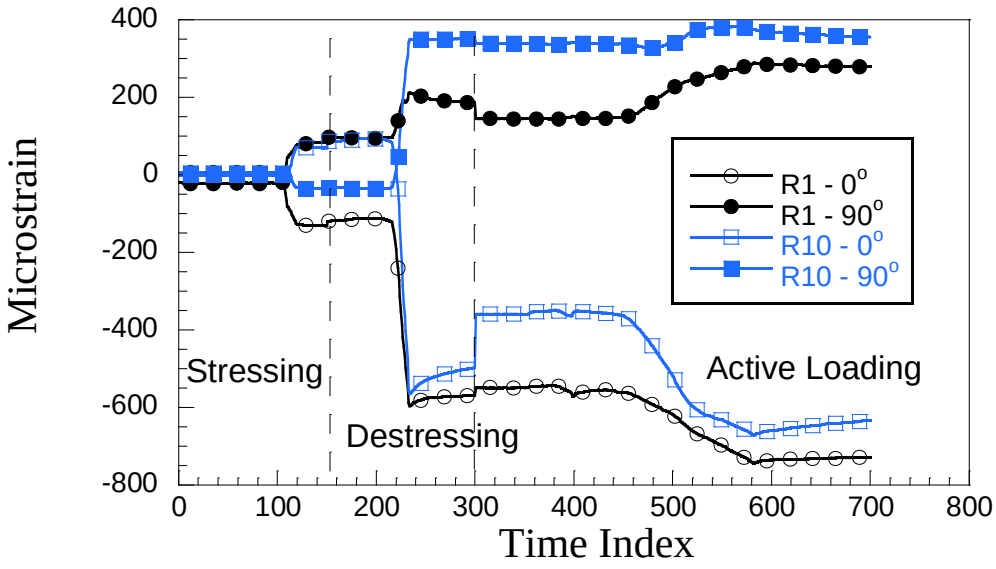

Figure 74. 12-strand – Second Specimen - R1 and R10 Time History

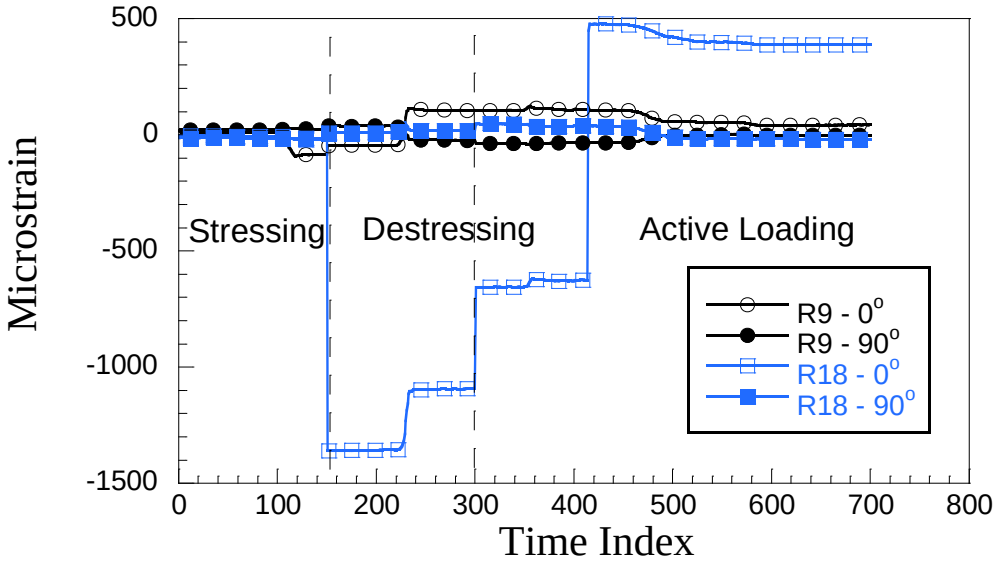

Figure 75. 12-strand – Second Specimen – R9 and R18 Time History

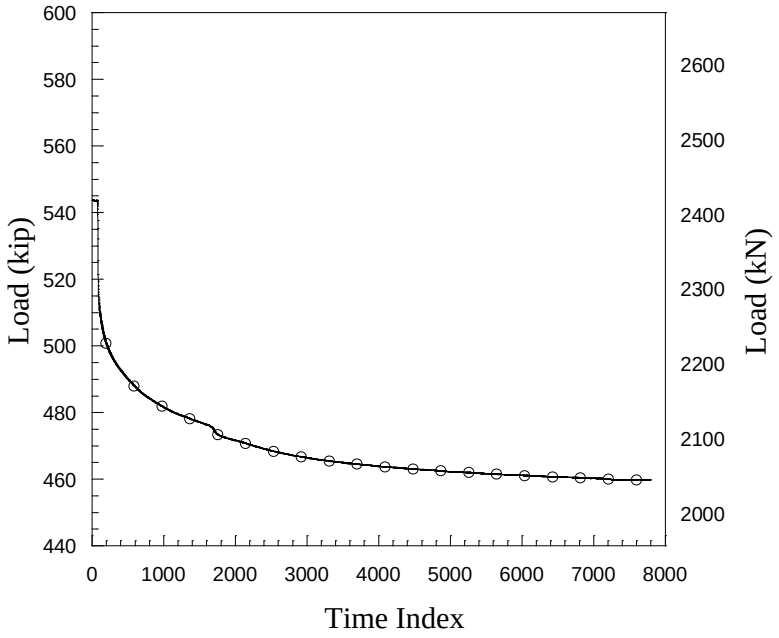

Figure 76. 12-strand – Second Specimen – Load at Active Loading End During De-stressing

The strain profile was also generated at different load increments during the de-stressing and active stressing. The axial strain profile for the top ($R1_0$-$R9_0$) gages during de-stressing is shown in Figure 77 and axial strain profile for the side ($R10_0$ – $R18_0$) gages is shown in Figure 79. Similarly, the circumferential strain profile for the top ($R1_{90}$-$R8_{90}$) gages and the side ($R9_0$ – $R12_0$) gages are shown in Figure 78 and Figure 80 respectively. The trends in the axial strain are consistent between the top and side axial gages. Since this specimen experienced a load loss of 84 kips of during de-stressing, the stressing force was not fully transferred; however, the specimen was able to sustain the load after the load loss. From the strain profiles the transfer length of this load (after the 84 kips of lost load) can be estimated at 28". There are irregularities in the strain profile observed on the active loading end of the pipe that are attributed to the errors in the strain gage readings and not any physical phenomena. However, The general trends along the pipe can be still seen.

Strain profiles were also generated for the active loading phase and are shown for the axial top and side strain gages in Figure 81 and Figure 83 respectively, and the circumferential strain for the top and side gages in Figure 82 and Figure 84 respectively. The same "grout plug formation" phenomenon observed in the second and third 7-strand specimens was observed in

the 2nd 12-strand specimen. During active loading it is observed from the axial strain distribution that the tendon pulling is causing the pipe to be in two different states, compression on the free face and tension on the active loading face. As the tendon is pulled, the axial strains were increasing in compression while the circumferential strains were increasing in tension. This grout plug anchored the tendon therefore placing the pipe in axial compression at the free face.

Estimating the development length from the active loading phase is not as obvious as the estimation of the transfer length from the de-stressing data due to grout plug formation. The PT force was not fully developed for this specimen. It can be seen that the grout plug formation allowed the specimen to hold 607 kips of pullout force.

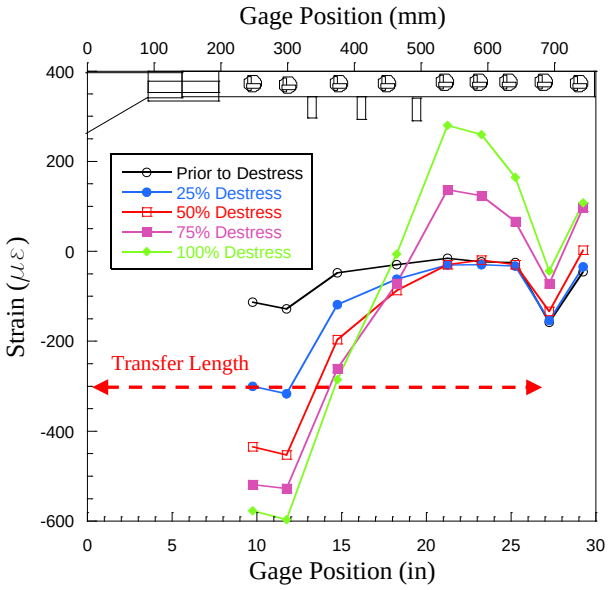

Figure 77. 12-strand - Second Specimen - Top Axial Strain Profile During De-stressing

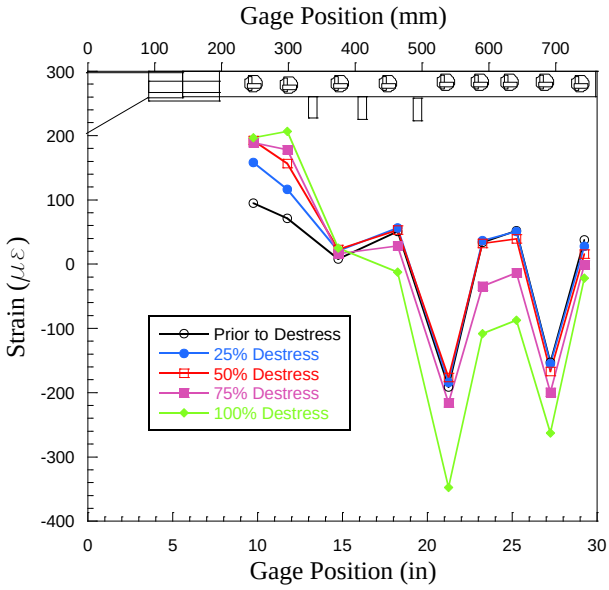

Figure 78. 12-strand - Second Specimen - Top Circumferential Strain Profile During De-stressing

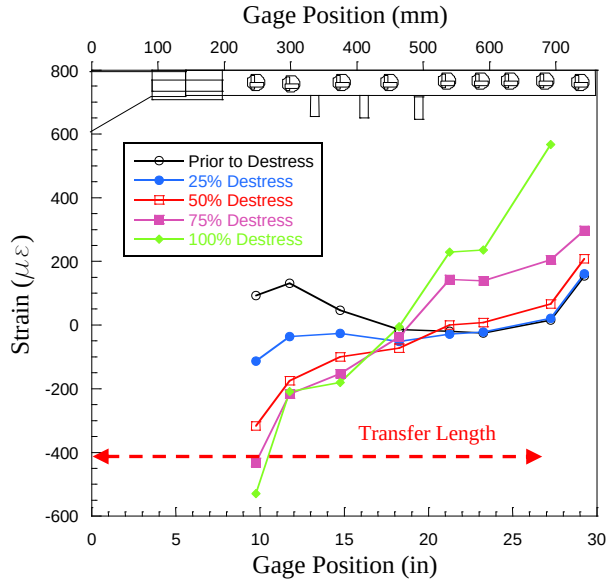

Figure 79. 12-strand - Second Specimen – Side Axial Strain Profile During De-stressing

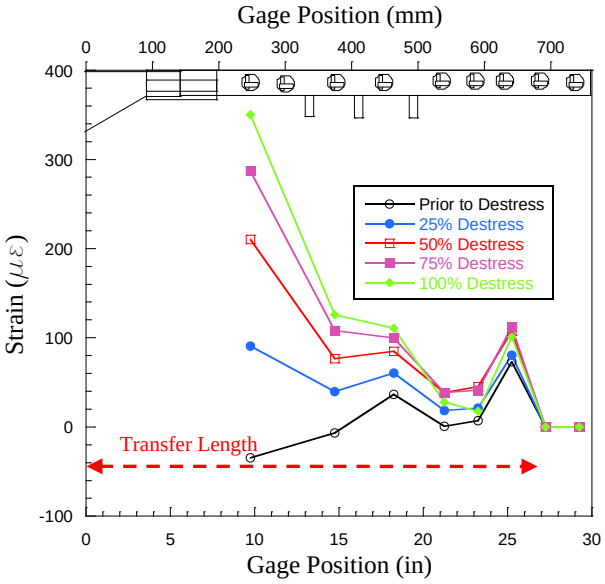

Figure 80. 12-strand - Second Specimen – Side Circumferential Strain Profile During De-stressing

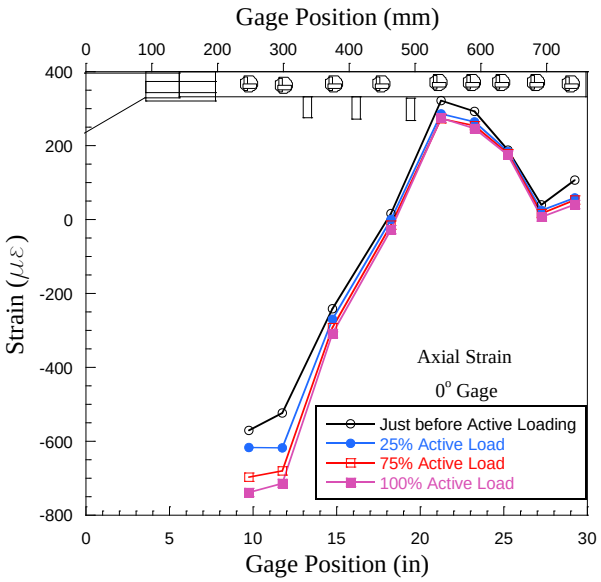

Figure 81. 12- strand - Second Specimen -Top Axial Strain During Active Loading

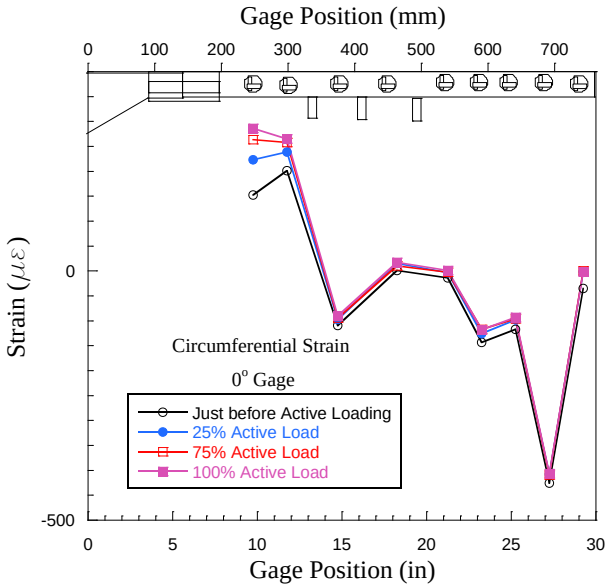

Figure 82. 12- strand - Second Specimen -Top Circumferential Strain During Active Loading

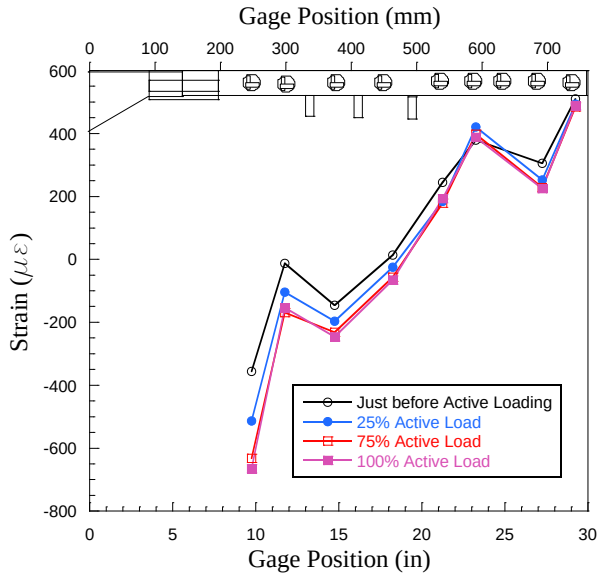

Figure 83. 12- strand - Second Specimen - Side Axial Strain During Active Loading

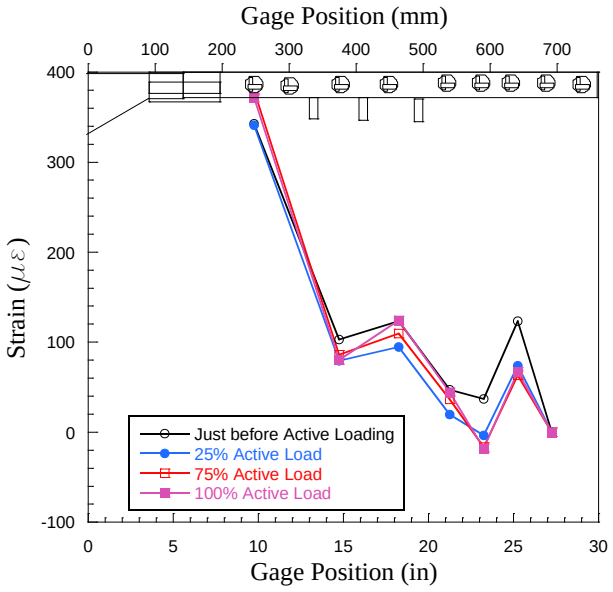

Figure 84. 12- strand - Second Specimen –Side Circumferential Strain During Active Loading

5.5.3 Post-test Observations

After active loading, the hydraulic jacks, and reaction fixtures were removed and DSI bars were de-stressed allowing the visual inspection of the specimen. The same post-active-loading observations that were recorded in the 2nd and 3rd 7-strand specimens were observed in the 2nd 12 strand specimen. There was visual indication of slippage between the tendons and PT grout from the active loading end (Figure 85). Once the grout blocker was removed from the free end of the specimen, slippage between the tendon and the grout was observed (Figure 86). No cracking was observed in the specimen block due to the active loading procedure.

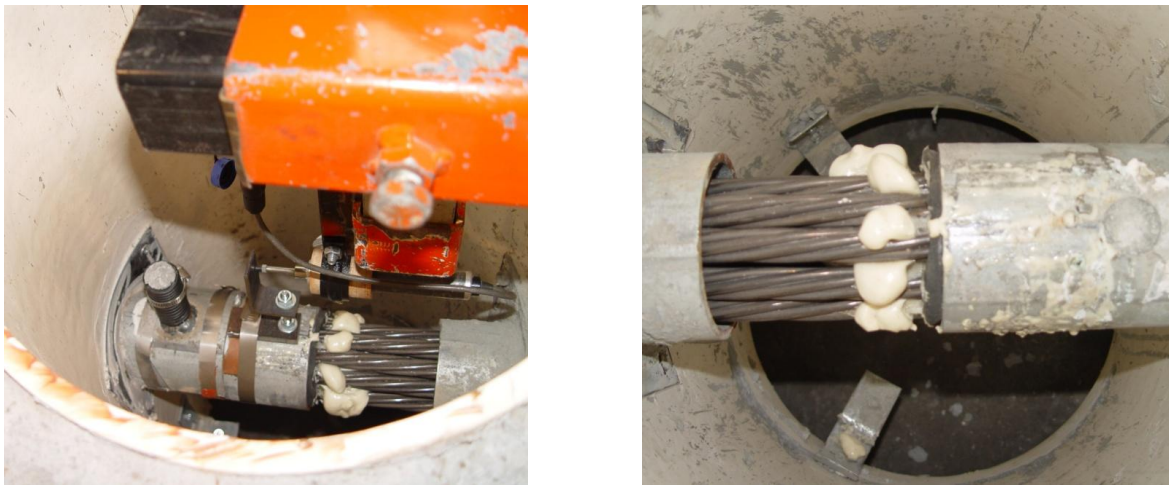

Figure 85. 12-strand – Second Specimen – Post-active Loading - Active Loading End Photo

Figure 86. 12-strand - Second Specimen – Post-active Loading – De-stressing End Photo

5.6 Third 12-strand Tendon Specimen (2 ft Bond Length)

5.6.1 Test Details

The third 12-strand specimen was stressed on 10/18/2010. There were no significant deflections of the specimen recorded during the stressing phase. The two load cells were reflecting loads with no discrepancies during stressing. During de-stressing, the load cell at the active loading end showed 86 kips of load loss.

Specimen grouting proceeded the following day (10/20/2010). The specimen block and test fixture were monitored overnight. There were no observed changes in specimen or fixture measurements. There were no problems observed during the grouting procedure and no grout leakage or bleeding was observed. De-stressing and active loading procedures were carried on 10/25/2010 and 10/26/2010 respectively. There were no problems observed with the DAQ system or loading procedures.

5.6.2 Numerical Test Results

The time history plots for this specimen are shown in Figure 87, Figure 88 and Figure 89. As in all the previous specimens, the horizontal axis does not reflect the real time of which the experiment was performed. These plots are meant to show the continuity of the loads and strains through the different stages: stressing of the tendon, load transfer from the tendon into the system (de-stressing), and active loading.

The load throughout the various portions of the testing procedure is shown in Figure 87. During stressing and de-stressing, the data from load cell at the free end was used. During active loading, the data from the load cell at the active loading end was used. The tendon load increases in the stressing phase, then decreases during de-stressing as the load is transferred to the system (grout, pipe and concrete block). During active loading, the load is increased to 632 kips. 90% of GUTS was not carried by the specimen and a sudden drop in the load was observed. As seen in Figure 73 the load decreases exponentially to a constant value allowing the tendon to slip. Then the load was increased to 632 kips (90% GUTS) and the same behavior occurred where the specimen was unable to hold the load. The latter part is not shown in the time history plot. The specimen was able to hold a constant load of 605 kips. The change in load with time can be correlated with the strain changes observed in the two subsequent plots. Figure 88 shows the

strain history in gages R1/R8 (the 2 sets of gages located at the free face) in the axial and circumferential directions on the pipe and Figure 89 shows a similar plot for the gages on the active loading end (R7/R14). Over the course of the test, several discontinuities in recorded strain values were observed due to environmental and accident interference. Data was post-processed to remove these discontinuities.

Figure 90 shows the load at the active loading end during de-stressing. This plot shows a load loss of 86 kips during de-stressing. Therefore, the stressing load was not fully transferred into the specimen during de-stressing and slip could have happened. After the 86 kip load loss, the specimen was able to hold the remaining load.

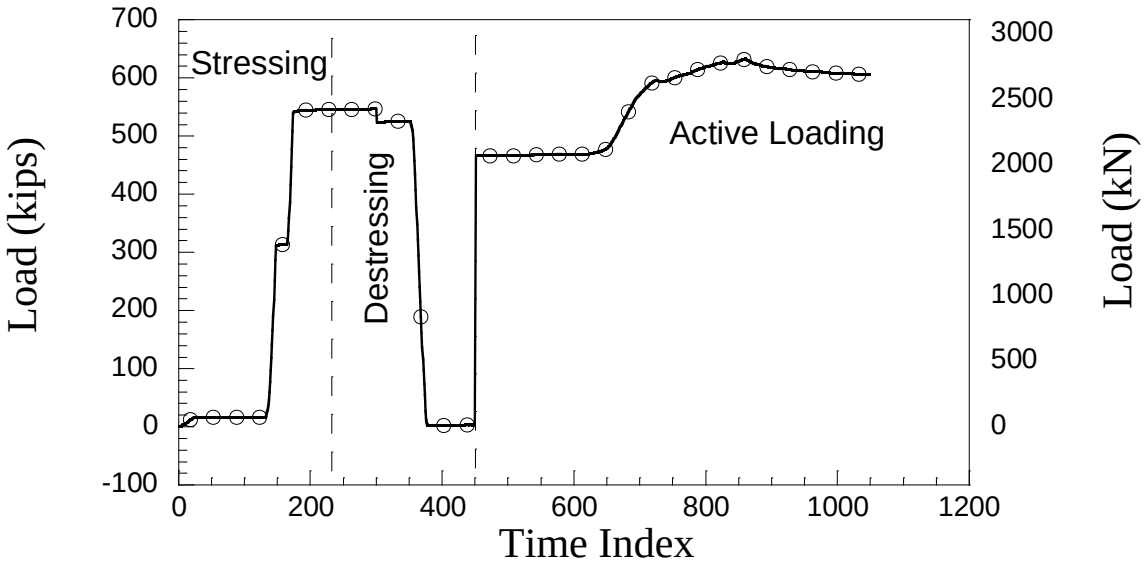

Figure 87. 12-strand – Third Specimen - Tendon Load Time History

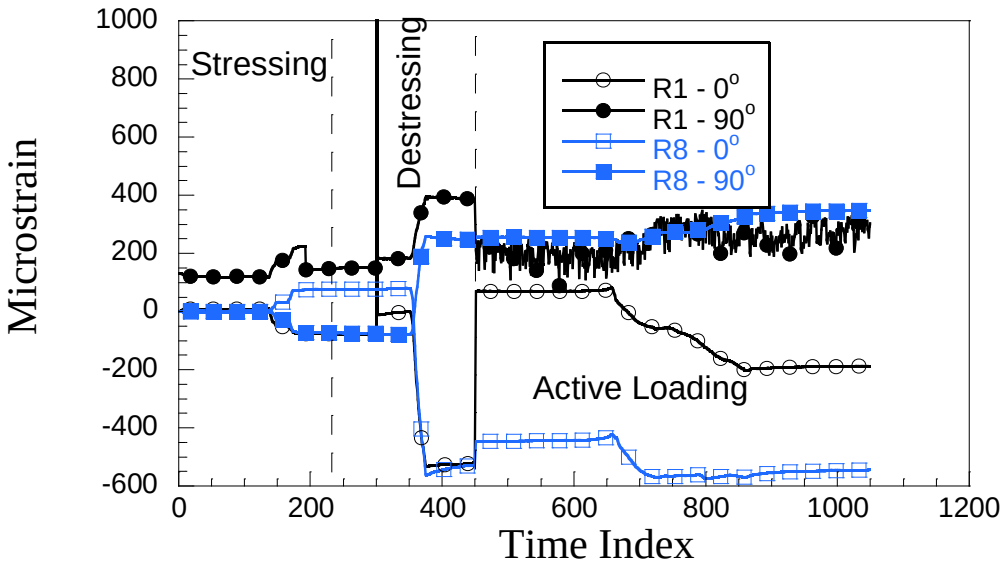

Figure 88. 12-strand – Third Specimen - R1 and R8 Time History

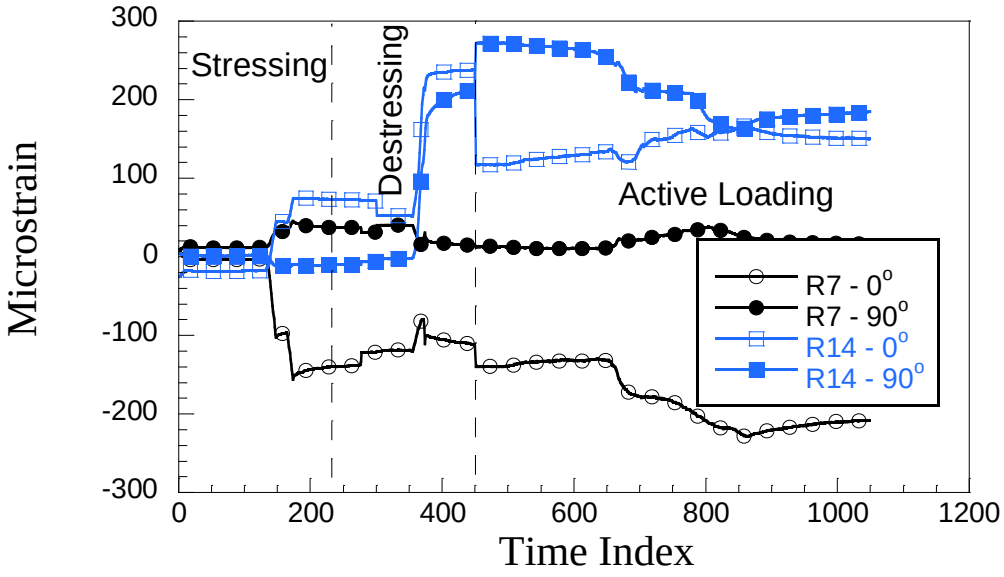

Figure 89. 12-strand – Third Specimen– R7 and R14 Time History

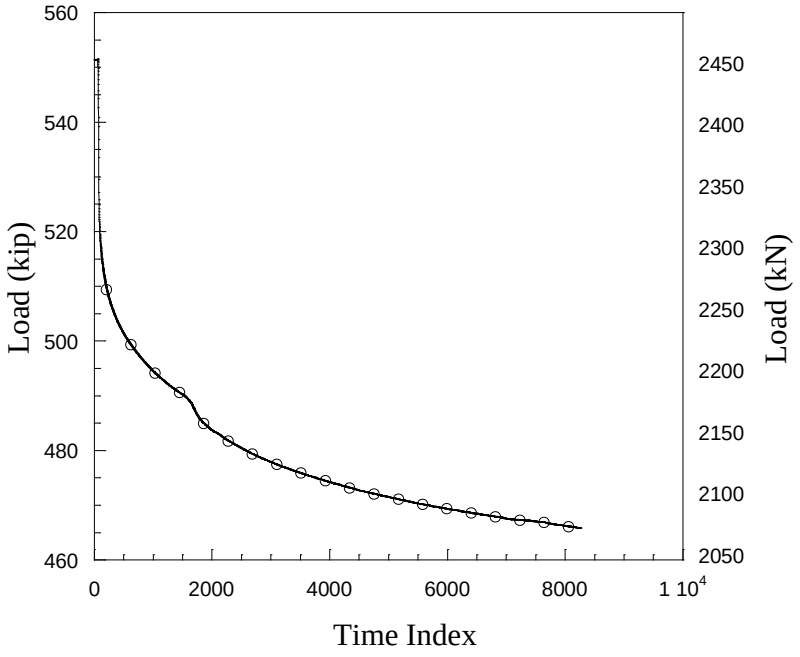

Figure 90. 12-strand - Third Specimen - Load at Active Loading End During De-stressing

The strain profile was also generated at different load increments during the de-stressing and active stressing. The top axial strain profile for the top ($R1_0$-$R7_0$) gages during de-stressing is shown in Figure 91 and axial strain profile for the side ($R8_0$ – $R14_0$) gages is shown in Figure 93. Similarly, the circumferential strain profile for the top ($R1_{90}$-$R7_{90}$) gages and the side ($R8_0$ – $R14_0$) gages are shown in Figure 92 and Figure 94 respectively. Since this specimen experienced a load loss of 86 kips of during de-stressing, the stressing force was not fully transferred; however, the specimen was able to sustain the load after the load loss. From the strain profiles the transfer length of this load (after the 86 kips of lost load) can be estimated at 21".

Strain profiles were also generated for the active loading phase and are shown for the axial top and side strain gages in Figure 95 and Figure 97 respectively, and the circumferential strain for the top and side gages in Figure 96 and Figure 98 respectively. The same "grout plug formation" phenomenon observed in the previous specimen is observed in this one. During active loading it is observed from the axial strain distribution that the tendon pulling is causing the pipe to be in two different states, compression on the free face and tension on the active loading face. As the tendon is pulled, the axial strains were increasing in compression while the circumferential strains were increasing in tension. This grout plug anchored the tendon therefore

placing the pipe in axial compression at the free face. As in the other specimen where a grout plug formed, the strain profile did not show a development length. The grout plug is main anchorage mechanism after the anchor head failure. The specimen was able to hold a pullout load of 605 kips due to this anchorage mechanism.

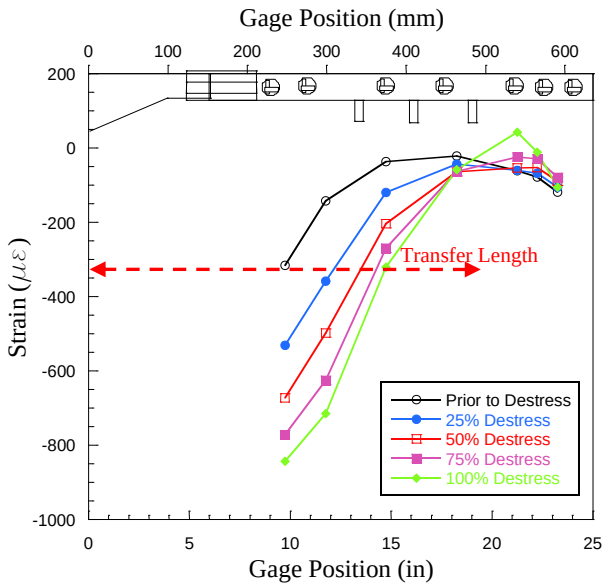

Figure 91. 12-strand – Third Specimen - Top Axial Strain Profile During De-stressing

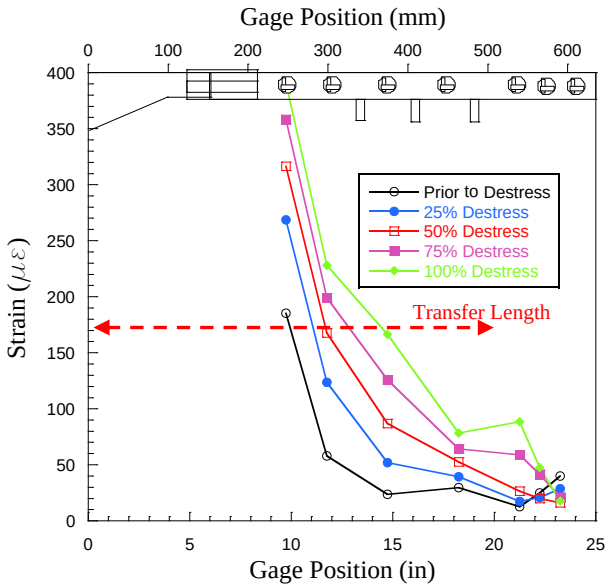

Figure 92. 12-strand – Third Specimen - Top Circumferential Strain Profile During De-stressing

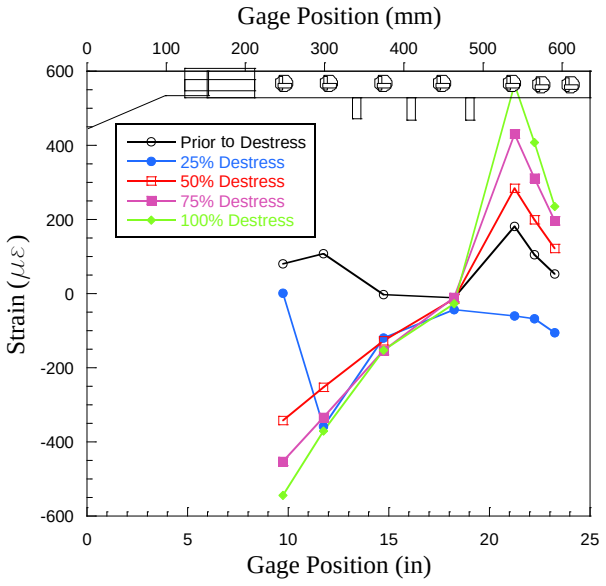

Figure 93. 12-strand - Third Specimen - Side Axial Strain Profile During De-stressing

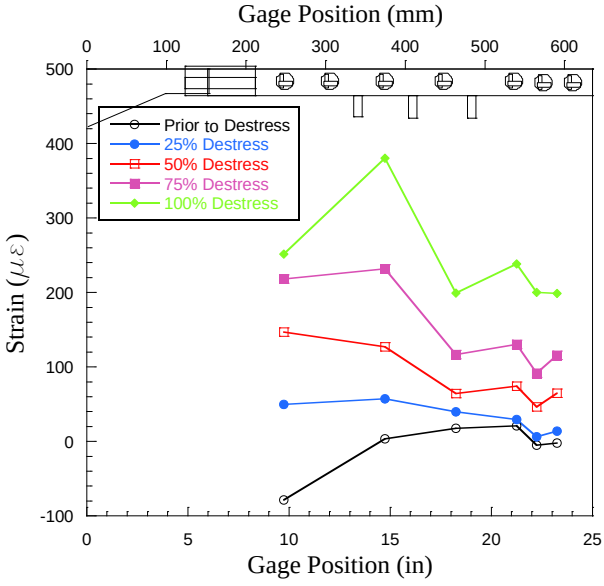

Figure 94. 12-strand – Third Specimen – Side Circumferential Strain Profile During De-stressing

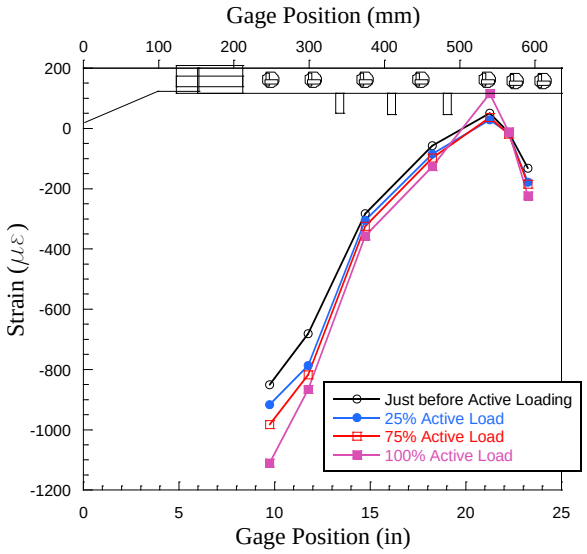

Figure 95. 12-strand – Third Specimen -Top Axial Strain During Active Loading

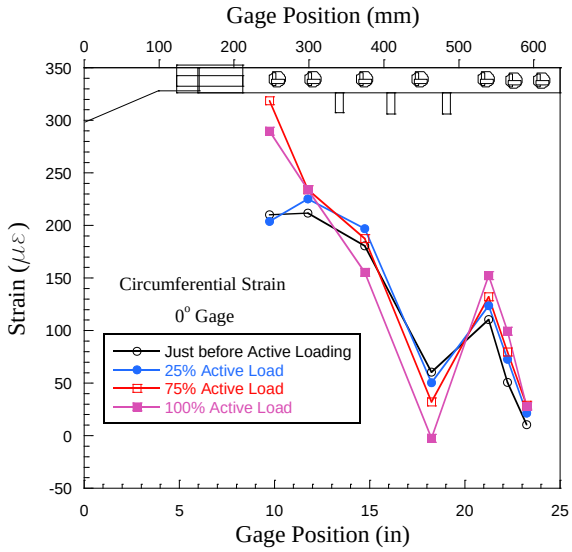

Figure 96. 12-strand – Third Specimen - Top Circumferential Strain During Active Loading

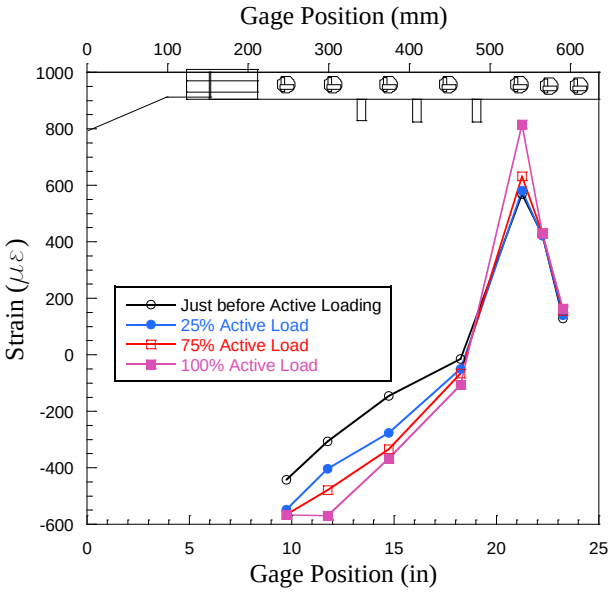

Figure 97. 12-strand – Third Specimen - Side Axial Strain During Active Loading

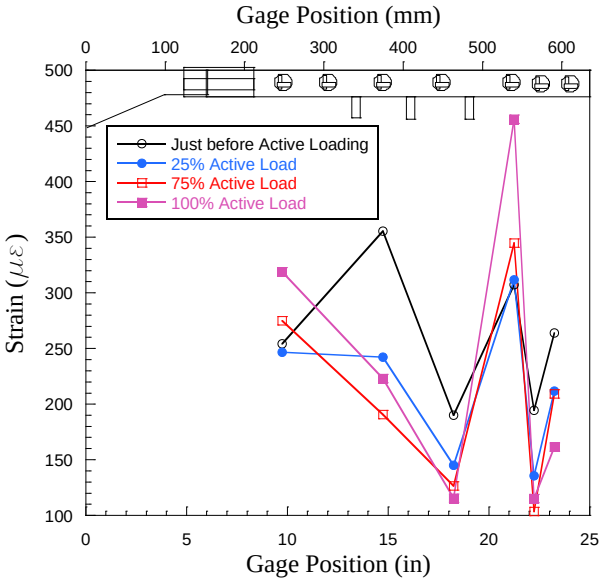

Figure 98. 12-strand – Third Specimen –Side Circumferential Strain During Active Loading

5.6.3 Post-test Observations

After active loading, the hydraulic jacks, and reaction fixtures were removed and DSI bars were de-stressed allowing the visual inspection of the specimen. The same post-active-loading observations that were recorded in the 2nd and 3rd 7-strand and the second 12-strand specimen were observed in this specimen. There was visual indication of slippage between the tendons and PT grout and pipe and PT grout from the active loading end. Once the grout blocker was removed from the free end of the specimen, slippage between the tendon and the grout as well as pipe and PT grout was observed. No cracking was observed in the specimen block due to the active loading procedure.

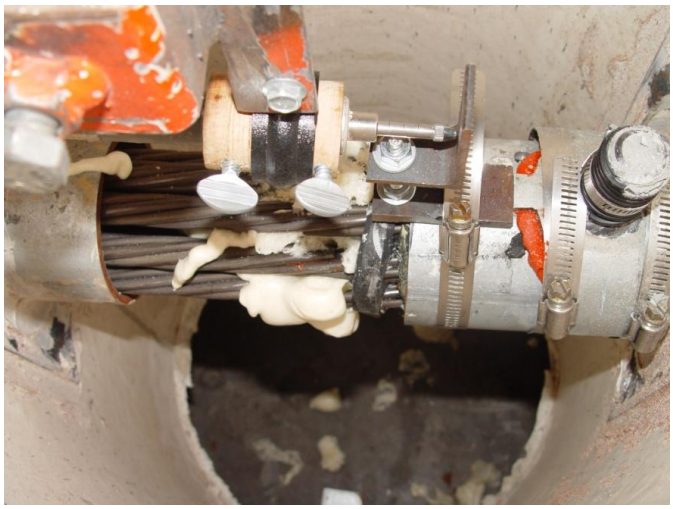

Figure 99. 12-strand - Third Specimen - Active Loading End – Post-active Loading Photo

Figure 100**. 12-strand - Third Specimen - Free Face – Post-active Loading Photo**

5.7 First 19-strand Tendon Specimen (6ft Bond Length)

5.7.1 Test Details

The 19-strand specimen was initially stressed on 1/21/2010. During stressing, a substantial discrepancy between load cells began to occur. Upon reaching at the lock-off force of 835 kips at the sliding fixture load cell, the load cell at the dead-end fixture measured approximately 705 kips. An immediate inspection of the test specimen and surrounding test fixtures was conducted. Inspection revealed that excessive friction was causing the free-end foam block to pull away from the specimen block (Figure 101). Load was immediately relieved for safety reasons. The grout blocking device was redesigned and stressing occurred at a later date. The grout blocking device used for the second stressing utilized a neoprene bearing pad and polished steel plate. Holes were drilled to allowed the strands to pass through the device.

On 1/28/2010 the 19-strand specimen was stressed for the second time. All tendon strands were replaced prior to conducting the second stressing procedure. During the stressing procedure there were no major problems. Although, as seen in previous specimens, there still was discrepancy in load cell measurements at lock-off. Grouting was commenced the following day (2/29/2010)

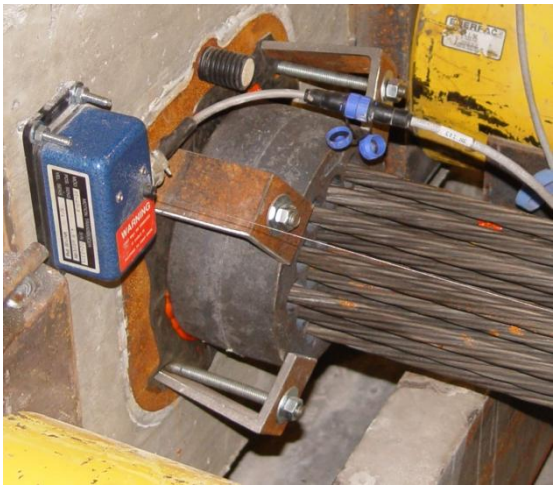

Figure 101. Free-end Grout Block Wedge Plate

Figure 102. New Grout Block Device

De-stressing and active loading procedures commenced on 2/4/2009 and 2/5/2009 respectively. There were no problems observed with the DAQ system or loading procedures. During the de-stressing procedure, a load drop in the order of 150 kips was measured in the dead-end load cell. A photo taken during the active loading procedure can be seen in Figure 103. Results from concrete cylinders and grout cubes can be found in Table 7.

Figure 103. 19-strand During Active Loading

Table 7. 19-strand Cube and Cylinder Strengths

Cubes		**Cylinders**	
Test Date	2/4/2010	*Test Date*	2/9/2010
Sample	Strength (psi)	Sample	Strength (psi)
1	9394	1	8842
2	9664	2	9334
3	9382	3	8447
Average	9480	Average	8874

5.7.2 Numerical Test Results

During de-stressing of the 19-strand, the load cell at the active loading end showed a loss of approximately 172kip as seen in Figure 104. The pipe displacement recorded in gage D1 showed a maximum movement of less than of 0.012" in Figure 105. Therefore, the dissipation of load in the active loading end load cell cannot be associated with pipe slip. Plotting the strain history for the gages closest to the free end during de-stressing in Figure 110 shows the corresponding changes in strain due to the Hoyer Effect in the circumferential direction as well the compression strains in the axial direction. The change in strain is largest at the free end during de-stressing; however, there were minor abrupt changes in the strains closest to the active loading end after the de-stressing is achieved (Figure 111). These changes are negligible compared to the changes that occur at the free end. It is also observed from Figure 111 that there were residual strains from the stressing phase that were in the region of 100 με. This was the case for all the rest of the gages except the R1 and R6, which are the gages closest to the free end. This could imply that the hypothesis proposed in the previous section about the bending of the pipe due to eccentric loading is still valid. From Figure 110 it was observed from the value of the axial strains that the pipe has yielded at that location as R6 (side gage) reached approximately 1100 με. The yielding of the pipe at that location is more apparent in the interpretation of the active loading data in the next paragraph.

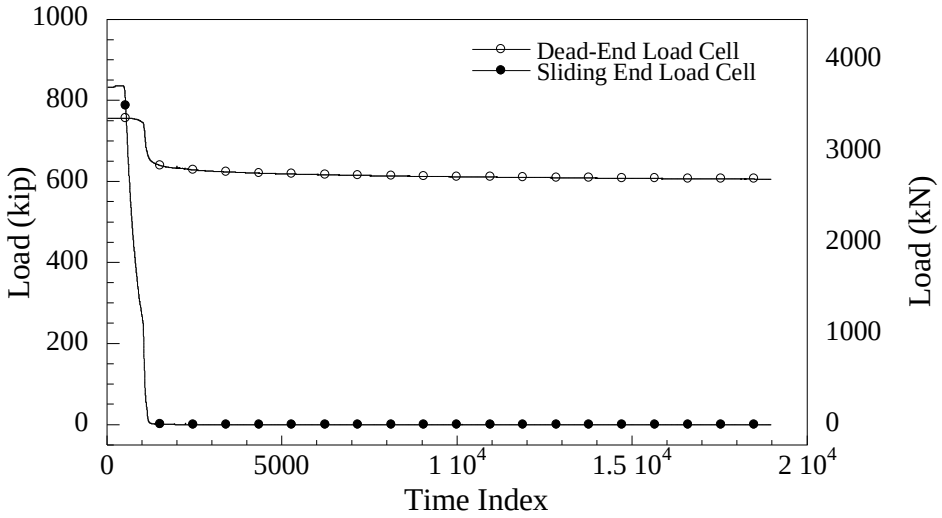

Figure 104. 19-strand – 1st Specimen - De-stressing Load History

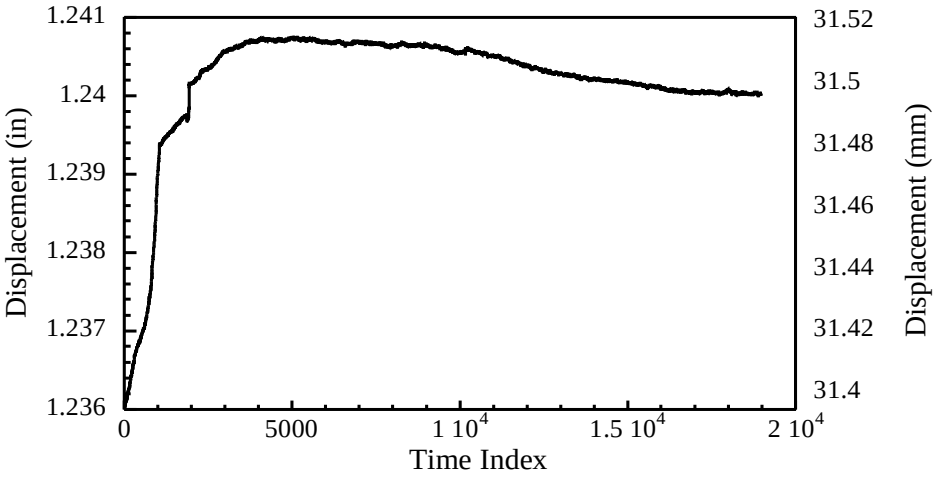

Figure 105. 19-strand 1st specimen - De-stressing Pipe Displacement History

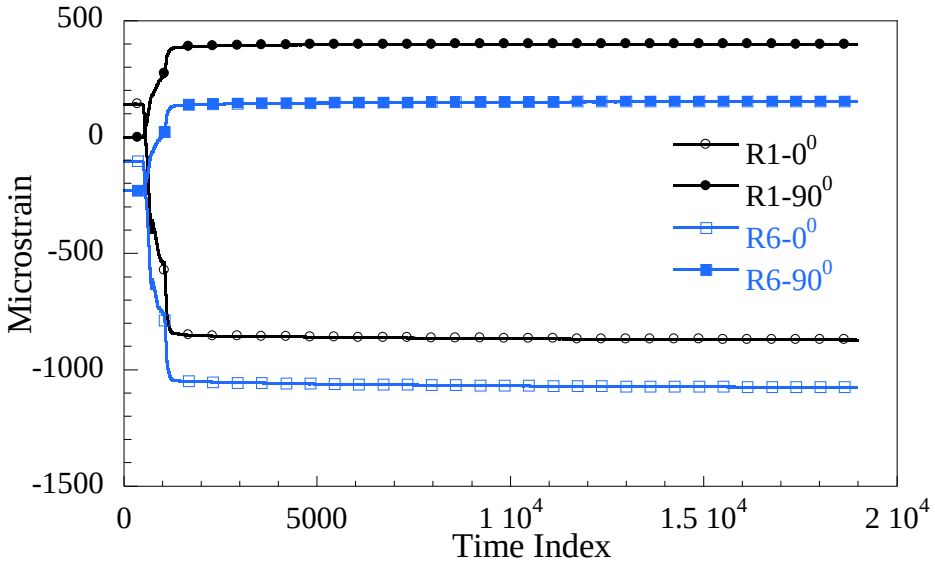

Figure 106. 19-strand – 1st Specimen - De-stressing Strain History: Gages 1 and 6

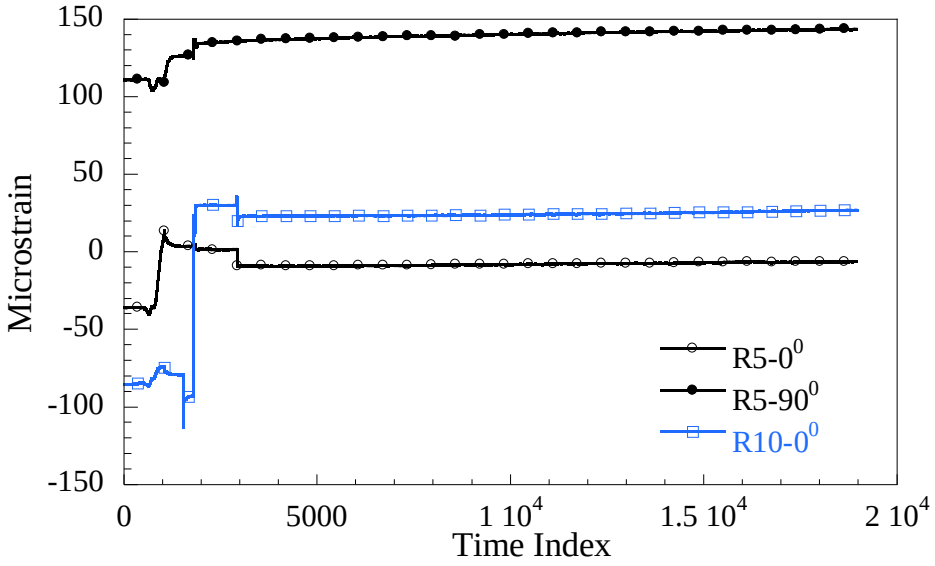

Figure 107. De-stressing Strain History: Gages 5 and 10

The distributions along the pipe, for both the axial and circumferential strains, followed the expected trend, where the Hoyer Effect is obvious in both figures. The gradual decrease of the strain along the pipe shows the rate of transfer of the force into the system, between the first two strain gages as the strains come close to zero within the vicinity of the second strain gage from the free end. From Figure 108 and Figure 109, it can be inferred that the length required for the PT force, after the losses, to be transferred into the system is approximately 60". It is apparent in Figure 110 that the circumferential strains follow the same expected trend for the Hoyer Effect and gradual transfer of the PT force, but the strains never go to zero. This behavior is apparent because as the load increases, the expansive stresses in the concrete block are increasing in the region of the DSI bars, which induces strains on the tube that are not necessarily due to the Hoyer Effect.

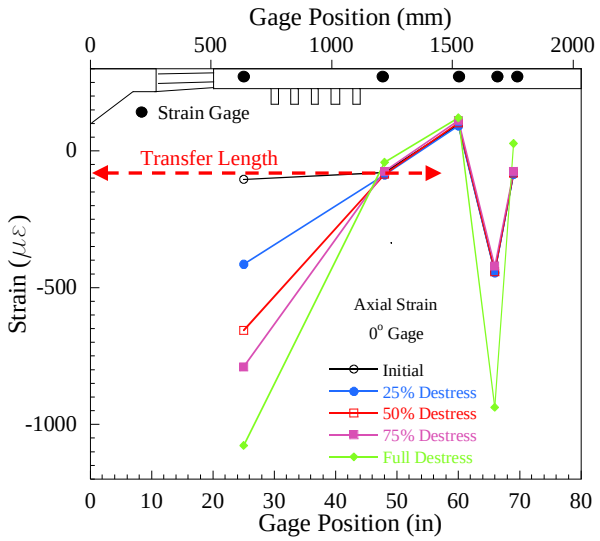

Figure 108. 19-strand Axial Strain Distribution: 0^0 Gage

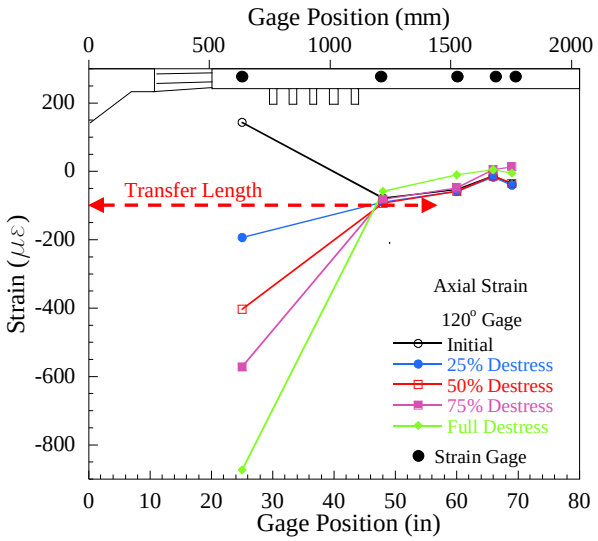

Figure 109 19-strand Axial Strain Distribution: 120^0 Gage

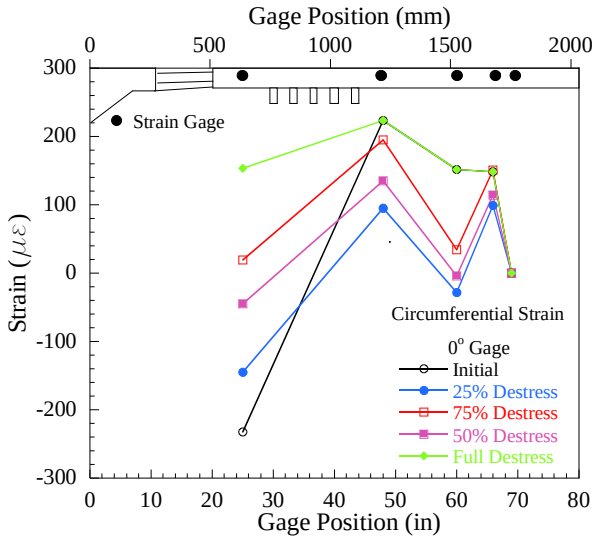

Figure 110. 19-strand Circumferential Strain Distribution: 0^0 Gage

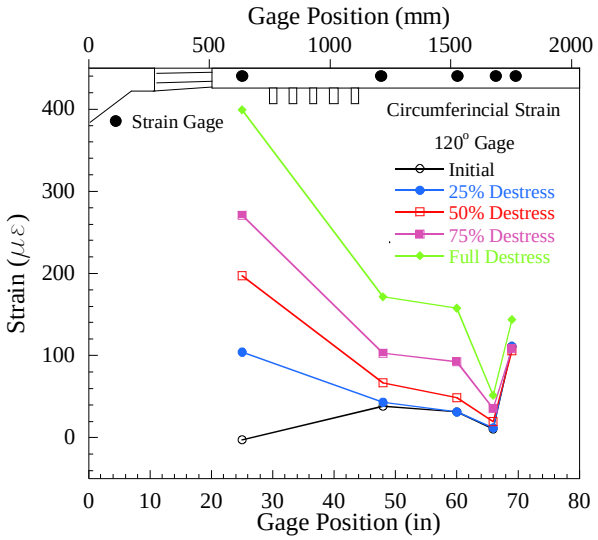

Figure 111. Circumferential Strain Distribution: 120^0 Gage

Between the de-stressing phase and the active loading phase, the load cell at the active loading end recorded negligible losses. During the active loading phase, major cracking of the specimen started to occur at 944kip (Figure 112). The load was increased until it reached

1001.5kip when sharp drops in the load indicated the failure of the specimen. Strain histories for R1 and R6, R2 and R7, and R5 and R10 are shown in Figure 114, Figure 115 and Figure 116. The very sharp increase in the strain values in gages R1 and R6 imply that the pipe has yielded. As the load was increased the strain gages failed. The same plots show that R2 and R7 also failed in tension.

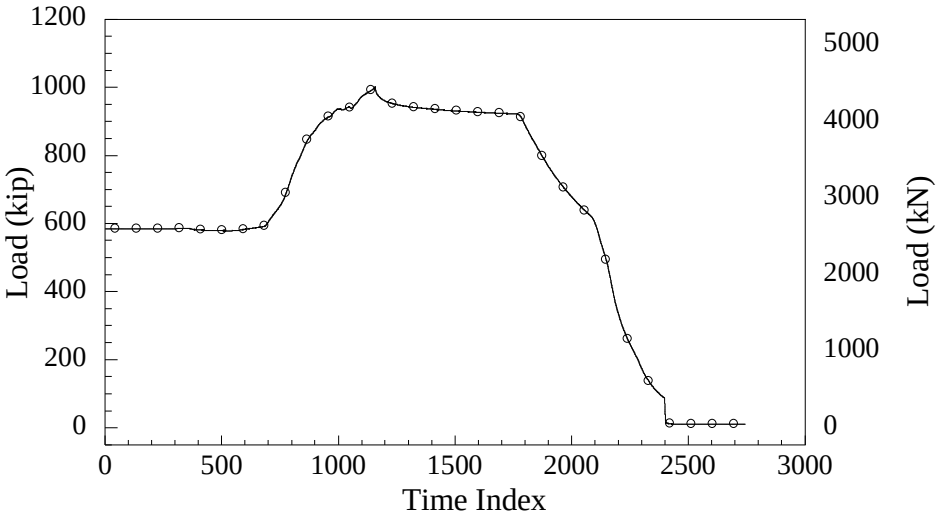

Figure 112. Loading History During Active Loading

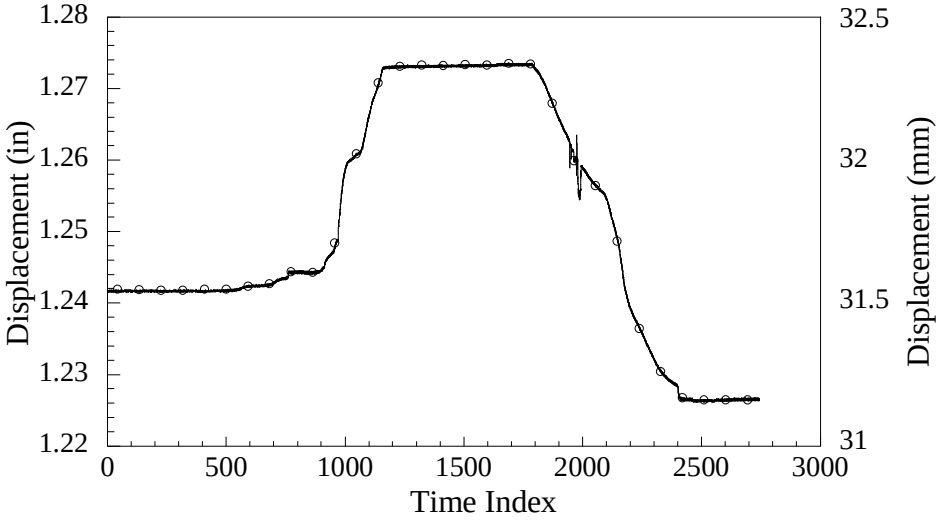

Figure 113. Pipe Displacement History during Active Loading

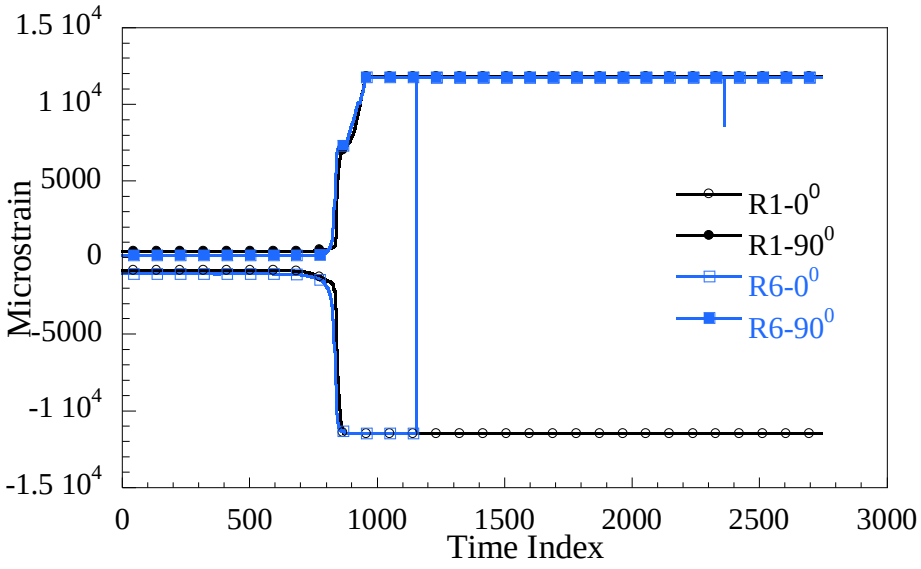

Figure 114. Active Loading Strain History for Gages 1 and 6

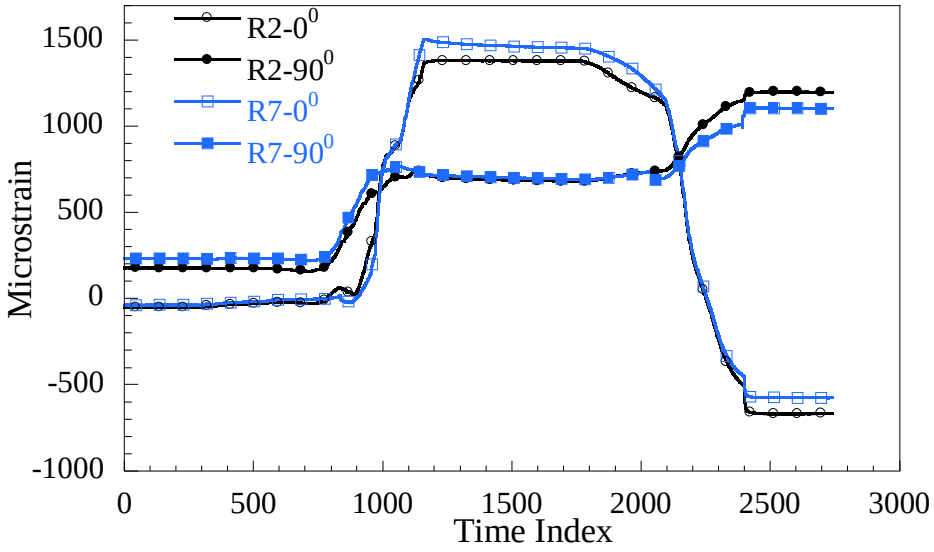

Figure 115. Active Loading Strain History for Gages 2 and 7

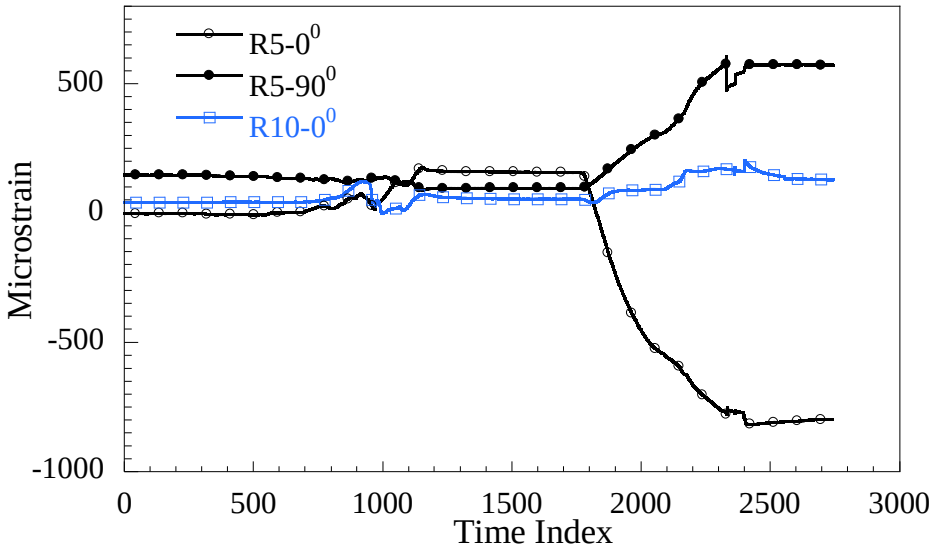

Figure 116. Active Loading Strain History for Gages 5 and 10

The strain distributions along the pipe are shown in Figure 117through Figure 120. It can be seen that the same mechanism that occurred in the 7 and 12 strand specimens was occurring in this specimen as well. However, due to very high compressive stresses in the steel tube at the free face, the tube started yielding in the de-stressing phase. As soon as the tendon was pulled from the active loading end, small increases in the load caused great increases in the strains, especially in gages R1 and R6 that already experienced yielding strains during de-stressing. As the load started to increase more, the pipe started to show yielding at the R2 and R7 locations where the axial and circumferential strains were increasing in tension as the pipe was expanding due to the great Hoyer stresses inside the tube.

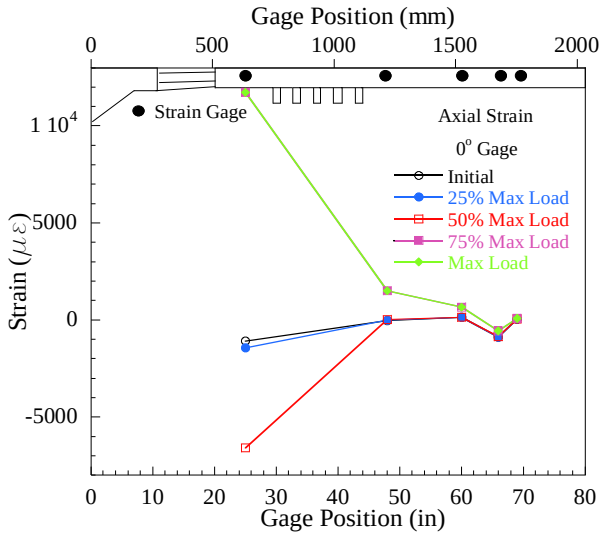

Figure 117. 19-strand Axial Strain Distribution During De-stressing: 0^0 Gage

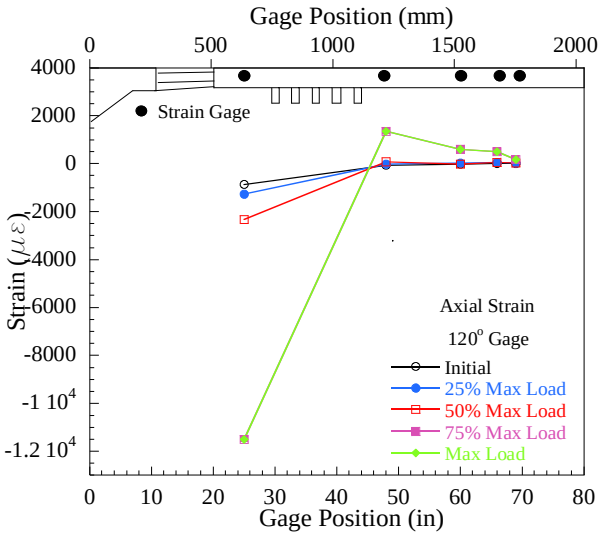

Figure 118. 19-Strand Axial Strain Distribution During De-stressing: 120^0 Gage

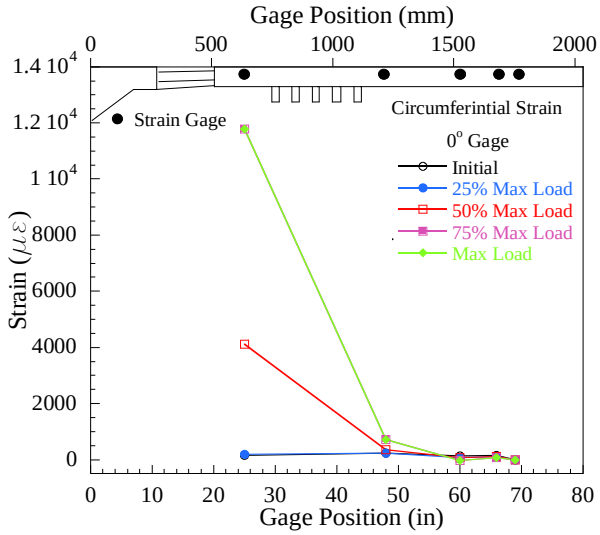

Figure 119. 19-Strand Circumferential Strain Distribution During De-stressing: 0^0 Gage

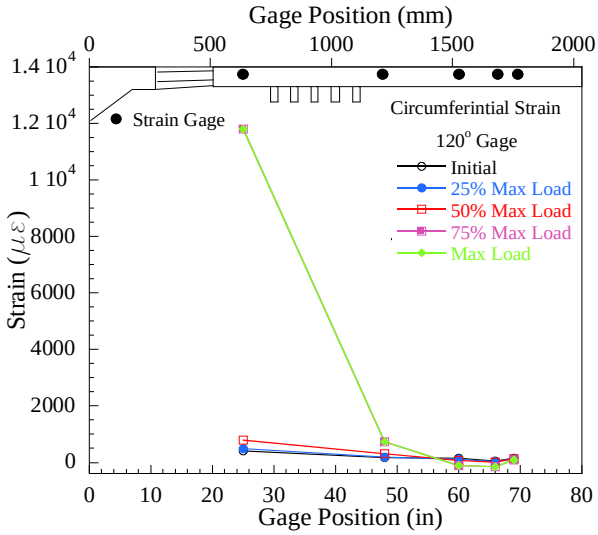

Figure 120. 19-Strand Circumferential Strain Distribution During De-stressing: 120^0 Gage

5.7.3 Post-Test Observations

After testing, an inspection of the 19-strand specimen revealed that a significant amount of cracking occurred within the specimen block. It can be seen in Figure 121 that cracks propagate diagonally from the active loading locations to the free face of the block. Furthermore, a large crack was found to have opened up through the tension tie region of the specimen block. Figure 122 shows cracks that have radial trajectories originating from the wedge plate bearing plate that were also found during inspection. Given the crack patterns that were found and data that was compiled from the test, it was decided to break the 19-strand specimen block apart and remove the steel pipe.

Upon removal, it was found that the pipe had expanded significantly at the free face. Furthermore, there was obvious local failure of R1 and R6 (Figure 123). This would imply that a schedule 40 steel pipe does not possess sufficient strength for such high stresses. The steel tube employed in this specimen was per VSL and FDOT specifications and it is the same tube used in the field. This raises questions about changing the specification of the steel tubing. However since this was not an objective in this research, the remaining 19-strand specimens were cast using the same schedule 40 pipe.

Figure 121. Photo of 19-Strand Specimen Block Cracking

Figure 122. Photo of Radial Cracking of the specimen around the tube

Figure 123. Deformed Location of 19-strand Pipe (R1/R6 location)

After thorough inspection of the removed pipe, the plastic trumpet and bearing plate were cut of the pipe section. Figure 124 shows the cured grout found under the removed trumpet section. It can be seen that excessive amount cracking occurred during either the de-stressing or active loading phases of the test. Crack trajectories would indicate high levels of compressive stress within the grout region. This cracking could also be partially due to radial expansion of embedded strand during de-stressing. Radial expansion of strand can be seen to have caused spalling near the removed bearing plate (Figure 125).

Figure 124. Grout as-found Under Removed Trumpet

Figure 125. Cracking Located at the Removed Bearing Plate

5.8 Second 19-strand Tendon Specimen (Shear Flanges at the Center of Pipe)

5.8.1 Test Details

The third 19-strand specimen was stressed on 11/23/2010. There were no significant deflections of the specimen recorded during the stressing phase. The two load cells were reflecting loads with no discrepancies during stressing. During de-stressing, the load cell at the active loading end showed 36 kips of load loss.

Specimen grouting proceeded the following day (11/24/2010). The specimen block and test fixture were monitored overnight. There were no observed changes in specimen or fixture measurements. There were no problems observed during the grouting procedure and no grout leakage or bleeding was observed. De-stressing and active loading procedures were carried on 11/30/2010 and 12/01/2010 respectively. There were no problems observed with the DAQ system or loading procedures. Results from concrete cylinders and grout cubes can be found in Table 8.

Table 8. 19-strand 2nd Specimen - Grout Cubes and Concrete Cylinder Strengths

Cubes		**Cylinders**	
Test Date	11/30/2010	*Test Date*	12/1/2010
Sample	Strength (psi)	Sample	Strength (psi)
1	8074	1	8622
2	--	2	8529
3	7692	3	8648
Average	7883	Average	8600

5.8.2 Numerical Test Results

The time history plots for this specimen are shown in Figure 126, Figure 127 and Figure 128. As in all the previous specimens, the horizontal axis does not reflect the real time of which the experiment was performed. These plots are meant to show the continuity of the loads and strains through the different stages: stressing of the tendon, load transfer from the tendon into the system (de-stressing), and active loading.

The load throughout the various portions of the testing procedure is shown in Figure 126. During stressing and de-stressing, the data from load cell at the free end was used. During active loading, the data from the load cell at the active loading end was used. The tendon load increases in the stressing phase, then decreases during de-stressing as the load is transferred to the system (grout, pipe and concrete block). During active loading, the load is increased to 811 kips. The specimen was unable to hold the load. As seen in Figure 126 the load decreases exponentially to a constant value allowing the tendon to slip. Then the load was increased to 933 kips (90% of GUTS) and the same behavior occurred where slip occurs between the grout and pipe. The specimen was able to hold a load of 770 kips after each reloading to 90% GUTS. The change in load with time can be correlated with the strain changes observed in the two subsequent plots. Figure 127 and Figure 128 show the strain history in gages R1/R16 (the 2 sets of gages located at the free face) in the axial and circumferential directions on the pipe and Figure 128 shows a similar plot for the gages on the active loading end (R15/R30). Over the course of the test, several discontinuities in recorded strain values were observed due to environmental and accident interference. Data was post-processed to remove these discontinuities.

Figure 129 shows the load at the active loading end during de-stressing. This plot shows a load loss of 36 kips during de-stressing. Therefore, the stressing load was not fully transferred

into the specimen during de-stressing and slip could have happened. After the 36 kip load loss, the specimen was able to hold the remaining load.

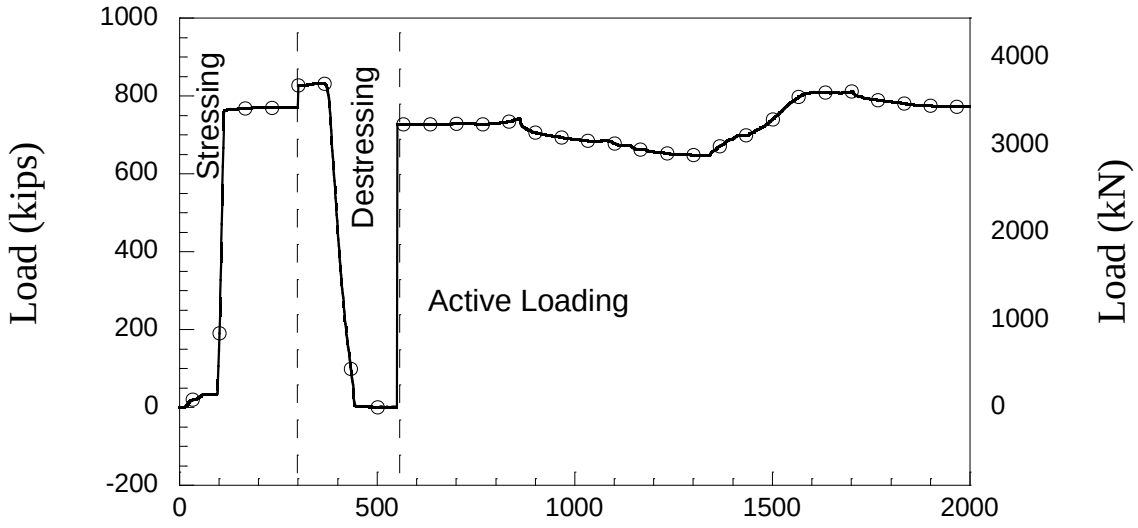

Figure 126. 19-strand – Second Specimen - Tendon Load Time History

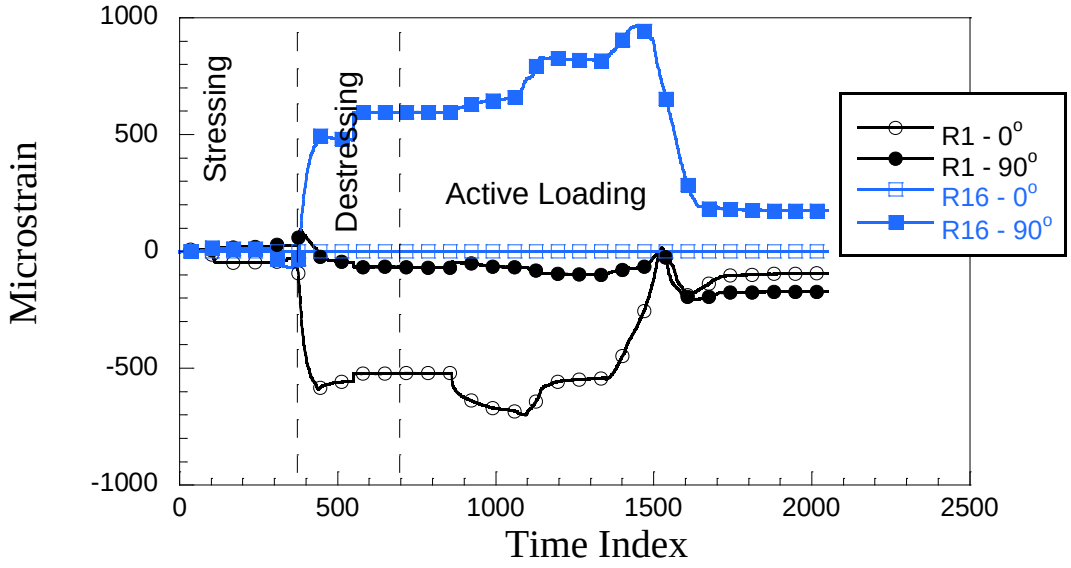

Figure 127. 19-strand – Second Specimen – R1 and R16 Time History

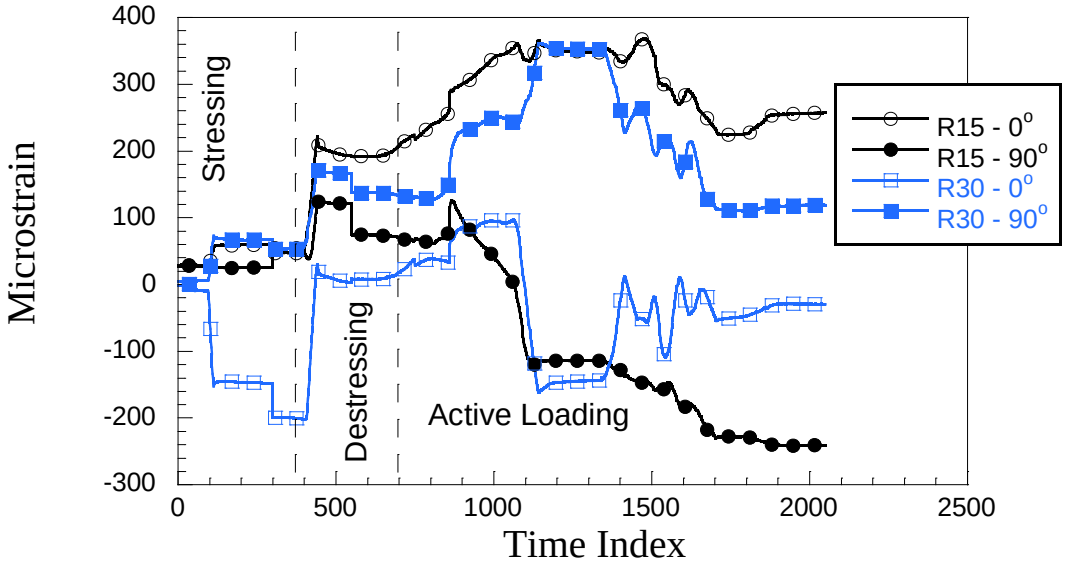

Figure 128. 19-strand – Second Specimen – R15 and R30 Time History

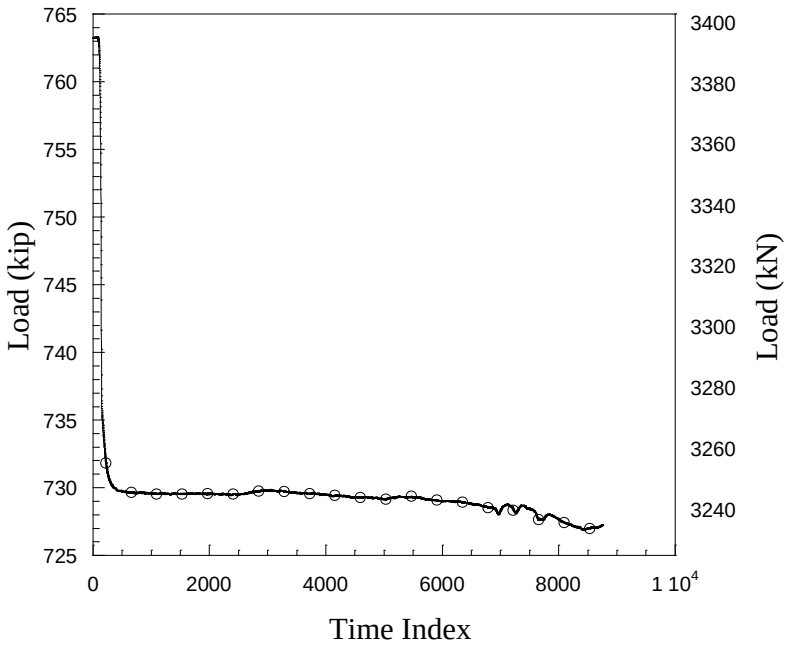

Figure 129. 19-strand - Second Specimen - Load at Active Loading End During Destressing

The strain profile was also generated at different load increments during the de-stressing and active stressing. The top axial strain profile for the top ($R1_0$-$R15_0$) gages during de-stressing is shown in Figure 130 and axial strain profile for the side ($R16_0$ – $R30_0$) gages is shown in

Figure 132. Similarly, the circumferential strain profile for the top ($R1_{90}$-$R15_{90}$) gages and the side ($R16_0$ – $R30_0$) gages are shown in Figure 131 Figure 133 respectively. Since this specimen experienced a load loss of 36 kips of during de-stressing, the stressing force was not fully transferred; however, the specimen was able to sustain the load after the load loss. From the strain profiles the transfer length of this load (after the 36 kips of lost load) can be estimated at 55".

Strain profiles were also generated for the active loading phase and are shown for the axial top and side strain gages in Figure 134 and Figure 136 respectively, and the circumferential strain for the top and side gages in Figure 135 and Figure 137, respectively. In this specimen, there was no grout plug formation observed. This can be particularly seen from Figure 134 where there are no irregularities in the strain readings. As the tendon is pulled a slip between the grout and pipe is observed then the tendon starts to develop. The strand in this specimen is not fully developed and slip of the tendon was observed. The specimen however, was able to hold a pullout load of 770 kips. From the strain profile plots, it appeared that the secondary anchorage was provided by two mechanisms: grout plug formation and strand development. The development length is estimated at approximately 58 inches.

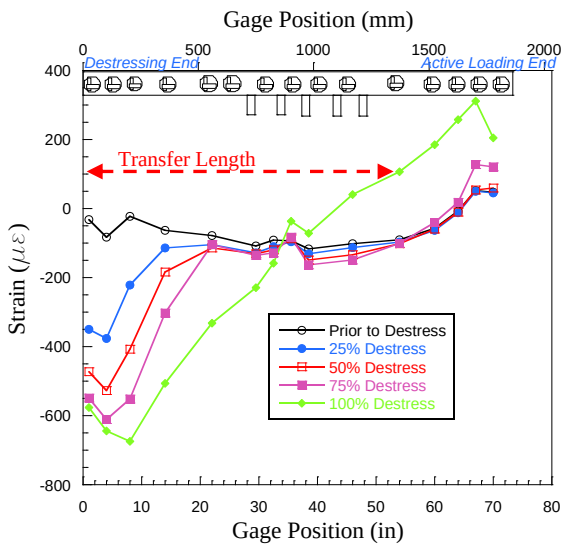

Figure 130. 19-strand – Second Specimen - Top Axial Strain Profile During De-stressing

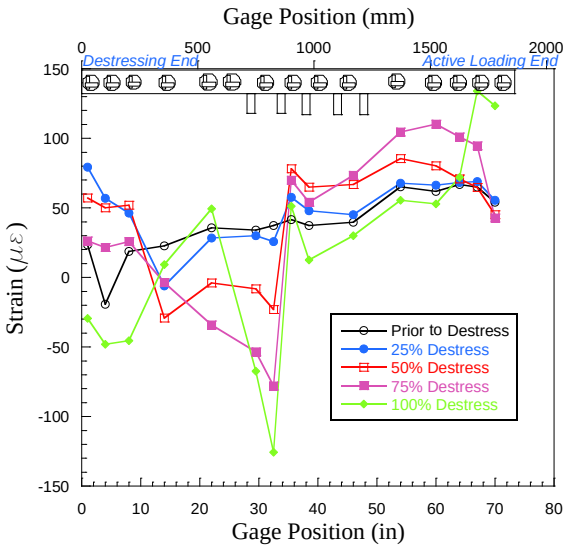

Figure 131. 19-strand – Second Specimen - Top Circumferential Strain Profile During De-stressing

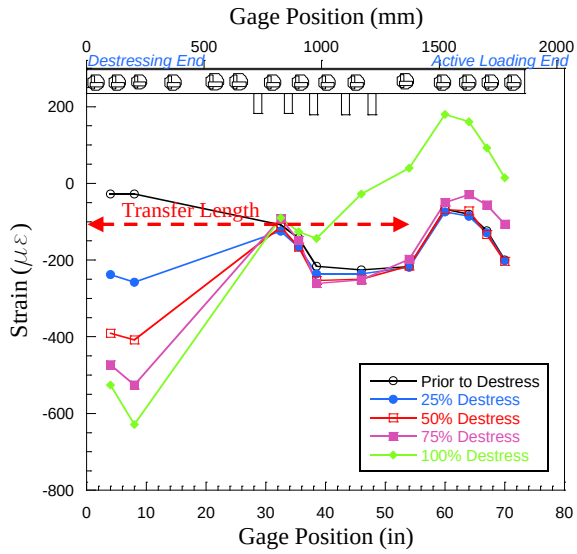

Figure 132. 19-strand – 2nd Specimen - Side Axial Strain Profile During De-stressing

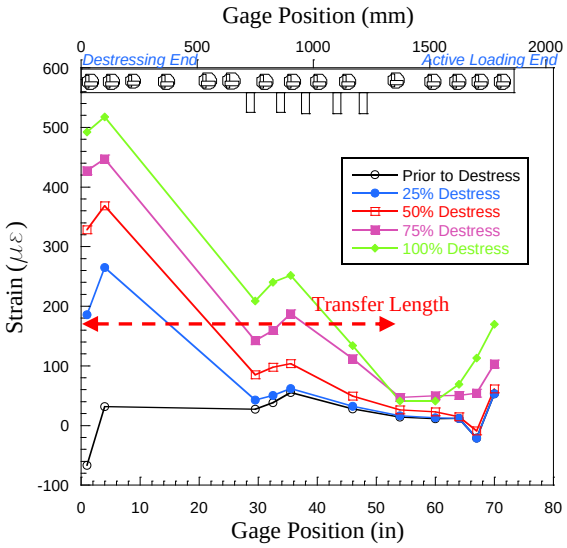

Figure 133. 19-strand – 2nd Specimen – Side Circumferential Strain Profile During De-stressing

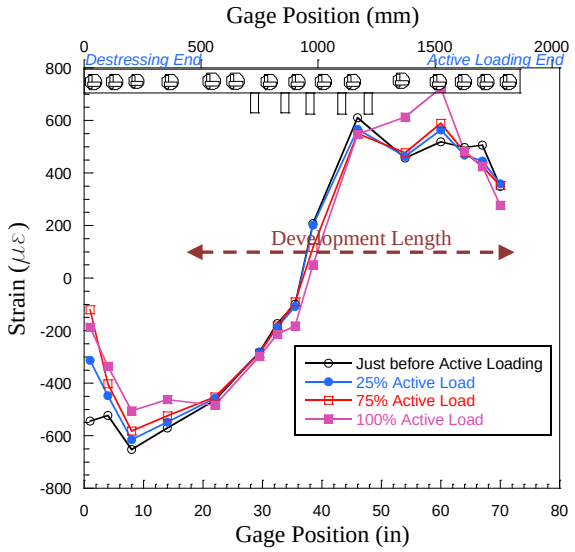

Figure 134. 19-strand – Second Specimen -Top Axial Strain During Active Loading

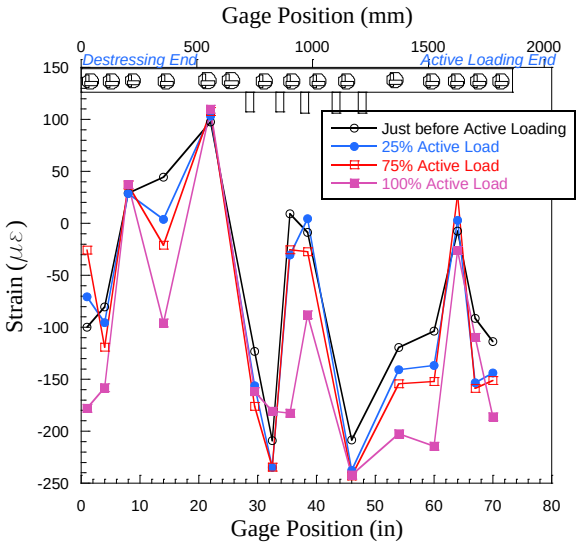

Figure 135. 19-strand – Second Specimen - Top Circumferential Strain During Active Loading

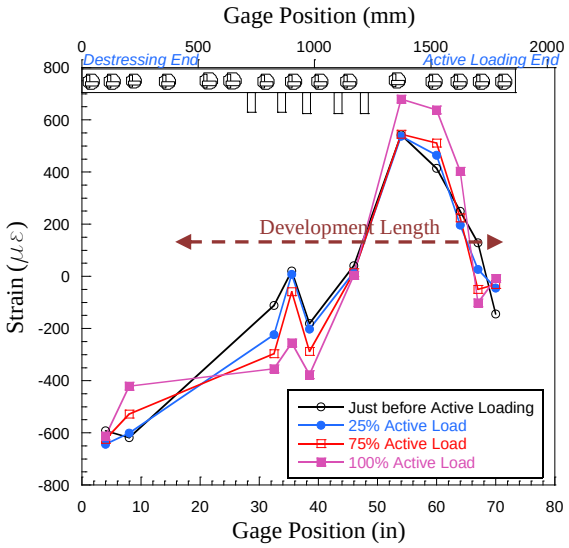

Figure 136. 19-strand – Second Specimen - Side Axial Strain During Active Loading

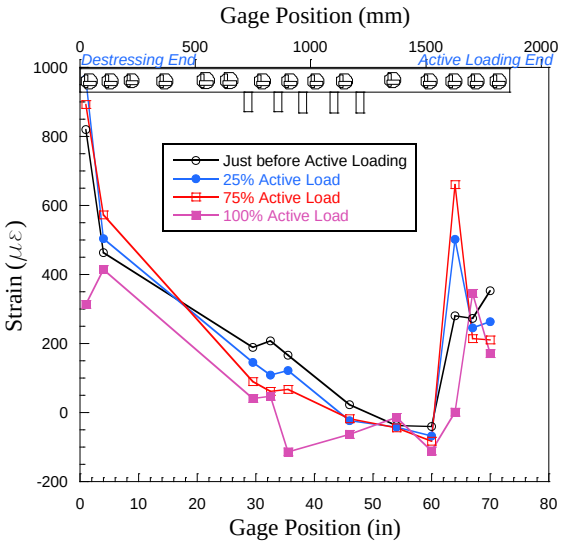

Figure 137. 19-strand – Second Specimen –Side Circumferential Strain During Active Loading

5.8.3 Post-test Observations

After active loading, the hydraulic jacks, and reaction fixtures were removed and DSI bars were de-stressed allowing the visual inspection of the specimen. Similar observations were recorded for this specimen as those seen in the observations that were recorded in the 2nd and 3rd 7-strand and 12-strand specimens. There was visual indication of slippage between the tendons and PT grout and pipe and PT grout from the active loading end. Once the grout blocker was removed from the free end of the specimen, slippage between the tendon and the grout and the pipe and grout was observed as seen in Figure 138. No cracking was observed in the specimen block due to the active loading procedure (Figure 139).

Figure 138. Second 19-strand Specimen Photo- Active Loading End After Pullout

Figure 139. Second 19-strand Specimen Photo- Destressing End - After Pulllout

5.9 Third 19-strand Tendon Specimen (Shear Flanges Spread out through Pipe)

5.9.1 Test Details

The third 19-strand specimen was stressed on 1/3/2010. There were no significant deflections of the specimen recorded during the stressing phase. The two load cells were reflecting loads with no discrepancies during stressing. During de-stressing, the load cell at the active loading end showed 117 kips of load loss.

Specimen grouting proceeded the following day (1/24/2010). The specimen block and test fixture were monitored overnight. There were no observed changes in specimen or fixture measurements. There were no problems observed during the grouting procedure. No grout leakage or bleeding was observed. De-stressing and active loading procedures were carried on 01/05/2010 and 01/06/2010 respectively. There were no problems observed with the DAQ system or loading procedures. Results from concrete cylinders and grout cubes can be found in Table 9.

Table 9. 19-strand 3rd Specimen - Grout Cubes and Concrete Cylinder Strengths

Cubes		**Cylinders**	
Test Date	1/10/2011	*Test Date*	1/12/2011
Sample	Strength (psi)	Sample	Strength (psi)
1	9637	1	9041
2	9521	2	8757
3	1080	3	9105
Average	9746	Average	8968

5.9.2 Numerical Test Results

The time history plots for this specimen are shown in Figure 140, Figure 141 and Figure 142. The horizontal axis does not reflect the real time of which the experiment was performed. These plots are meant to show the continuity of the loads and strains through the different stages: Stressing of the tendon, load transfer from the tendon into the system de-stressing, and active loading.

The tendon load, in Figure 140, increases in the stressing phase, then decreases during de-stressing as the load is transferred to the system (grout, pipe and concrete block). During active loading, the load is increased to 933 kips (90% of GUTS). The specimen was unable to hold the load. As seen in Figure 140 the load decreases exponentially to a constant value allowing the tendon to slip. Then the load was increased to 90% of GUTs and the same behavior occurred where slip occurs between the grout and pipe. The latter part is not shown in the time history plot. The change in load with time can be correlated with the strain changes observed in the two subsequent plots. Figure 141 show the strain history in gages R1/R16 (the 2 sets of gages located at the free face) in the axial and circumferential directions on the pipe and Figure 142 shows a similar plot for the gages on the active loading end (R15/R30). Over the course of the test, several discontinuities in recorded strain values were observed due to environmental and accident interference. Data was post-processed to remove these discontinuities.

Figure 143 shows the load at the active loading end during de-stressing. This plot shows a load loss of 117 kips during de-stressing. Therefore, the stressing load was not fully transferred into the specimen during de-stressing and slip could have happened. After the 36 kip load loss, the specimen was able to hold the remaining load.

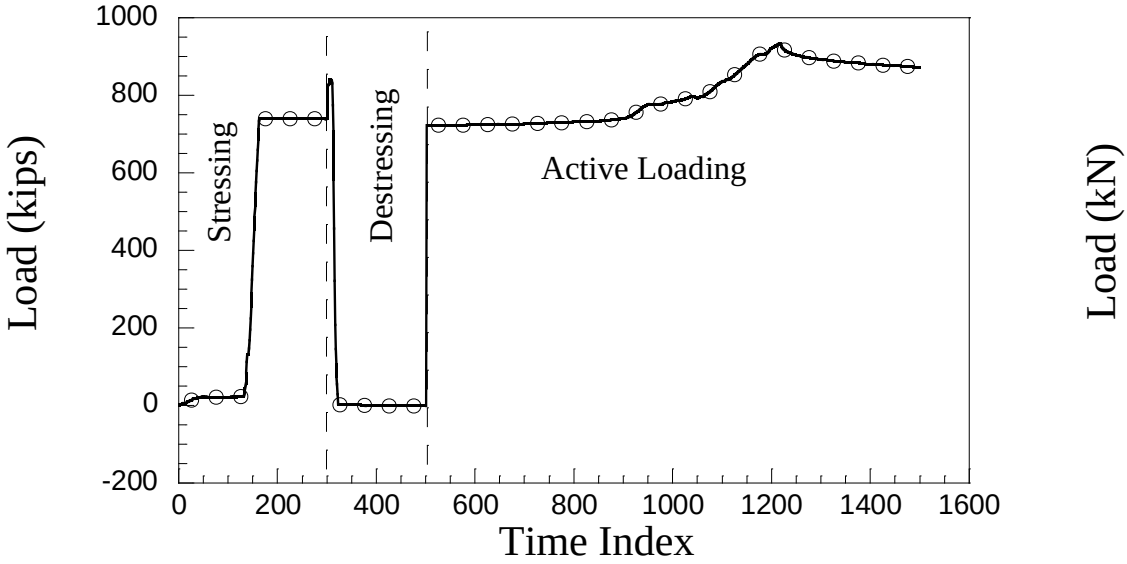

Figure 140. 19-strand – Third Specimen - Tendon Load Time History

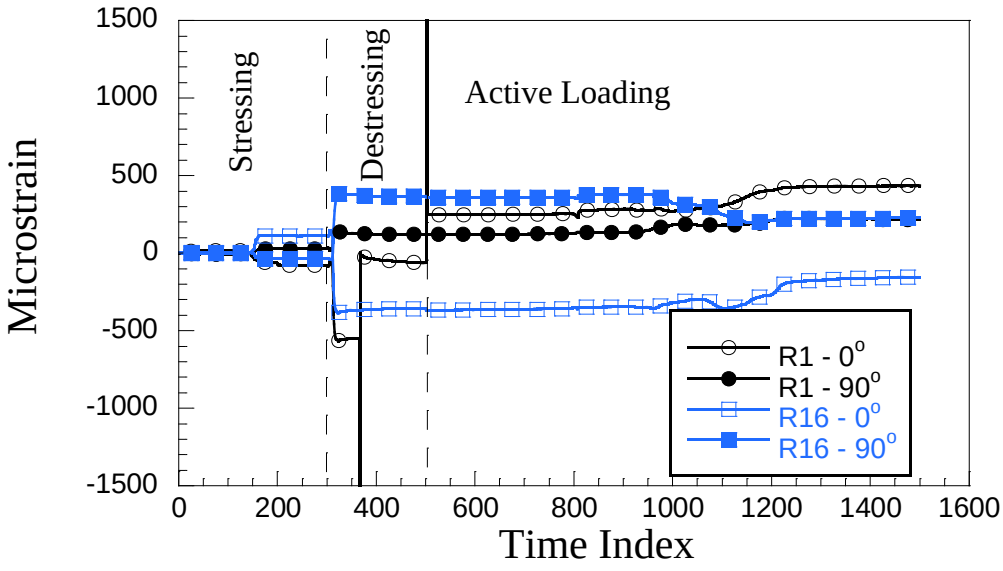

Figure 141. 19-strand – Third Specimen – R1 and R16 Time History

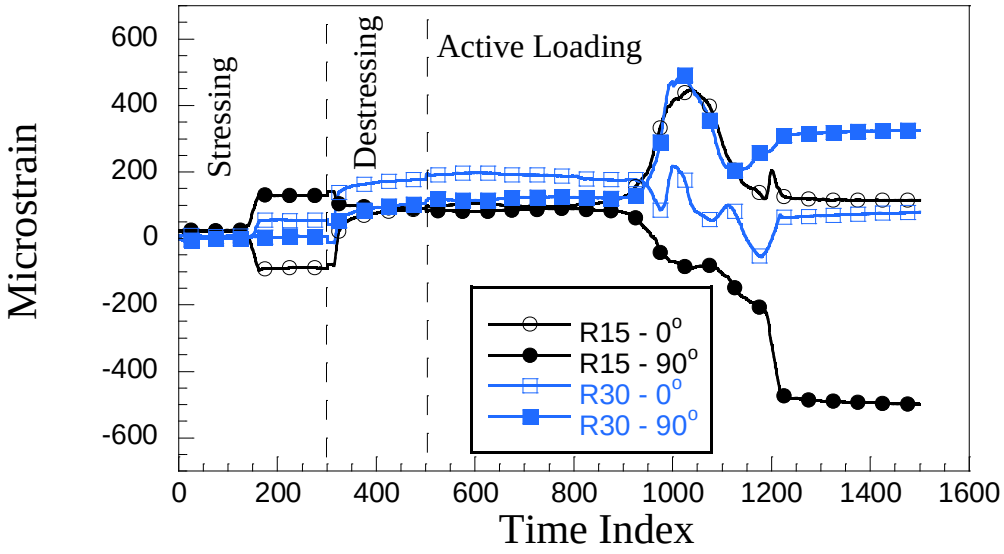

Figure 142. 19-strand – Third Specimen – R15 and R30 Time History

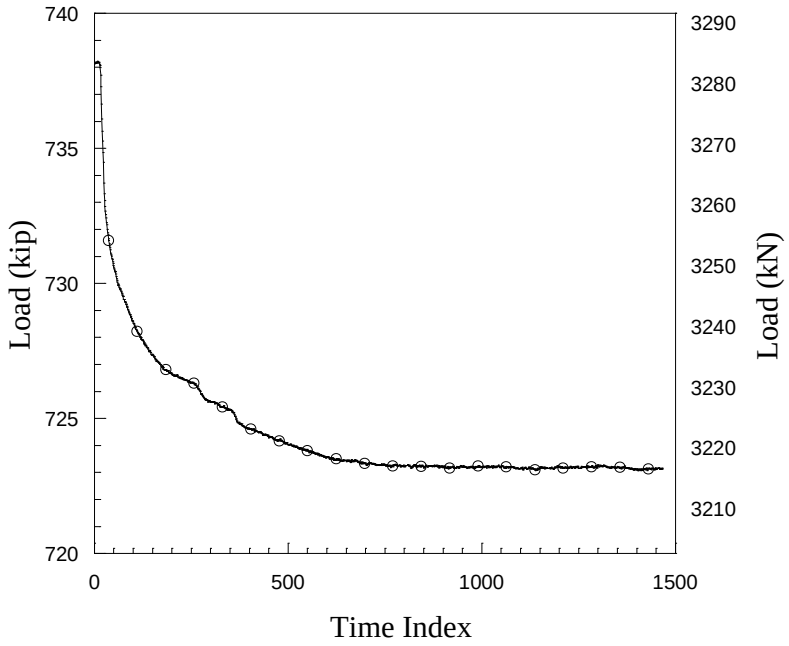

Figure 143. 129-strand - Third Specimen - Load at Active Loading End During De-stressing

The strain profile was also generated at different load increments during the de-stressing and active stressing. The top axial strain profile for the top ($R1_0$-$R15_0$) gages during de-stressing is shown in Figure 144 and axial strain profile for the side ($R16_0$ – $R30_0$) gages is shown in Figure 146. Similarly, the circumferential strain profile for the top ($R1_{90}$-$R15_{90}$) gages and the

side ($R16_0$ – $R30_0$) gages are shown in Figure 145 and Figure 147, respectively. Since this specimen experienced a load loss of 117 kips of during de-stressing, the stressing force was not fully transferred; however, the specimen was able to sustain the load after the load loss. From the strain profiles the transfer length of this load (after the 117 kips of lost load) can be estimated 50".

Strain profiles were also generated for the active loading phase and are shown for the axial top and side strain gages in Figure 148 and Figure 150 respectively, and the circumferential strain for the top and side gages in Figure 149 and Figure 151, respectively. In this specimen, there formation of grout plug is not apparent from Figure 148 through Figure 151. The strand appeared to be developing over a length of 50 inches from the strain profile plots (Figure 148 through Figure 151) ; however, the 90% GUTS pullout load was not held and the strand slipped. The load specimen sustained a load of 872 kips, but kept decreasing at a very slow rate. Therefore, it is concluded that the specimen did not have enough length and strength to fully develop the 90% GUTS pullout load.

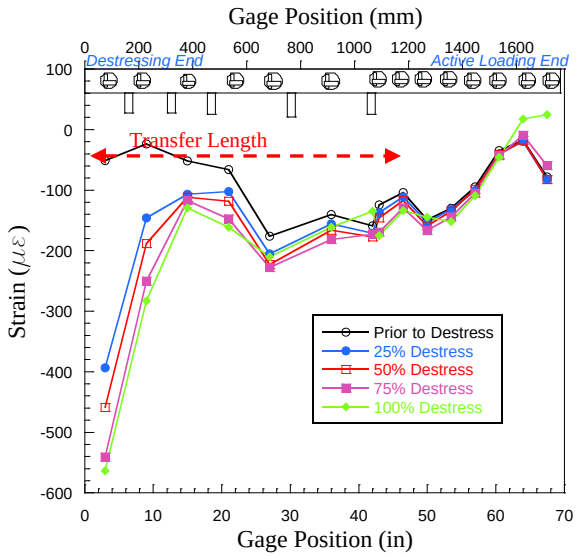

Figure 144. 19-strand – Third Specimen - Top Axial Strain Profile During De-stressing

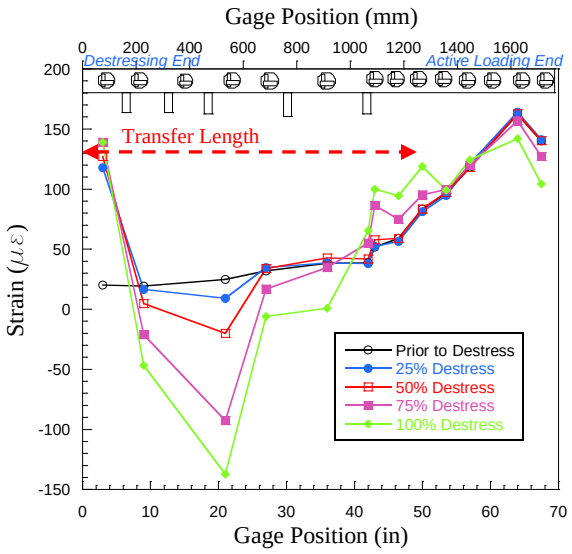

Figure 145. 19-strand – Third Specimen - Top Circumferential Strain Profile During De-stressing

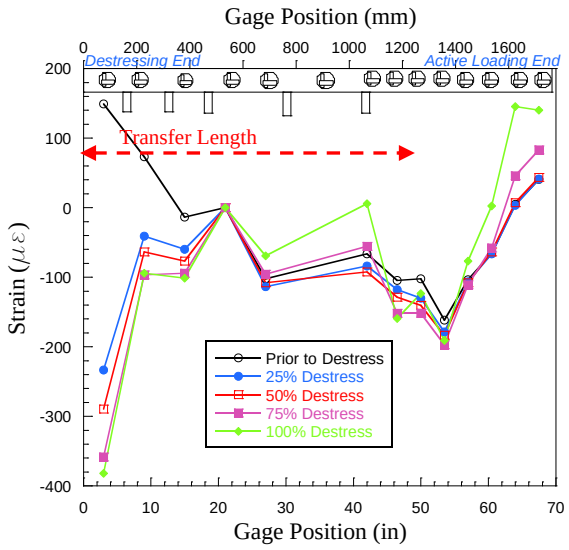

Figure 146. 19-strand – Third Specimen - Side Axial Strain Profile During De-stressing

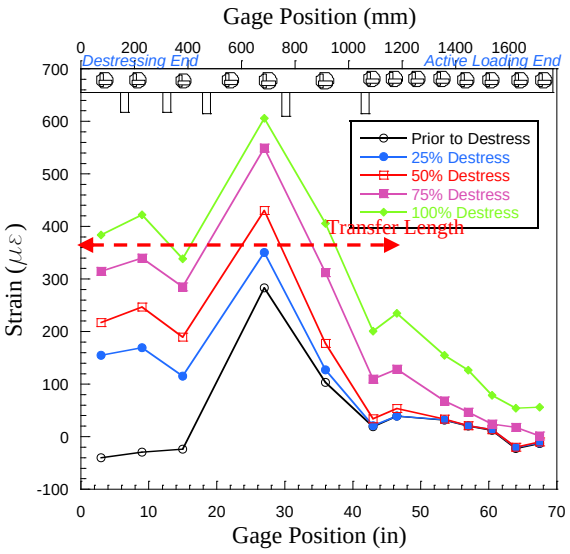

Figure 147. 19-strand – Third Specimen – Side Circumferential Strain Profile During De-stressing

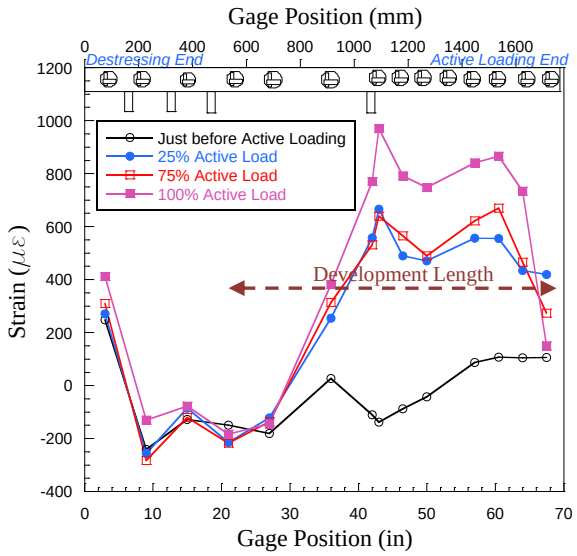

Figure 148. 19-strand – Third Specimen -Top Axial Strain During Active Loading

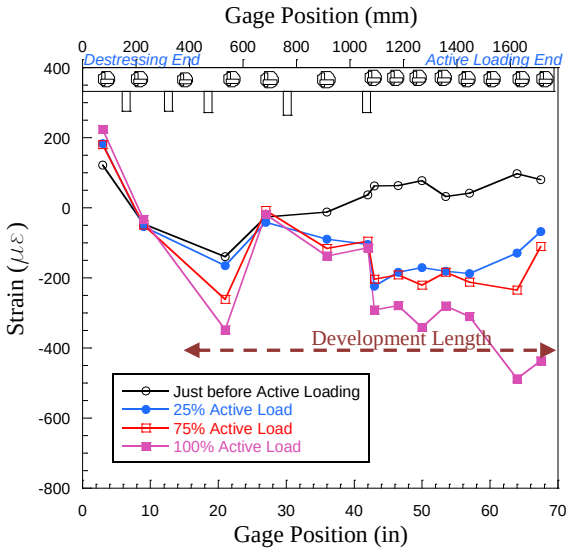

Figure 149. 19-strand – Third Specimen - Top Circumferential Strain During Active Loading

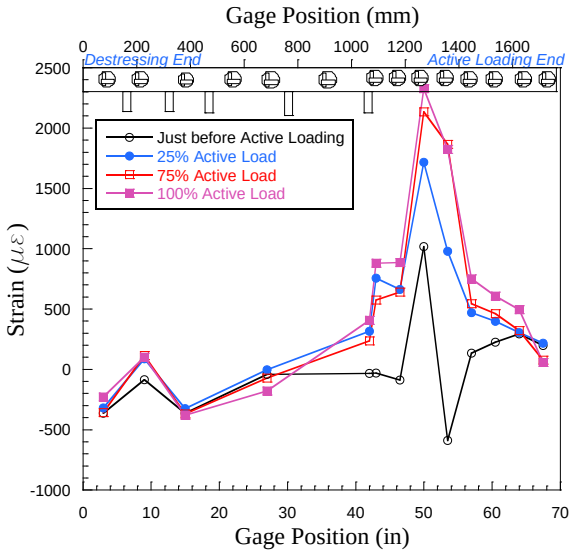

Figure 150. 19-strand – Third Specimen - Side Axial Strain During Active Loading

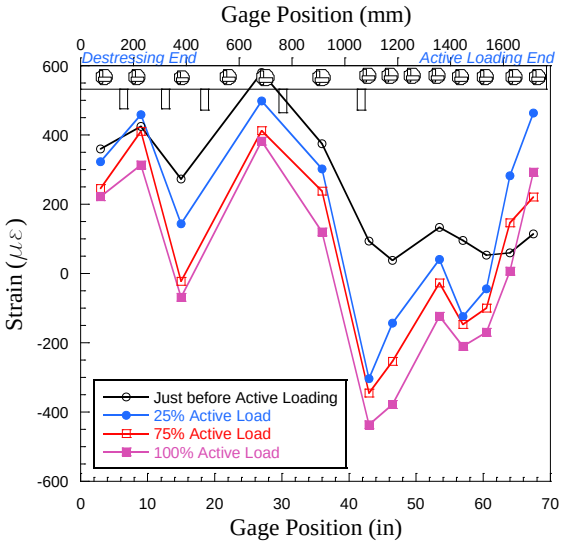

Figure 151. 19-strand – Third Specimen –Side Circumferential Strain During Active Loading

5.9.3 Post-test Observations

After active loading, the hydraulic jacks, and reaction fixtures were removed and DSI bars were de-stressed allowing the visual inspection of the specimen. The same post-active-loading observations that were recorded in the 2nd and 3rd 7-strand and the second 12-strand specimen were observed in this specimen. There was visual indication of slippage between the tendons and PT grout from the active loading end. Visible signs of tendon slippage were observed in Figure 152. No cracking was observed in the specimen block due to the active loading procedure (Figure 153).

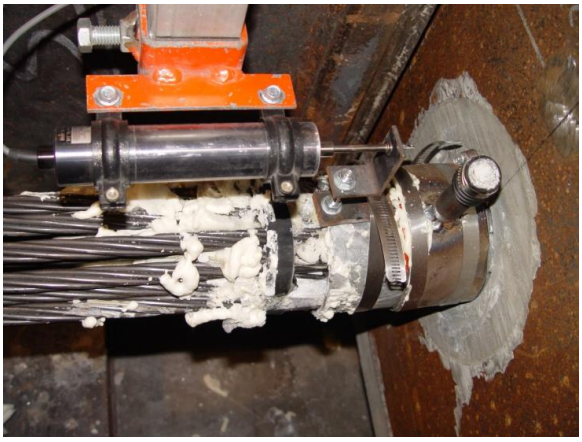

Figure 152. Third 19-strand Specimen Photo- After Pullout- Active Loading End

Figure 153. Third 19-strand Specimen Photo - Destressing End- After Active Loading

Chapter 6: Analytical Model

A finite element model was generated in OpenSees (Opensees, 2002) in order to study the behavior of the experiment from a theoretical perspective and to see whether the experimental data can be predicted with a model of known parameters. It was necessary to implement staged analysis to mimic the actual experimental testing procedure. Modeling was purposely restricted to the linear elastic material domain for stress transfer before significant material or contact nonlinearities developed. Therefore, it is anticipated that the agreement of the experimental and analytical data is better during de-stressing (transfer).

In addition, no parameter optimization studies were performed to minimize the discrepancy between experimental and analytical strain values. The analysis was not calibrated to predict the development length and maximum strain magnitudes on the pipe as there are several portions of the model that would require more substantial meshing and material/interface characterization. Such complex nonlinearities, geometries, and boundary conditions are left for future study. However, the analytical model enables several parameter studies. The two key variations included here are the general behavior of the system when replacing the steel pipes with PVC, and the variation in pipe strains due to different boundaries (and relative movement) at the load cell locations.

6.1 Modeling

6.1.1 Model Geometry and Materials

The geometry of the concrete blocks was defined per the dimensions of each specimen. The dimensions of the pipe were obtained from the manufacturer. These dimensions are listed in Table 3. The tendons were modeled as a single cylinder (as opposed to elements defining each strand individually) with an effective diameter as specified by the manufacturer of the tendons (VSL). The dimensions of the 7-strand, 12 strand, and 19 strand are shown in Table 10. The reinforcing rebar, DSI bars, shear flanges and specimen supports were not included in the model.

Table 10. Effective Area and Diameter of Strands (VSL)

Tendon	Effective Diameter (in)	Effective Area (in^2)
7-strand	1.3912	1.52
12-strand	1.8195	2.6
19-strand	2.29	4.12

The concrete and grout test data were obtained, and the modulus of elasticity for each was calculated per the ACI code. The material properties of the strand and pipe were obtained from the manufacturers. VSL specified a modulus of elasticity of 28500 ksi for the steel tendons, and the pipe had a specified modulus of elasticity of 29000 ksi per AISC standards. When the PVC pipe alternative was studied, a modulus of elasticity of 410 ksi was used (The Engineering ToolBox, 2011).

6.1.2 Elements and Constitutive Model

Standard brick elements, which use a triangular isoparametric formulation in OpenSees, were used to construct the model. Multiaxial material models must be used for modeling 3D elements in OpenSees. These NDMaterial objects represent stress-strain relationships at the integration point of continuum and force-deformation elements. It was assumed that both the steel and cementitious materials could be assumed elastic and isotropic. In this project the FEM model will not be calibrated to obtain the exact results obtained in the experiment; elastic material modeling is considered sufficient to predict the behavior of the system and predict a transfer length.

6.1.3 Mesh

The concrete block was meshed around the steel pipe in four portions, the top, bottom, right and left portions. After that the pipe was meshed with the same manner over a specific thickness (depending on specimen). The pipe end nodes were rigidly connected to the concrete block. This meshing strategy allowed maximum mesh refinement in the pipe region and general element size increase at the extents of the mesh.

The grout was then meshed and connected to the steel pipe. The same number of layers were used through the pipe and grout thickness. The tendon was meshed as a single circular block with an effective diameter defined in Table 10. The parameter nodes of the tendon were not connected to the grout until the stressing of the tendon was performed. After stressing the tendon 1-D gap elements were added connecting the tendon parameter nodes to the grout nodes. This procedure ensured that no restoring force was imparted into the grout due to the initial stress state developed during stressing.

The nodes and elements locations were exported from OpenSees in text format and plotted in Matlab and shown in Figure 154.

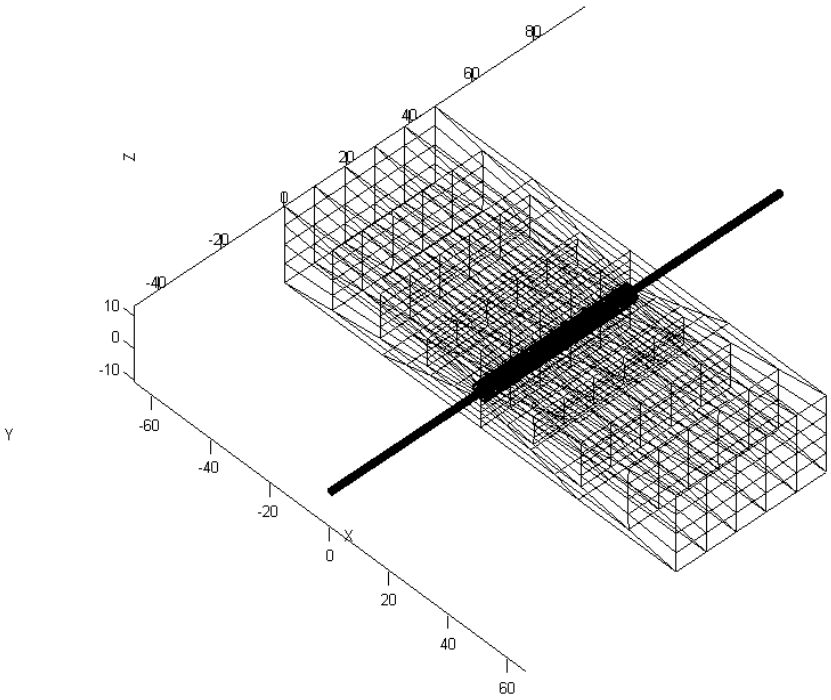

(a) Mesh of full system

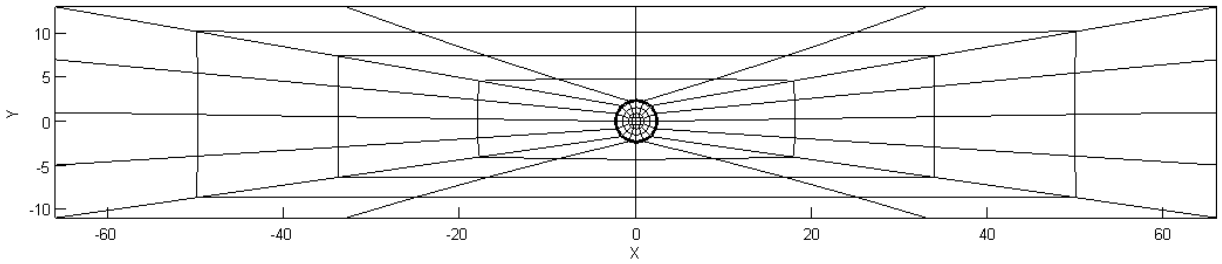

(b) Front face of specimen

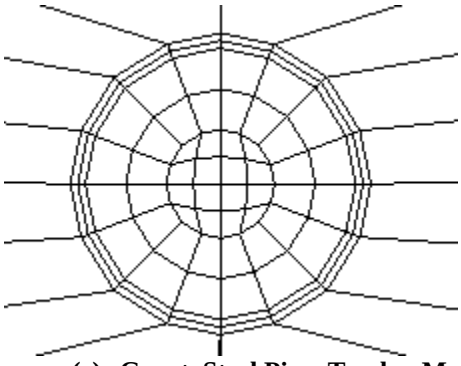

(c) Grout, Steel Pipe, Tendon Meshing

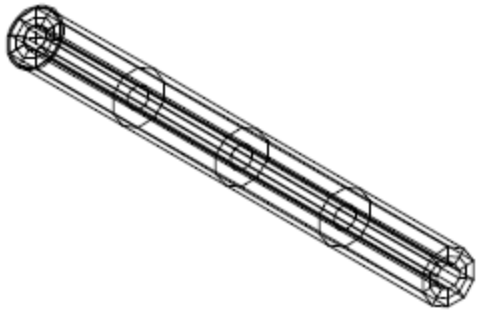

(d) Grout Mesh in 3 dimensions

Figure 154. Mesh as Exported from Opensees

6.1.4 Boundary Conditions and Loads

The tendon was modeled 4 times the length of the specimen block. The tendon nodes were fixed on one end and the stressing load was applied linearly in 20 steps for all 3 specimens. After adding the link (gap) elements between the tendon and the grout, the stressing load was released linearly in 20 steps as well. The constraints were then removed and the active loading was performed from the end where the constraints were present. The 7 strand active loading was applied in 28 steps while the 12 and 19 strand loads were applied in 25 and 24 respectively. The difference in the loading pattern was done only for programming issues and not to compensate the rate of the load during the experiment since the constitutive model is time independent.

The specimen was fixed at the bottom in all three directions. Changes to the boundary conditions did not reveal any changes to the analytical results: The hydraulic jacks were replaced by pins that resist forces in X and Z directions (transverse to the loading and parallel to the loading respectively) and the bottom of the specimen was fixed with pins that resist the forces in the y direction.

6.1.5 Load Pattern and Analysis

In Opensees the analysis was performed in three steps. First the load pattern was defined. A plain Pattern is used to define linear static nodal loads in our model. The second step was defining the analysis and its features. The integrator command is used in this project to determine the predictive step for time t+dt, specify the tangent matrix, and determine the incremental displacements. Then the 3rd step is analyzing; using incremental solution strategies implemented in Opensees analysis object, the static solution is obtained incrementally.

The stresses at the integration points are provided by Opensees. Using the elasticity matrix, these stresses are converted into strains.

6.2 FEM Results

Figure 155 through Figure 166 show the results of the finite element model analysis for the 7-, 12-, and 19-strand specimens plotted along with the obtained results from the experiments. The FEM model results perfectly show the predicted behavior of the system if there is no slip. For the 7- and 12- strand specimens, during de-stressing the model predicts the behavior of the system very closely even though the magnitudes of the strains are different. These magnitude differences are attributed to the stiffness property of the finite elements. A mesh refinement analysis would bring the strain values to a closer magnitude observed during the experiments. In addition to mesh refinement, better boundary conditions, incorporation of shear flanges and trumpets as well as nonlinearities would influence the results.

In order to show that there is de-bonding, link elements between the tendon and grout are removed over a predetermined length. The strain profile for the 7-strand specimen after the removal of those link elements is shown in Figure 167 and Figure 168.

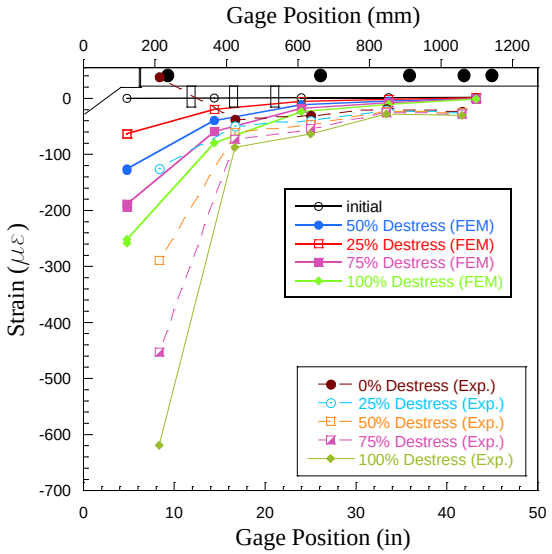

Figure 155. Axial Strain Distribution for the 7-strand specimen During De-stressing: FEM vs. Experimental

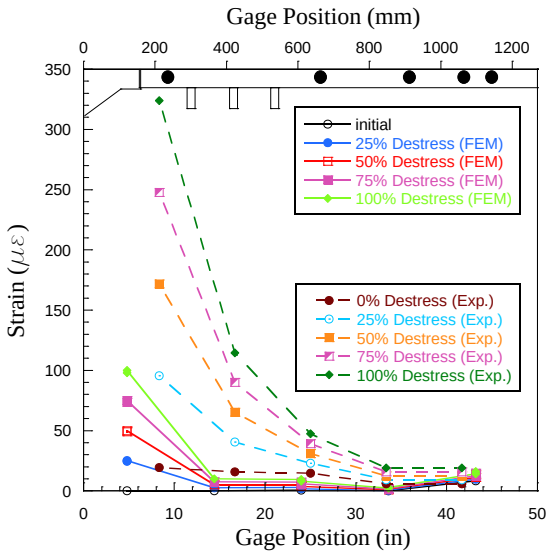

Figure 156. Circumferential Strain Distribution for the 7-strand specimen During De-stressing: FEM vs. Experimental

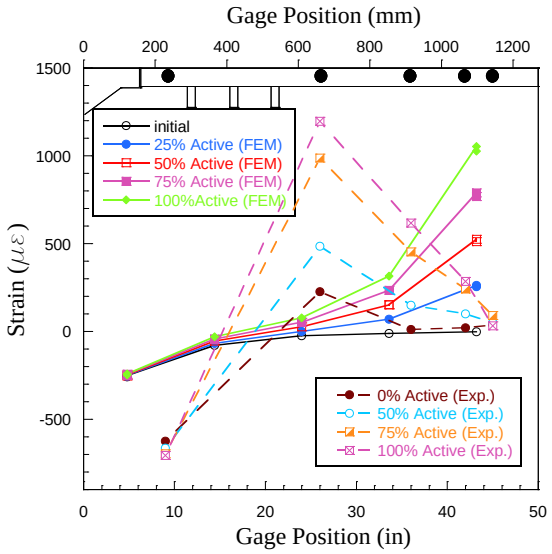

Figure 157. Axial Strain Distribution for the 1st 7-strand specimen During Active Loading: FEM vs. Experimental

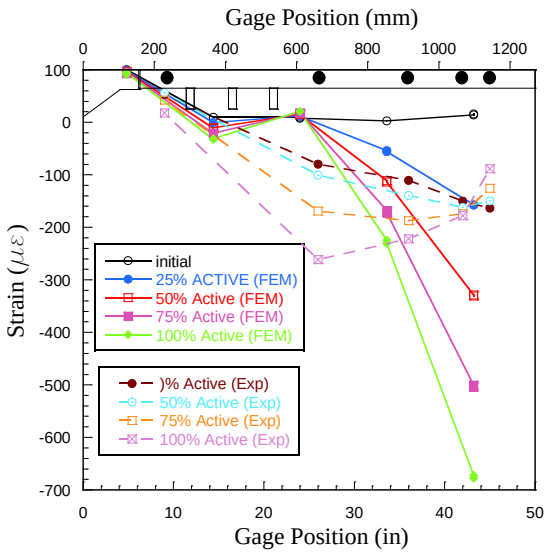

Figure 158. Circumferential Strain Distribution for the 1st 7-strand specimen During Active Loading: FEM vs. Experimental

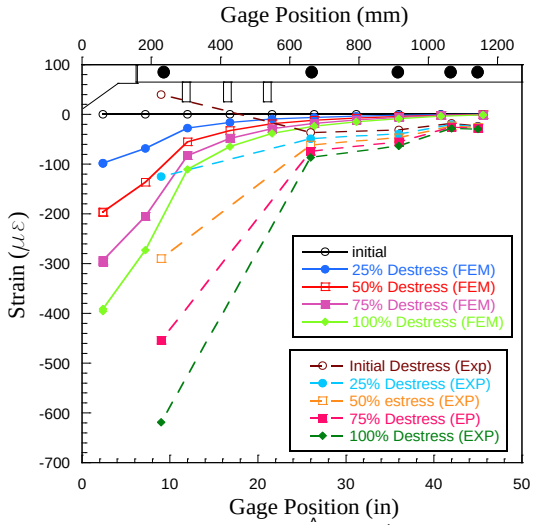

Figure 159. Axial Strain Distribution for the 1st 12-strand specimen During De-stressing: FEM vs. Experimental

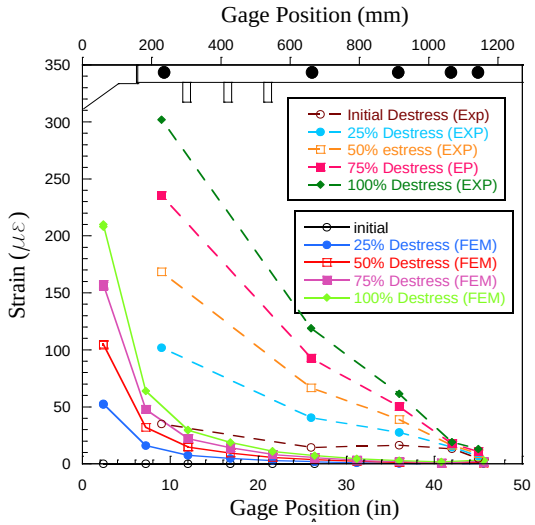

Figure 160. Circumferential Strain Distribution for the 1st 12-strand specimen During De-stressing: FEM vs. Experimental

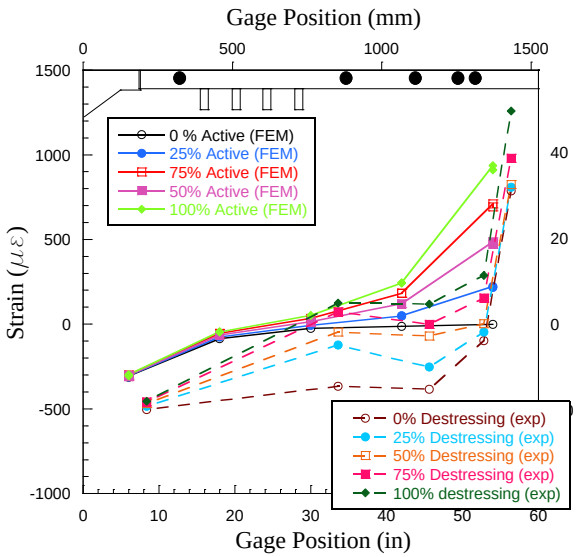

Figure 161. Axial Strain Distribution for the 1st 12-strand specimen During Active Loading: FEM vs. Experimental

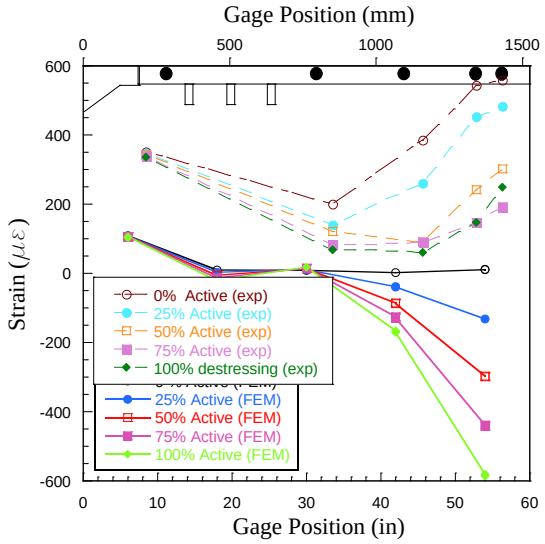

Figure 162. Circumferential Strain Distribution for the 1st 12-strand specimen During Active Loading: FEM vs. Experimental

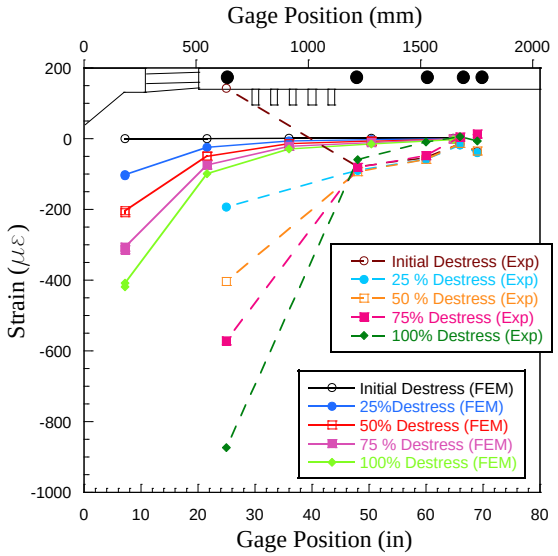

Figure 163. Axial Strain Distribution for the 1st 19-strand specimen During De-stressing: FEM vs. Experimental

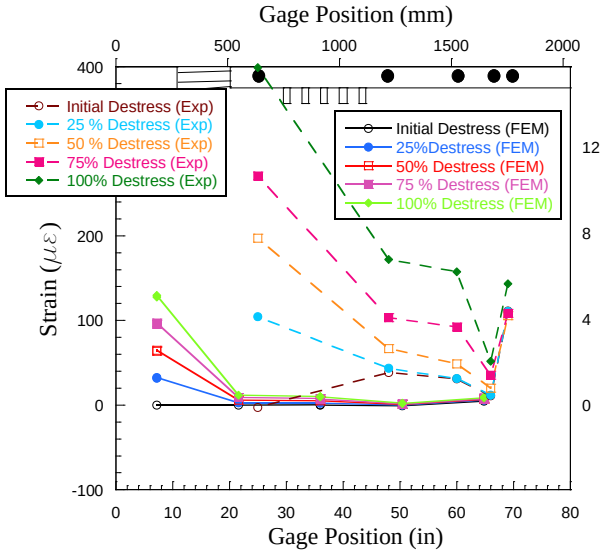

Figure 164. Circumferential Strain Distribution for the 1st 19-strand specimen During De-stressing: FEM vs. Experimental

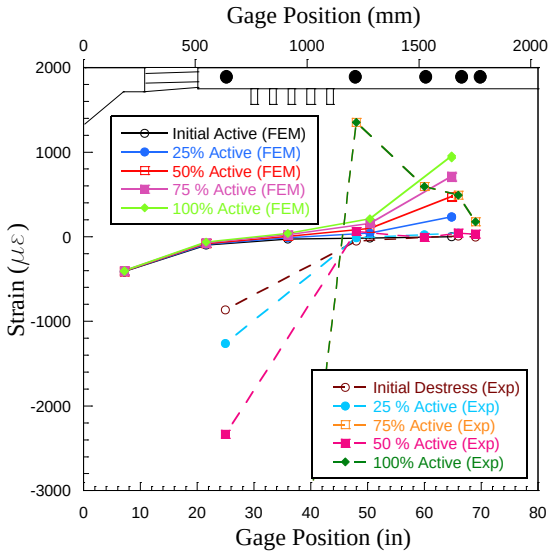

Figure 165. Axial Strain Distribution for the 1st 19-strand specimen During Active Loading: FEM vs. Experimental

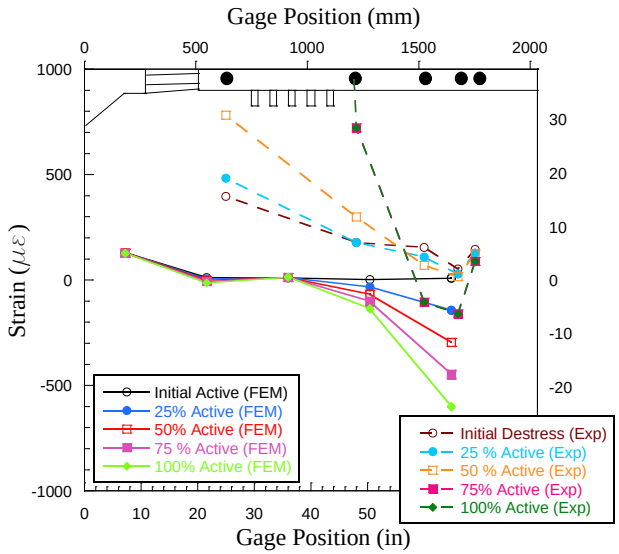

Figure 166. Axial Strain Distribution for the 1st 19-strand specimen During Active Loading: FEM vs. Experimental

The expected behavior during de-stressing was shown in the FEM results for all specimens. The Hoyer Effect was reflected by the great increase of circumferential tension strains during de-stressing. The expected axial compressive strain profile during de-stressing was also observed. The transfer length was less than what is expected in the experimental results. This is because there are many boundary conditions that were not modeled such as the shear flanges, hydraulic jack loads, and VSL anchorage. The ability to model the VSL anchorage as well as shear flanges could change the results significantly especially for the 19-strand results where there are relatively higher compressive strains which might in turn cause a short column effect between the VSL anchorage and shear flanges.

The links were removed at approximately 25 inches from the free face. It can be seen from Figure 167 that the pipe is in compression axially at the points closest to where the link elements are added. This is due to strain compatibility: As the tendon is pulled the pipe where the link elements are added is in tension axially which causes the section that is not connected to the grout to go into compression. This also applies for the circumferential strain profile in Figure 168.

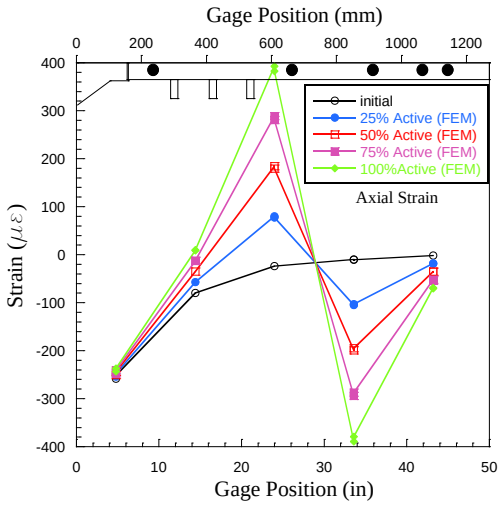

Figure 167. FEM Axial Strain After Removing Link Elements During Active Loading

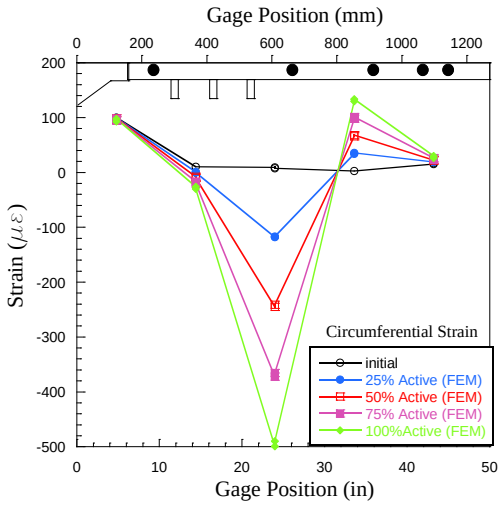

Figure 168. FEM Circumferential Strain After Removing Link Elements During Active Loading

A postulated explanation for the differences between the top and side strain gage readings was the differential movement of the specimen in the X Z plane causing flexure in the pipe due to the two load application points. As explained in the experimental results section, the LVDTs at the two corners of the specimen reflected this behavior. This phenomenon was studied by subjecting the specimen block in the FEM to the same shearing effect. The results of the strains are shown in Figure 169 and Figure 170. It can be seen that there are major strain differences between the top and side strains on the pipe which supports the behavior observed in the experimental results.

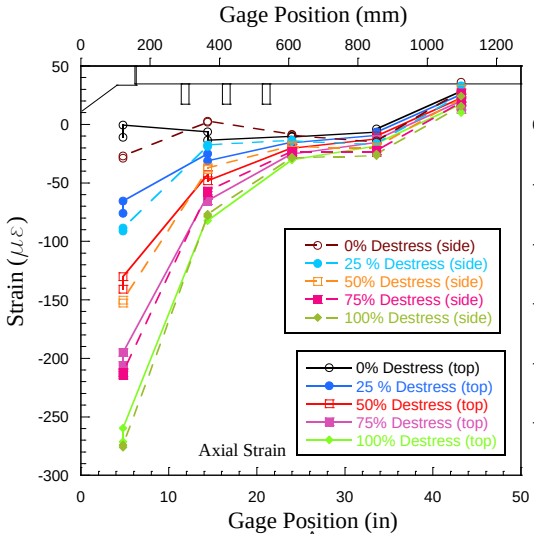

Figure 169. FEM Axial Strain Distribution During De-stressing (top and side)

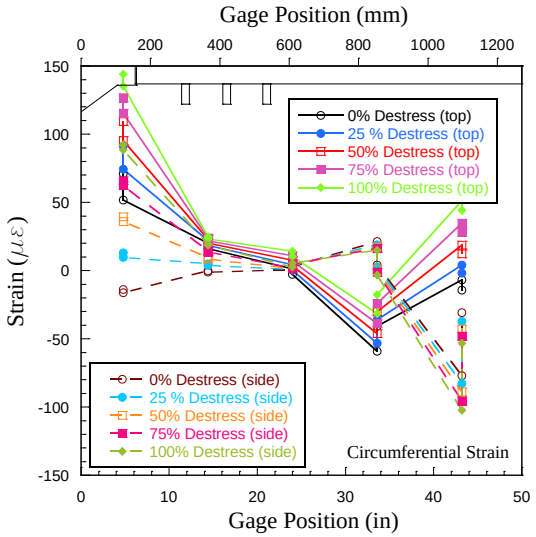

Figure 170. FEM Circumferential Strain Distribution During De-stressing (top and side)

6.3 PVC Alternative

In order to investigate the use of a PVC pipe alternative to the steel one used in the experiments, the finite element model was altered to incorporate the PVC properties. Figure 171 and Figure 172 show the strain on the exterior circumference of the pipe in the axial direction during de-stressing and active loading respectively. It can be seen from these plots that the strain values have increased significantly on the outside circumference of the pipe. The pipe would experience very high stresses which in the case of 7-strand would fail at about 56% of full pullout force. Having such large magnitude of forces being transferred from the tendon to the

grout and then to the PVC pipe, leads to believe that using the PVC pipe will not allow the force to be transferred to the concrete block; therefore, the failure mechanism observed in this experiment would be entirely different. The most probable type of failure based on these results would be a grout-PVC interface failure.

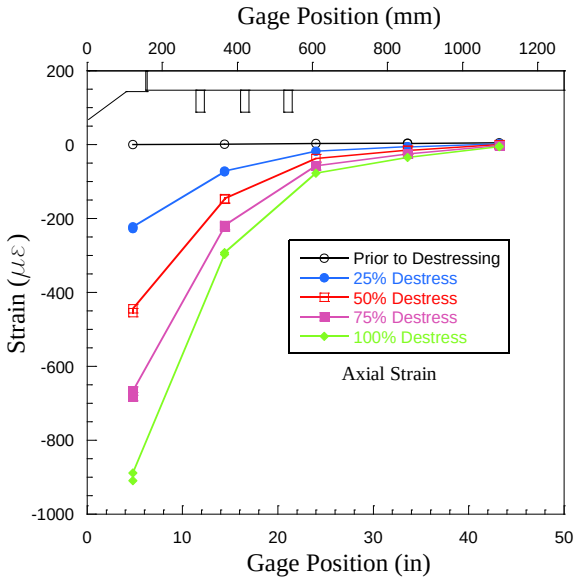

Figure 171. 7-strand – PVC Pipe – Axial Strain Analytical Results for De-stressing

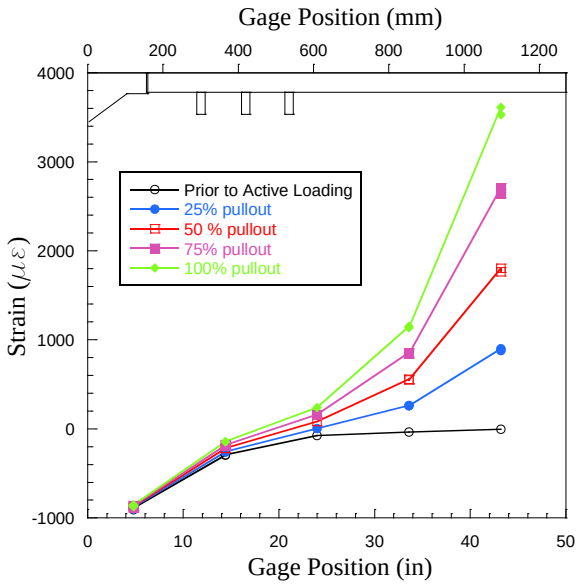

Figure 172. 7-strand – PVC Pipe – Axial Strain Analytical Results for Active Loading

Chapter 7: NASP

7.1 NASP Background

Since the mid 1990s, researchers tried developing a standardized test to assess the bond characteristics of individual prestressing strands. It was suspected that strand produced by different manufacturers had different bonding characteristics. To that end, many testing programs were undertaken to assess the viability of various "standardized tests" and the suitability of such tests for predicting the bond ability of prestressing strand. The latest were testing and research sponsored by the North American Strand Producers Association (NASP). These led to the development of a standard bond test, called "the NASP Bond Test". Many of the original results were not published, according National Cooperative Highway Research Program (NCHRP) report (NCHRP, 2008). Research concentrated on this standard and determined that the NASP Bond Test provided the best repeatability (Ramirez & Russel, 2008). According to the same report, experimental results showed that there were differences that existed in the bond of prestressing strands from various manufacturers. The standardization of the NASP bond test received endorsement by many researchers.

7.2 Application in This Project

To determine the bond performance between the VSL 0.6" diameter strand used and the PT grout, it was decided to perform a standard NASP PT strand bond test as described in Appendix H of NCHRP Technical Report 603. Six pullout samples were prepared and tested at the University of Central Florida Structural Analysis Laboratory. Pictures from the experimental setup are shown in Figure 173.

(a) Full NASP Test Set-up

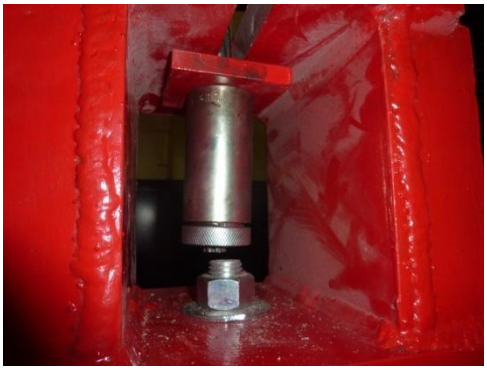

(b) Chuck Location

(c) Specimen Bearing Location

Figure 173. Photos From the NASP Setup

7.3 Instrumentation and Testing

The pull out test set-up shown in Figure 173 is can be summarized in a schematic shown in Figure 174. The tendon is pulled from the lower end of the specimen. The slip is measured from the top of the strand. Two LVDTS were mounted from a reference frame. One measured the displacement of the top of the strand and the other that of the top of the grout. The slip was estimated by subtracting the displacements of the strand from those of the grout.

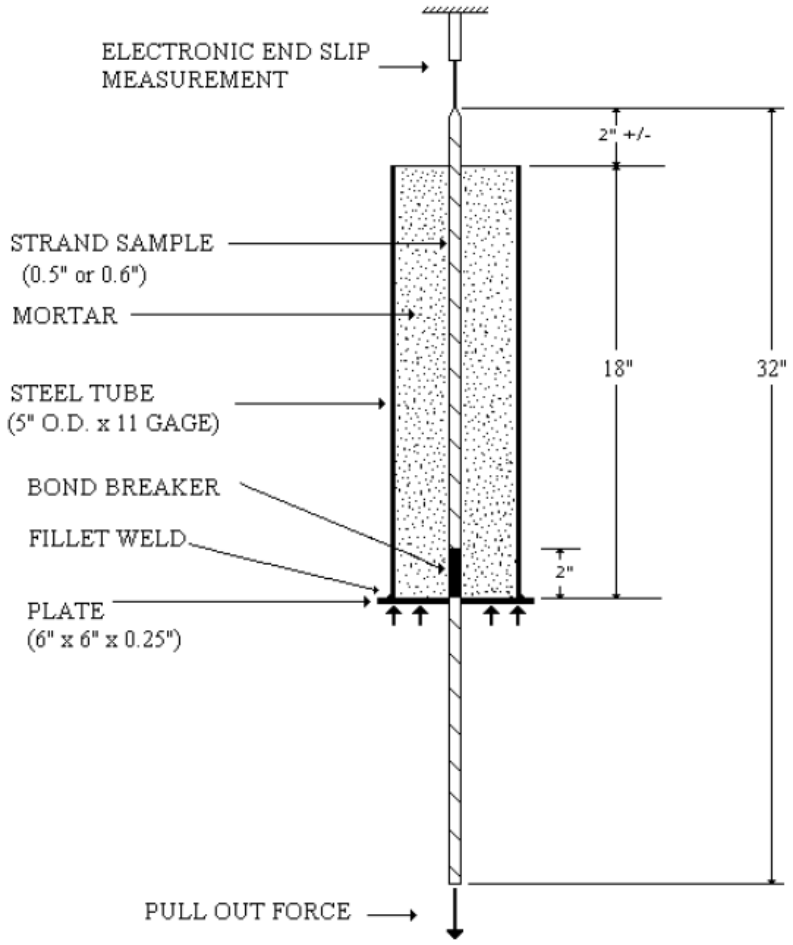

Figure 174. NASP Schematic

The first specimen (Batch 1) was cast on 12/15/2009 and tested on 1/30/2010. The second through sixth specimens were cast on 12/17/2009 and tested on 2/4/2010. Grout cubes were taken just before grouting the specimen and tested on 2/5/2010. The grout strength is listed in Table 11. All the grouting procedures were performed following ASTM C 109.

Table 11. Grout Cube Strength

Batch No.	Cube ID	Strength (ksi)	Batch No.	Cube ID	Strength (ksi)
1	A	11.59	2	A	12.57
	B	11.58		B	12.22
	C	11.45		C	12.19
Average		11.54	**Average**		12.33

The first specimen was tested on 1/30/2010. The load reached 25 kips and the test procedure was stopped. Problems with the data acquisition prevented getting the load that caused 0.01 in displacement. The same specimen was retested on 2/3/2010. The strand showed 0.01 in displacement at 13 kips. The strands of specimen 2, 3, 4, and 6 slipped 0.01 inches at 22.63kips, 23.68 kips, 23.47 kips, and 20.13 kips respectively. Specimen 3 was omitted due to a malfunction in the DAQ during testing. The slip-versus-load plots are shown in Figure 175 through Figure 179.

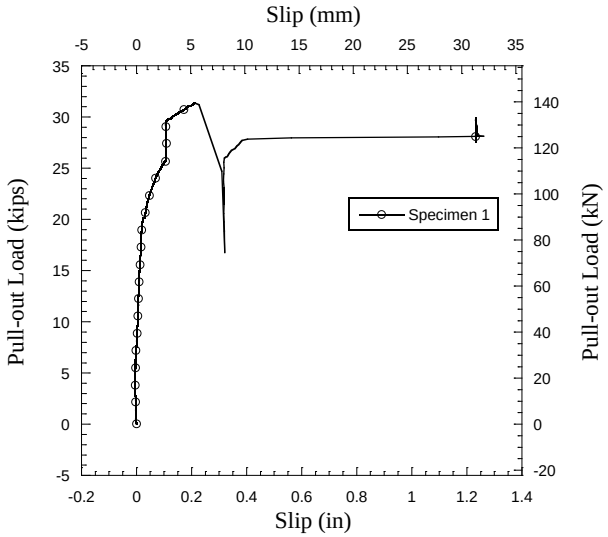

Figure 175. NASP Specimen 1 (Redo) Pullout Load vs. Slip

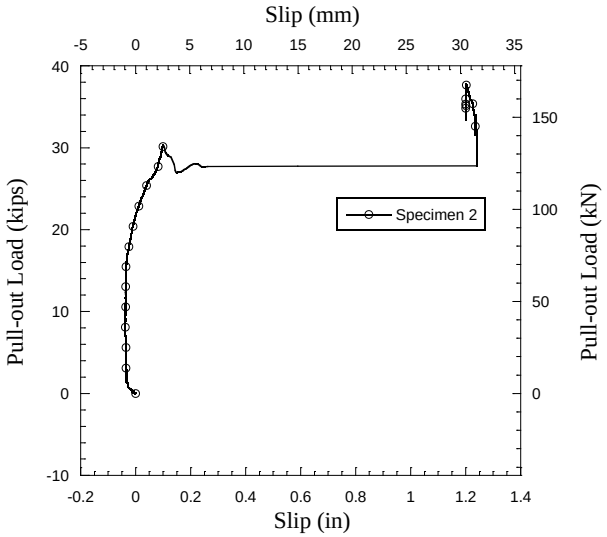

Figure 176. NASP Specimen 2 Pullout Load vs. Slip

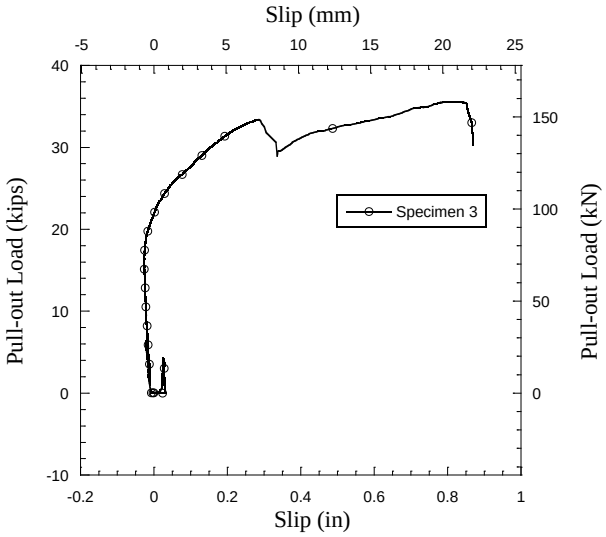

Figure 177. NASP Specimen 3 Pullout Load vs. Slip

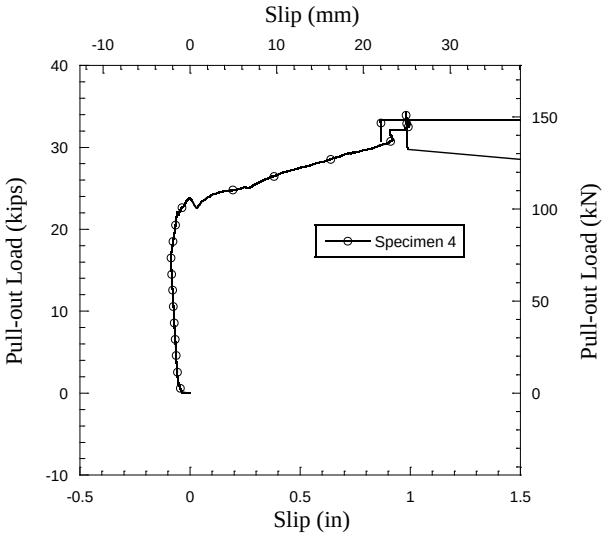

Figure 178. NASP Specimen 4 Pullout Load vs. Slip

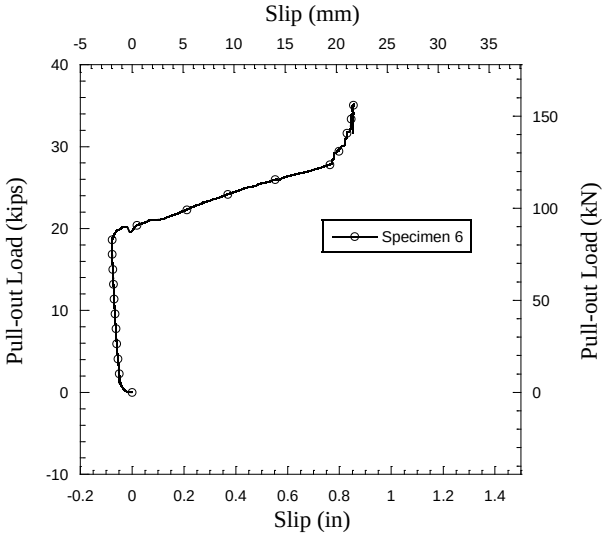

Figure 179. NASP Specimen 6 Pullout Load vs. Slip

All the specimens were tested until the strand slipped at least 2 inches. When the first specimen was re-tested, sudden failure occurred at 31 kips with a popping sound. The same failure happened when testing the third specimen. The latter failed at 35 kips. The tendon from the rest of the specimens was pulled out gradually, with no sudden failures. Surface cracks

developed during curing that radiate from the strand but no new cracks developed after the testing Figure 180.

Figure 180. Specimen before (left) and after (right) testing

.

Additional 6 specimens were casted and tested within 24 hours of casting. Specimens 1, 2 and 3 were tested following the same recommended procedure for NASP per NCHRP report 603. Specimens 4, 5, 6 were prestressed up to 80% of GUTS and de-stressed by heating and cutting the strand from the top side of the specimen. While casting specimen 5, grout bleeding occurred. The specimen was, therefore, 3 inches shorter than the rest. Figure 181 shows the load vs. displacement of the 6 specimens. The data shows that while the prestressed specimens were able to sustain more load until significant pullout to occur, the stiffness had decreased. This can be attributed to the change in bond properties that occurred during de-stressing. The circumferential expansion and axial contraction of the tendon caused the bond properties between grout and tendon to change. On the other hand the Hoyer Effect increased the capacity of the prestressed specimens to sustain more pullout load.

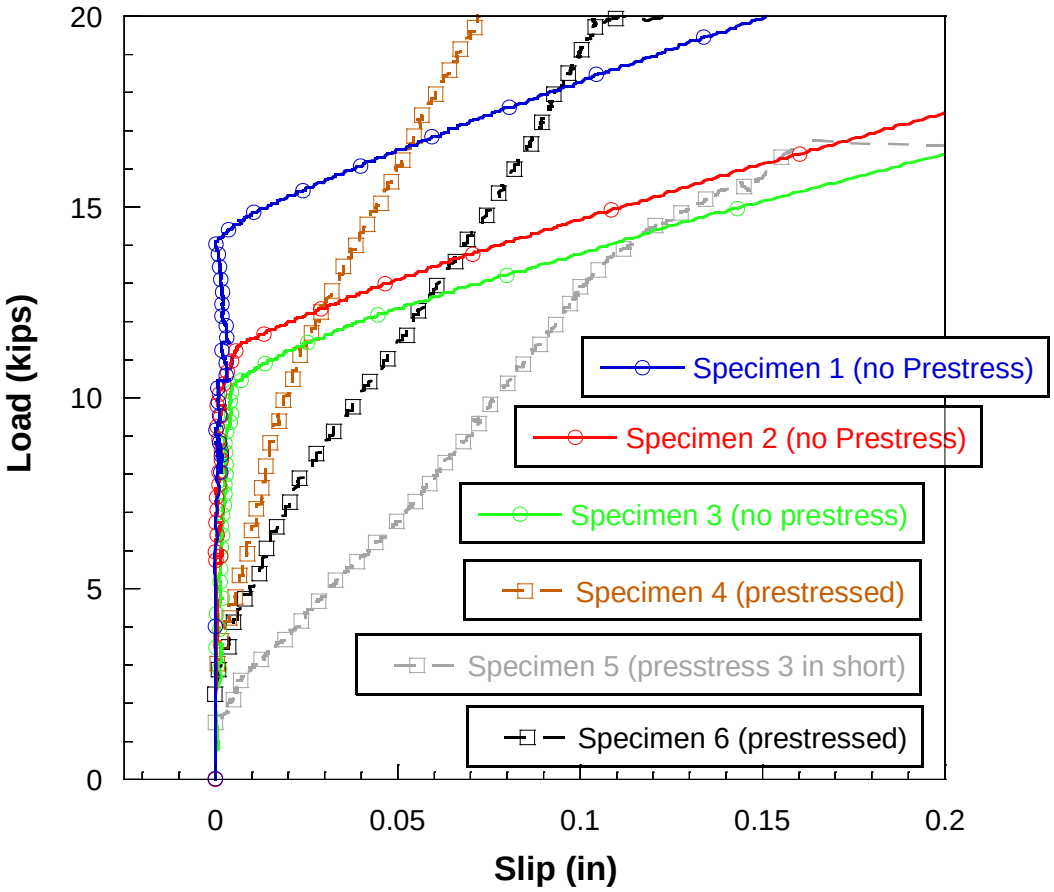

Figure 181. 2nd NASP Batch: Specimens 1, 2, 3, 4, 5, 6 Load vs. Slip

Chapter 8: Conclusions & Recommendations

8.1 Conclusions

The results obtained from the nine specimens indicate that the pier anchors and deviator blocks have potential to provide secondary anchorage. This secondary anchorage is dependent on adequate grouting operations. Based on the 7-strand results a 38” of development length provides sufficient anchorage in case of anchor head failure as the strand is loaded up to 90% of GUTS. The 12-strand results indicate that a transfer length of 50” will provide sufficient anchorage without failure as the strands are loaded up to 90% of GUTS. These recommendations are based on the first 7- and 12-strand specimens as no failure was indicated by data analysis or observed experimentally.

Using the VSL anchorage specifications and shear flanges, there was one common ductile failure mechanism among the specimens that did not hold 90% GUTS during active loading. The 7-, 12-, and 19-strand specimens that did not hold the full 90% GUTS pullout force showed a formation of a grout plug at the free face that anchored the tendon and induced large axial and circumferential strains on the pipe. It is also observed that after the initialization of failure, the tendon slippage would stop and the tendon would be able to sustain 80 to 85% of GUTS without losses. Increasing the load to 90% of GUTS would only initialize the ductile slip of the tendon from the grout and the tendon would go back to being able to hold the same previously sustained load.

The results of the 19-strand test indicate that the pipe did not have sufficient strength in it to allow anchorage when the VSL specifications for anchorage are used. The high strains induced on the pipe due to the grout plug formation allowed the local failure of the pipe and the concrete block. De-stressing data showed that the pipe yielded at the location of the first strain gage from the free face due to the high stresses inside the pipe from the Hoyer Effect. During active loading, the anchorage mechanism provided by Hoyer Effect at the free face exerted more axial compressive strain, increasing the circumferential strains. The increased stresses and strains caused the yielding of the pipe, thus releasing a large amount force from the tube into the specimen. The release of this stress caused the slip of the grout and strand from the pipe from the active loading end. When the VSL specifications were altered and the anchor head was removed,

the grout plug did not form at the free face. The VSL specifications, specifically the trumpet at the anchor head, induce undesirable failure of the pipe when it does not have sufficient strength to withhold the high strains as in the case of the 1st 19-strand specimen.

The only development length equations that are developed in the current code provisions deal with prestressed concrete beams and segmental bridge girders (ACI 318-05 and AASHTO LRFD). Using these equations provide a very conservative and uneconomical and even unpractical solutions for calculating the transfer length. Based on these provisions the minimum requirement for strand development, the measured development lengths for the 7- and 12-strand specimens exceeded these requirements by 55%.

8.2 Recommendations

The recommended minimum development length for a 7-strand tendon is 38" and that for the 12-strand is 50" for no failure to occur at 90 % of GUTS tendon load. To use the same development for the 19-strand tendon as those recommended in sections 5.8 and 5.9 of this report, stronger pipe that can resist more expansive forces is required in order to allow ductile failure and time for inspection and repair.

When similar VSL systems are used, the failure of the 7 and 12 strand bridge piers is slow and ductile and allow time for inspection and repair. Using the same specifications for the 19-strand could potentially lead to brittle and undesirable failures.

To use the same development for the 19-strand tendon as those recommended in sections 5.8 and 5.9 of this report, stronger pipe that can resist more expansive forces is required in order to allow ductile failure and time for inspection and repair. However, the 6' specimen length used in the specimens in this study exhibited either progressive slip or significant expansive failure of the surrounding concrete and may therefore be more detectable.

References

American Assiciation of State Highway and TransportationOfficials (AASHTO). (2004). *AASHTO LRFD Bridge Design Specifications.* Washington, D.C.: AASHTO.

American Concrete Institute (ACI) 318-02. (2002). *Building Code Reqirements for Structural Concrete.* Farmington Hills, MI: American Concrete Institute.

American Concrete Institute (ACI) Committee 318. (2005). *Building Code requirements for Structural Concrete (ACI 3118-05).* Farmington Hills, MI: ACI.

American Concrete Institute (ACI) Committee 318. (2005). *Building Code Requirements for Structural Concrete (ACI 318-05) and Commentary (ACI 318R-05).* Detroit: American Concrete Institute.

American Society for Testing and Materials. (2008). *Standard Test Method for Compressive Strength of Hydraulic Cement Mortars (Using 2-in or [50mm] Cube).* West Conshohocken, PA: ASTM International.

Buckner, C. D. (1994). *An Analysis of Transfer and Development Length for Pretensioned Concrete Structures.* Washington DC: Federal Highway Administration (FHWA).

Cousins, E. E., Johnston, D. W., & Zia, P. (1993). *Effect of Strand Spacing on Development of Prestressing Strands.* Alaska Department of Transportation and Public Facilities.

Cousins, T. E., Johnston, D. W., & Zia, P. (1990). Transfer and Development Length of Epoxy Coated and Uncoated Prestressing Strand. *PCI Journal* , 92-103.

Deatherage, J. H., Burdette, E., & Chew, C. (1994). Development Length and Lateral Spacing Requirements of Prestressing Strand for Prestressed Concrete Bridge Girders. *PCI Journal* , 70-83.

Diephuis, J. R. (2004). Factors Affecting Bond in Multi-Strand Post-Tensioning Tendons Including the Effect of Emulsifiable Oils. Austin, Texas: University of Texas.

Hoyer, E., & Friedrich, E. (1939). Beitrag Zur Frage der Hatspannung in Eisen Betonbauteilen. *Beton and Eisen* , vol. 38, No. 6, 107-110.

Janney, J. R. (1954). Nature of Bond in Pretensioned Prestressed Concrete. *Journal of the American Concrete Institute* , 717-736.

Marshall, W. T. (1966). A Theory for End-Zone Stresses in Pretensioned Concrete Beams. *Journal of Prestressed Concrete Institute* , 45-51.

Martin, L. D., & Scott, N. L. (1976). Development of Prestressing Strand in Pretensioned Members. *ACI Journal* , 453-456.

Mitchell, D., Cook, W. D., Khan, A. A., & Tham, T. (1993). Influence of High Strength Concrete on Transfer Length and Development Length of Pretensioning Strand. *PCI Journal* , 52 - 66.

Oh, B. H., Kim, W. S., & Choi, Y. C. (2006). Theoretical Analysis of Transfer Lengths in Pretensioned Prestressed Concrete Members. *Journal of Engineering Mechanics at ASCE* , 1057-1066.

Opensees, 2. (2002). *University of California at Berkeley*. From http://opensees.berkeley.edu/

Prestressed Concrete Institute. (1978). *PCI Design Handbook (2nd ed.).* Chicago.

Rajagopalan, I. N. (2002). Transmission and Anchorage. In I. N. Rajagopalan, *Prestressed Concrete* (pp. 303-331). Pangbourne: Alpha Science International.

Ramirez, J. A., & Russel, B. W. (2008). *(NCHRP) Report 603 - Transfer, Development, and Splice Length for Strand Reinforcement in High Strength Concrete.* Washington, D.C.: Transportation Research Board.

Russel, B. W., & Burns, N. H. (1993). *Design Guidelines for Transfer, Development, and Debonding of Large Diameter Seven Wire Strands in Pretensioned Concrete Girders.* Austin: Research Report 1210-5f, CTR, The University of Texas at Austin.

Russel, B. W., & Burns, N. H. (1996). Measured Transfer Lengths of 0.5 and 0.6 in. Strands in Pretensioned Concrete. *PCI Journal* , 44-63.

Russel, B. W., & Burns, N. H. (1997). Measurement of Transfer Lengths on Pretensioned Concrete Elements. *Journal of Structural Engineering* , 541 - 549.

Russel, B. W., & Tuan, C. Y. (1997). Measurement of Transfer Lengths on Pretensioned Concrete Elements. *Journal of Structural Engineering* , 541 - 549.

Sengupta, A. K., & Menon, D. (n.d.). Lecture Notes. *Prestressed Concrete Structures* . Indian Institute of Technology.

Sowlat, K., & Rabbat, B. (1984). *Testing of Segmental Bridges.* Skokie, IL: COnstruction Technology Laboratories.

The Engineering ToolBox. (2011). From http://www.engineeringtoolbox.com/physical-properties-thermoplastics-d_808.html

Xia, Z. (2004). Shear Transfer Device Pullout Test. *VSL Test No. 434* .